UC San Diego

UC San Diego Electronic Theses and Dissertations

Title

Collisional relaxation of an isotopic, strongly magnetized pure ion plasma and topics in resonant wave-particle interaction of plasmas

Permalink

https://escholarship.org/uc/item/2fg4055s

Author

Chim, Chi Yung

Publication Date

2016

Peer reviewed|Thesis/dissertation

UNIVERSITY OF CALIFORNIA, SAN DIEGO

Collisional relaxation of an isotopic, strongly magnetized pure ion plasma and topics in resonant wave-particle interaction of plasmas

A dissertation submitted in partial satisfaction of the
requirements for the degree
Doctor of Philosphy

in

Physics

by

Chi Yung Chim

Committee in charge:

   Professor Thomas O'Neil, Chair
   Professor Charles Fred Driscoll
   Professor Daniel Dubin
   Professor George Tynan
   Professor William Young

2016

The Dissertation of Chi Yung Chim is approved, and it
is acceptable in quality and form for publication on mi-
crofilm and electronically:

_____

_____

_____

_____

_____

Chair

University of California, San Diego

2016

DEDICATION

To my parents, Gladys and Man Kit, for their endless effort and support in raising me up and teaching me to be a proper person.

EPIGRAPH

"Rabbit's clever," said Pooh thoughtfully.

"Yes," said Piglet, "Rabbit's clever."

"And he has Brain."

"Yes," said Piglet, "Rabbit has Brain."

There was a long silence.

"I suppose," said Pooh, "that that's why he never understands anything."

—A.A. Milne, Winnie-the-Pooh

TABLE OF CONTENTS

LIST OF TABLES

ACKNOWLEDGEMENTS

I would like to first of all acknowledge my advisor Professor Thomas M. O'Neil for all of his guidance in this dissertation. He always focuses on the physical properties and concepts of any problem, and tries to explain and treat the difficulties and uncertainties with the greatest clarity possible. I have enjoyed working through the research problems with him, learning to identify and understand the physics of the phenomena being studied. He has put in so much effort in guiding me and giving me advice on writing papers and giving presentations, far more than what he is supposed to do as an advisor. I am very glad to have the opportunity to learn from and with him throughout these years.

I also want to thank Professor C. Fred Driscoll, Professor Daniel H.E. Dubin, Dr. Francois Anderegg and Dr. Andrey Kabantsev for all of their advice in all the private discussions and Tuesday group meetings. Professor Driscoll has been serious on the physical details and the consistency between theories and observations. Professor Dubin always has in mind the many different ways to solve a problem and the proper and productive ways to compute and to perform simulation. Dr. Anderegg and Dr. Kabantsev have provided a lot of views on how the actual experiment compares with our theories. The discussion with them has provided me with different viewpoints to understand the research problem and to interpret my results.

I would like to acknowledge as well my graduate student colleagues Arash Ashouvan, Daniel Walsh and Matthew Affolter. They have input a lot in terms of views, suggestions and reminders throughout the process of solving problems and giving presentations. My gratitude also goes to Jo Ann Christina for her secretarial work in keeping the group running well.

I want to extend my appreciation to the rest of the dissertation committee - Professors George Tynan and William Young, for all of their time, useful discussion and valuable feedback in the research work for this dissertation.

Thank you my parents, Gladys and Man Kit, for working so hard for decades to take care of me and providing me with the important guidance and education. I want to thank as well my family and friends for all the support and accompaniment. My gratitude also goes to my teachers for giving me the enlightenment and interest. Particularly, I have been very lucky to have met from my secondary school Ms Rachel Chan and Ms Lai Yee Lam, who have been listening to me about life issues, and giving me opinions and advice, even after I left my hometown to study in this country. I have taken something from every one of you to get to this point of life.

Chapter 1, in parts, is taken from the papers appearing in Physics of Plasmas as C.Y. Chim, T.M. O'Neil, D.H.E. Dubin, *Physics of Plasmas* **21**, 042115 (2014), C.Y. Chim, T.M. O'Neil, *Physics of Plasmas* **23**, 072113 (2016), and C.Y. Chim, T.M. O'Neil, *Physics of Plasmas* **23**, 050801 (2016). The dissertation author was the primary investigator and author of these papers.

Chapter 2, in full, is a reprint of the material as it appears in Physics of Plasmas. C.Y. Chim, T.M. O'Neil, D.H.E. Dubin, *Physics of Plasmas* **21**, 042115 (2014). The dissertation author was the primary investigator and author of this paper.

Chapter 3, in full, is a reprint of the material as it appears in Physics of Plasmas. C.Y. Chim, T.M. O'Neil, *Physics of Plasmas* **23**, 072113 (2016). The dissertation author was the primary investigator and author of this paper.

Chapter 4, in full, is a reprint of the material as it appears in Physics of Plasmas. C.Y. Chim, T.M. O'Neil, *Physics of Plasmas* **23**, 050801 (2016). The

dissertation author was the primary investigator and author of this paper.

VITA

2009   B. S. in Physics, Chinese University of Hong Kong, Hong Kong

2009-2011   Graduate Teaching Assistant, University of California, San Diego

2015   M.S., University of California, San Diego

2016   Ph.D., University of California, San Diego

PUBLICATIONS

A. Splendiani, L. Sun, Y. Zhang, T. Li, J. Kim, C. Y. Chim, G. Galli, F. Wang, "Emerging photoluminescence in monolayer MoS_2", Nano Letters 10 (4), 1271-1275, 2010.

C. Y. Chim, T. M. O'Neil, D. H. E. Dubin, "Collisional relaxation of a strongly magnetized two-species pure ion plasma", Phys. Plasmas **21**, 042115 (2014).

A. A. Kabantsev, C. Y. Chim, T. M. O'Neil, C. F. Driscoll, "Diocotron and Kelvin mode damping from a flux through the critical layer", Phys. Rev. Lett. **112**, 115003 (2014).

C. Y. Chim, T. M. O'Neil, "Flux-driven algebraic damping of diocotron modes", in NON-NEUTRAL PLASMA PHYSICS IX: 11th International Workshop on Non-Neutral Plasmas, Vol. 1668, AIP Publishing, 2015.

C. Y. Chim, T. M. O'Neil, "Flux-driven algebraic damping of $m = 1$ diocotron mode", Phys. Plasmas **23**, 072113 (2016).

C. Y. Chim, T. M. O'Neil, "A mechanistic interpretation of the resonant wave-particle interaction", Phys. Plasmas **23**, 050801 (2016).

FIELDS OF STUDY

Major Field: Physics

Study in Classical Mechanics
Professor Daniel Arovas

Study in Electrodynamics
Professor Thomas O'Neil

Study in Mathematical Physics
Professor Raj Pathria

Study in Quantum Mechanics
Professor George Fuller

Study in Non-equilibrium Statistical Physics
Professor Terence Hwa

ABSTRACT OF THE DISSERTATION

Collisional relaxation of an isotopic, strongly magnetized pure ion plasma and topics in resonant wave-particle interaction of plasmas

by

Chi Yung Chim

Doctor of Philosphy in Physics

University of California, San Diego, 2016

Professor Thomas O'Neil, Chair

First in Chapter 2, we discuss the collisional relaxation of a strongly magnetized pure ion plasma that is composed of two species with slightly different masses, but both with singly-ionized atoms. In a limit of high cyclotron frequencies Ω_j, the total cyclotron action $\mathcal{I}_j$ for the two species are adiabatic invariants. In a few collisions, maximizing entropy yields a modified Gibbs distribution of the form $\exp[-H/T_\parallel - \alpha_1\mathcal{I}_1 - \alpha_2\mathcal{I}_2]$. Here, H is the total Hamiltonian and α_j's are related to parallel and perpendicular temperatures through $T_{\perp j} = (1/T_\parallel + \alpha_j/\Omega_j)^{-1}$. On a longer timescale, the two species share action so that α_1 and α_2 relax to a common

value α. On an even longer timescale, the total action ceases to be a constant of the motion and α relaxes to zero.

Next, weak transport produces a low density halo of electrons moving radially outward from the pure electron plasma core, and the $m = 1$ mode begins to damp algebraically when the halo reaches the wall. The damping rate is proportional to the particle flux through the resonant layer at the wall. Chapter 3 explains analytically the new algebraic damping due to both mobility and diffusion transport. Electrons swept around the resonant "cat's eye" orbits form a dipole ($m = 1$) density distribution, setting up a field that produces $\mathbf{E} \times \mathbf{B}$-drift of the core back to the axis, that is, damps the mode.

Finally, Chapter 4 provides a simple mechanistic interpretation of the resonant wave-particle interaction of Landau. For the simple case of a Vlasov plasma oscillation, the non-resonant electrons are driven resonantly by the bare electric field from the resonant electrons, and this complex driver field is of a phase to reduce the oscillation amplitude. The wave-particle resonant interaction also occurs in 2D $\mathbf{E} \times \mathbf{B}$-drift waves, such as a diocotron wave. In this case, the bare electric field from the resonant electrons causes $\mathbf{E} \times \mathbf{B}$-drift motion back in the core plasma, thus damping the wave.

Chapter 1

General introduction

My dissertation research is documented in 5 publications[1, 2, 3, 4, 5], as listed in the reference section and publication section. In the publication section, paper 2 discusses the theory of collisional relaxation for a strongly magnetized two species pure ion plasma, reprinted in Chapter 2. Papers 3 through 5 describe the flux-driven algebraic damping of diocotron modes. This novel damping is a close cousin of, but distinct from, the Landau damping of diocotron modes. Paper 4 describes the experimental observation of the damping as well as a short theoretical explanation. This explanation is described in more detail in paper 5. The explanation has the advantage of brevity, but leaves questions unanswered and raises conceptual issues. Paper 4 resolves these issues and provides a more rigorous treatment. Chapter 3 is a reprint of paper 5. Paper 6, which is reprinted in Chapter 4, provides a new and simple physical interpretation of Landau damping generally, including traditional Landau damping as well as the new flux-driven algebraic damping of papers 3 through 5. Chapter 2, 3 and 4 are taken from papers on which I was the first author. The following sections provide overviews of the three research topics.

1.1 Collisional relaxation of a strongly magnetized two-species pure ion plasma

There is good agreement between theory and experiment for the collisional relaxation of strongly magnetized single species plasmas[6, 7, 8, 9, 10]. The relaxation is novel because the collisional dynamics is constrained by adiabatic invariants associated with the cyclotron motion. In Chapter 2 we extend the theory to the case of a two-species plasma, where the charges of the two species are the same ($e_1 = e_2$) and the masses differ only slightly (i.e., $|m_1 - m_2| \ll m_1, m_2$). We have in mind a pure ion plasma that is composed of two isotopes. Such isotopically impure ion plasmas are often used in experiments[11, 12].

In Section 2.3, we begin with an analysis of a collision between two isotopically different ions that move in the uniform magnetic field $\mathbf{B} = B\hat{z}$. For sufficiently strong magnetic field, the collision looks very different from Rutherford scattering; the two ions approach and move away from one another in tight helical orbits that follow magnetic field lines.

We will find that the sum of the cyclotron actions for the two ions, $I_1 + I_2 = m_1 v_{\perp 1}^2/(2\Omega_1) + m_2 v_{\perp 2}^2/(2\Omega_2)$, is an adiabatic invariant that is nearly conserved in the collision. Here, $m_j v_{\perp j}^2/2$ and $\Omega_j = eB/(m_j c)$ are the cyclotron kinetic energy and cyclotron frequency for the two ions ($j = 1, 2$). More specifically, the change in the total action is of order $\Delta(I_1 + I_2) \sim \exp[-\Omega_c \tau]$, where $\Omega_1 \simeq \Omega_2 \equiv \Omega_c$ and τ is a time that characterizes the duration of the collision. The time is shortest, and the change $\Delta(I_1 + I_2)$ largest, for nearly head-on collisions, where $\tau \simeq (\pi/2)(b/v_\parallel)$. Here $v_\parallel$ is the initial relative velocity of the ions parallel to the magnetic field, $b =$

$2e^2/(\mu v_\parallel^2)$ is the minimum separation between the ions allowed on energetic grounds, and $\mu \equiv m_1 m_2/(m_1 + m_2)$ is the reduced mass. This estimate of τ uses guiding center drift dynamics as a zeroth order approximation to the orbits and so assumes that the cyclotron radii for the two ions are small compared to the ion separation [i.e., $v_{\perp j}/\Omega_j \ll b$]. For sufficiently large B, the product $\Omega_c \tau = (\pi/2)(\Omega_c b/v_\parallel)$ is large compared to unity and the change $\Delta(I_1 + I_2) \sim \exp[-(\pi/2)(\Omega_c b/v_\parallel)]$ is exponentially small.

The same analysis shows that the change in the individual actions is of order $\Delta I_1 \simeq -\Delta I_2 \sim \exp[-|\Omega_1 - \Omega_2|\tau]$, which also is exponentially small if $|\Omega_1 - \Omega_2|[\pi b/(2v_\parallel)]$ is large. By assumption, the ion masses, and therefore the ion cyclotron frequencies, differ only slightly, so we have the ordering $\Omega_1, \Omega_2 \gg |\Omega_1 - \Omega_2| \gg v_\parallel/b$, which implies the conclusion

$$I_1, I_2 \gg |\Delta I_1| \simeq |\Delta I_2| \gg |\Delta(I_1 + I_2)|. \tag{1.1}$$

The individual actions are well conserved, and the sum of the two actions is conserved even better.

In Section 2.4, we determine how these adiabatic invariants constrain the collisional relaxation of a strongly magnetized plasma composed of such ions. We say that the plasma is strongly magnetized when

$$\bar{b} \gg \frac{\bar{v}_{\perp,jk}}{\Omega_j} \text{ and } |\Omega_1 - \Omega_2| \gg \frac{\bar{v}_{jk}}{\bar{b}}, \tag{1.2}$$

where $\bar{v}_{ij} = \sqrt{T_\parallel/\mu_{ij}}$ is the relative parallel thermal velocity, $\bar{b} = 2e^2/(\mu_{jk}\bar{v}_{jk}^2) = 2e^2/T_\parallel$ is the distance of closest approach, $\bar{v}_{\perp j} = \sqrt{2T_{\perp j}/m_j}$ is the perpendicular

thermal velocity for species j, and μ_{jk} is the reduced mass of two interacting particles from species j and k. As we will see, the temperatures $T_\parallel$, $T_{\perp 1}$ and $T_{\perp 2}$ need not be equal during the evolution to thermal equilibrium. The condition $\Omega_1, \Omega_2 \gg |\Omega_1 - \Omega_2|$ plus inequalities (1.2) imply that all collisions between unlike ions are in the strongly magnetized parameter regime.

Note that this definition of strong magnetization is more restrictive than that used previously for the case of single-species plasmas[8, 9]. The requirement $|\Omega_1 - \Omega_2| \gg \bar{v}_{jk}/\bar{b}$ has replaced the less restrictive requirement $\Omega_1, \Omega_2 \gg \bar{v}_{jk}/\bar{b}$.

As a first step in determining the influence of the adiabatic invariants on the evolution, we note that the difference between the cyclotron frequencies of like ions is zero, so the change in the individual actions is not exponentially small. Of course, the change in the sum of the two actions for the like ions is exponentially small.

Thus, on the timescale of a few collisions, one expects that like ions will interchange cyclotron action with each other, but not with unlike ions. On this timescale, the total cyclotron action of species 1 (i.e., $\mathcal{I}_1 = \sum_{j=1}^{N_1} I_{1j}$) and the total cyclotron action of species 2 (i.e., $\mathcal{I}_2 = \sum_{j=1}^{N_2} I_{2j}$) along with the total Hamiltonian $\mathcal{H}$ are constants of the motion, and a modified Gibbs distribution, $\exp[-\mathcal{H}/T_\parallel - \alpha_1 \mathcal{I}_1 - \alpha_2 \mathcal{I}_2]$ is established[13]. Here $T_\parallel$, α_1 and α_2 are thermodynamic variables. From the velocity dependence in $\mathcal{H}$, $\mathcal{I}_1$ and $\mathcal{I}_2$, one can see that $T_\parallel$ is the temperature that characterizes velocity components parallel to the magnetic field and that $T_{\perp 1} = [1/T_\parallel + \alpha_1/\Omega_1]^{-1}$ and $T_{\perp 2} = [1/T_\parallel + \alpha_2/\Omega_2]^{-1}$ are the temperatures that characterize the perpendicular velocity components for species 1 and 2.

Inequalities (2.2) imply that on a longer timescale particles of the two species interchange action with each other conserving the sum $\mathcal{I}_1 + \mathcal{I}_2$. On this timescale, the

variables α_1 and α_2 evolve to a common value, yielding the distribution $\exp[-\mathcal{H}/T_{\parallel} - \alpha(\mathcal{I}_1 + \mathcal{I}_2)]$, where α is that common value. On a still longer timescale, $\mathcal{I}_1 + \mathcal{I}_2$ is not conserved, and α evolves to zero, yielding the usual Gibbs distribution $\exp[-\mathcal{H}/T_{\parallel}]$.

The purpose of Chapter 2 is to calculate the rate at which α_1 and α_2 evolve to the common value α and the much slower rate at which α evolves to zero. We will find that $\alpha_1 - \alpha_2$ satisfies the equation

$$\frac{d}{dt}(\alpha_1 - \alpha_2) = -\nu_a(\alpha_1 - \alpha_2) \tag{1.3}$$

and that α satisfies the equation

$$\frac{d}{dt}\alpha = -\nu_b\alpha, \tag{1.4}$$

where ν_a is of the order $\mathcal{O}[n\bar{b}_0^2\bar{v}_{11,0}\Lambda_2(\bar{b}|\Omega_1 - \Omega_2|/\bar{v}_{12})(\bar{v}_{11}/(\bar{b}\Omega_1))^2]$ and ν_b is of the order $\mathcal{O}[n\bar{b}_0^2\bar{v}_{11,0}\Lambda_1(\bar{b}\Omega_1/\bar{v}_{11})]$, and subscript 0 refers to initial values before equilibration. $\Lambda_1(\bar{\kappa})$ and $\Lambda_2(\bar{\kappa})$ decrease exponentially with increasing $\bar{\kappa}$. In the limit of $\bar{\kappa} \gg 1$, $\Lambda_1(\bar{\kappa})$ and $\Lambda_2(\bar{\kappa})$ are approximated by the asymptotic expressions

$$\Lambda_1(\bar{\kappa}) \simeq 3.10\bar{\kappa}^{-7/15}e^{-5(3\pi\bar{\kappa})^{2/5}/6}, \tag{1.5}$$

$$\Lambda_2(\bar{\kappa}) \simeq 3.87\bar{\kappa}^{13/15}e^{-5(3\pi\bar{\kappa})^{2/5}/6}. \tag{1.6}$$

In $\Lambda_1(\bar{\kappa})$, $\bar{\kappa}$ is the magnetization $\bar{\kappa}_{ij} = \bar{b}\Omega_i/\bar{v}_{ij}$, whereas in $\Lambda_2(\bar{\kappa})$, $\bar{\kappa}$ is the magnetization difference $|\bar{\kappa}_{12} - \bar{\kappa}_{21}|$.

1.2 Theory of flux-driven algebraic damping of dio-cotron modes

1.2.1 Azimuthal mode number $m = 1$

Diocotron modes are dominant features in the low frequency dynamics of non-neutral plasmas confined in Malmberg-Penning traps[14, 15, 16, 17]. In an ideal limit, these modes involve only cross magnetic field $\mathbf{E} \times \mathbf{B}$ drift motion and are described by the drift-Poisson equations[14]. These equations are isomorphic to Euler's equations for the ideal (i.e., incompressible and inviscid) flow of a neutral fluid, and the diocotron modes are analogues of a Kelvin modes on a fluid vortex[18, 19].

There has been much previous work on diocotron mode instabilities[15, 20, 21, 22] and on diocotron mode damping[18, 19, 23, 24, 25, 26]. This paper focuses on damping.

Previously identified damping mechanisms include a spatial version of the Landau resonance[18, 23], the rotational pumping of bulk viscosity[24, 25], axial velocity dissipation on a separatrix for plasma columns with trapped and passing particles[27], and a strong damping mechanism when the radial magnetron field from end cylinders dominates over the radial space charge field[26]. The Landau mechanism fits into the ideal 2D $\mathbf{E} \times \mathbf{B}$ drift framework, but others, such as rotational pumping, involve physics beyond the ideal model.

Chapter 3 discusses a damping mechanism that is a close cousin of Landau damping, so we begin with a review of the spatial Landau resonance.

The nonneutral plasma column is immersed in a uniform axial magnetic field $B\hat{z}$, has a radial space charge electric field $E(r)\hat{r}$, and consequently undergoes an

azimuthal $\mathbf{E} \times \mathbf{B}$ drift rotation. Here, (r, θ, z) is a cylindrical coordinate system with the z-axis coincident with the axis of the trap. We consider the plasma column to be a pure electron plasma in this paper.

A diocotron mode of azimuthal mode number m can experience a resonant interaction with the rotating plasma flow at a critical plasma radius $R_{\mathrm{res}}(m)$, where $\omega_m = m\omega_E[R_{\mathrm{res}}(m)]$. Here, m is the azimuthal mode number, ω_m is the mode frequency, and $\omega_E(r) = -cE(r)/Br$ is the local rotation frequency of the plasma.

Linear mode theory[18, 19, 23] predicts that this spatial Landau resonance produces exponential mode damping when the slope of the radial density distribution is small and negative at the critical radius, and this damping has been observed experimentally for low order azimuthal modes with $m > 1$[23].

The $m = 1$ mode is special in that the resonant radius is at the wall where typically there are no particles. It was long thought that an $m = 1$ mode would not experience damping due to a Landau resonance[18].

However, recent experiments[2, i.e. paper 3 in publication list] have observed a novel algebraic damping of the $m = 1$ mode, which we believe is a close cousin of Landau damping. In these experiments, transport produces a low density halo of particles that gradually extends out from the plasma core until it reaches the wall. The algebraic damping begins when the halo reaches the resonant region (the wall for $m = 1$), and the damping rate is proportional to the flux of particles through the resonance.

Fig. (1.1), taken from Ref. 2 (paper 3 in publication list), shows the normalized amplitudes of an $m = 1$ mode versus time for several values of the transport flux. The amplitudes of an $m = 1$ mode is characterized by the displacement D (D_1 in the
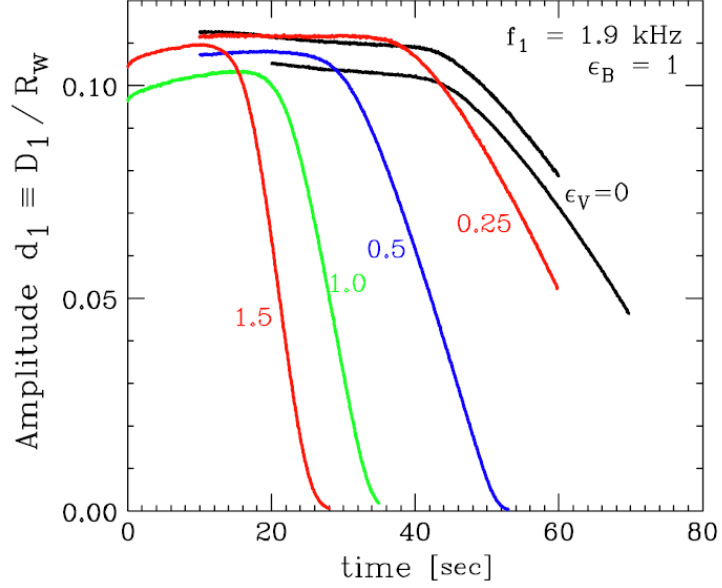
Figure 1.1: Normalized amplitude of $m = 1$ mode vs time for several values of transport flux. The flux is controlled by quadrupole wall voltage ϵ_v in Volts and magnetic field tilt angle ϵ_B in radians. This figure is taken from Ref. 2 (paper 3 in publication list).

figure) of the plasma column off the trap axis, and in Fig. (1.1), this displacement is normalized to the radius R_w of the conducting wall that bounds the confinement region. In the experiments the transport flux can be varied in a controlled way. The algebraic damping begins when the radially expanding halo reaches the wall. Fig. (1.2), also taken and edited from Ref. 2 (paper 3 in the publication list), shows that the algebraic damping rate $\gamma_1 = \dot{D}/R_w$ is proportional to the normalized rate $|\dot{N}|/N$ at which particles are lost to the wall. $|\dot{N}|$ ($|\dot{N}_L|$ in the figure) is the number of particles per unit length lost to the wall per unit time. N (N_L in the figure) is the number of core particles per unit length.

The theoretical picture that we envision for this flux driven algebraic damping is similar to, but distinct from, spatial Landau damping. In both cases, the damping results from an interaction of the mode field with resonant particles, but the particu-
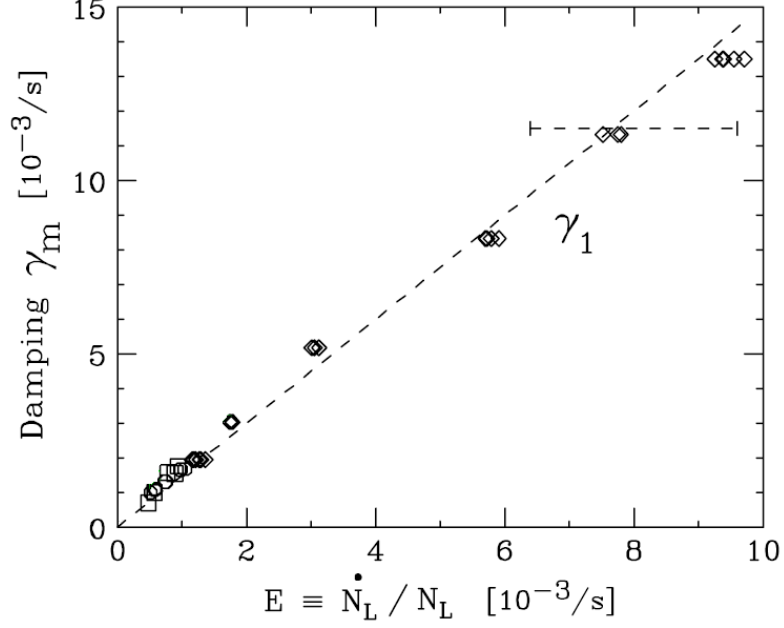
Figure 1.2: Damping rate of $m = 1$ mode vs normalized rate at which particles are lost to the wall. This figure is taken and edited from Ref. 2 (paper 3 in publication list).

lars of the interactions are very different in the two cases. In spatial Landau damping, the resonant particles are present before the mode is excited, and the damping results from a mode-driven rearrangement of particles near the resonant radius. The analysis is linear and leads to exponential damping.

In contrast, for the new flux-driven algebraic damping, there are no particles initially at the resonant radius. The transport gradually brings particles to the resonant radius, and the mode field then sweeps the particles around the nonlinear cat's eye orbits to a scrape-off layer, causing the damping.

As will be discussed later, the scrape-off layer is a thin region adjacent to the wall where guiding center drift theory breaks down and particles (electrons) are rapidly absorbed by the wall. The scrape-off layer is at least as thick as a cyclotron radius. We will assume that the thickness of the layer is much smaller than the mode

amplitude.

While the new theory can be described within a 2D flow framework, the transport and the truncation of particle orbits by the wall are non-ideal elements beyond the $\mathbf{E} \times \mathbf{B}$ drift description.

The paper that reported the experimental results on the new damping also included a short theoretical explanation[2, 3, i.e. papers 3 and 4 in publication list]. To help understand this theory consider Fig. 1.3, which shows the cross section of an electron plasma column that has been displaced off the trap axis through the excitation of an $m = 1$ diocotron mode. The displacement is of magnitude D and direction $\bar{\theta} = 0$. The gray lines are equipotential contours as seen in the mode frame. In this frame the $\mathbf{E} \times \mathbf{B}$ drift flow is along the equipotential contours. The orange shaded region represents the relatively high density plasma core. In this region, the mode potential can be described by linear theory, and the equipotential curves are simply displaced circles. The resonant region is near the wall, and there nonlinear effects distort the circles. Near the left side of the figure are the "cat's eye" orbits, which describe the motion of particles that are trapped in the wave trough. In order to make the "cat's eye" orbits easier to see in Fig. 1.3, the ratio of the displacement to the wall radius (i.e. D/R_w) was taken to be the largest of experiment values at 0.1.

In addition to the $\mathbf{E} \times \mathbf{B}$ drift flow, there is a slow transport flow. The transport produces a low density halo that gradually extends out from the plasma core. A given particle slowly spirals out, moving successively from one contour to another of larger radius.

The green dot-dashed equipotential contours in Fig. 3.1 is the critical contour

that just misses the blue dashed scrape-off layer at $\bar{\theta} = 0$. When transport moves an electron through this critical contour, the electron hits the scrape-off layer and is absorbed by the wall before returning to $\bar{\theta} = 0$. The red solid curve in Fig. 1.3 shows the trajectory of such an electron.
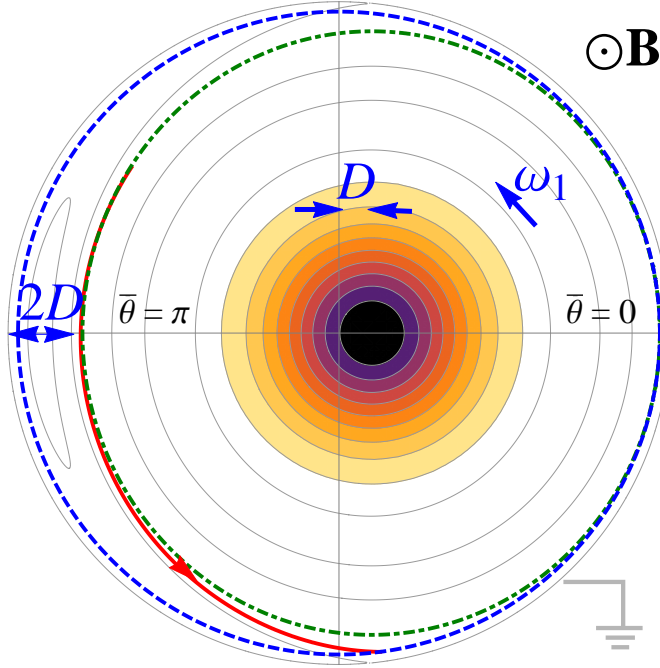
Figure 1.3: Cross section of the electron plasma column in a $m = 1$ mode. The orange shaded region is the plasma core. The gray lines are equipotential contours in the mode frame. The blue dashed curve is the scrape-off layer. The green dot-dashed curve is the critical contour. The red solid curve is a particle trajectory.

The previous theory focuses on the transfer of canonical angular momenta from the plasma core to such electrons. In the guiding center drift approximation, the canonical angular momentum for an electron in the uniform magnetic field of the trap is simply $P_\theta = eBr^2/2c$, where the radial position r is measured from the center of the trap, B is the magnetic field strength and $e = -|e|$ is the electron charge[28, 29]. When an $m = 1$ diocotron mode is excited, the plasma core is displaced off the trap

axis by a small amount D, and the core canonical angular momentum per unit length is changed by $N(eB/2c)D^2$[23]. This change in angular momentum is called the canonical angular momentum of the mode.

When an individual electron $\mathbf{E} \times \mathbf{B}$ drifts in a nearly circular orbit around the displaced center of the plasma core, the radius of the electron measured from the center of the trap oscillates by order $\Delta r \sim D \cos[\bar{\theta}(t)]$. Thus, the electron continually trades angular momentum back and forth with the core, or equivalently with mode. However, the orbit for an electron that crosses the critical contour is truncated by the wall, so there is a net change in angular momentum. Since the thickness of the "cat's eye" orbit is of order D, the net change in angular momentum is of order $\Delta P_\theta \sim (eB/2c)[R_w^2 - (R_w - D)^2] \sim (eB/c)R_w D$. More precisely, the previous derivation[2] obtained the average change in canonical angular momentum $\langle \Delta P_\theta \rangle = (2/\pi)(eB/c)R_w D$.

Balancing the rate of change of the mode angular momentum against the rate of change of halo particle angular momentum yields the equation

$$\frac{d}{dt}N\frac{eB}{2c}D^2 + \left|\frac{dN}{dt}\right|\langle\Delta P_\theta\rangle = 0. \tag{1.7}$$

Substituting for $\langle\Delta P_\theta\rangle$ yields the damping rate equation

$$\frac{dD}{dt} = -\frac{2}{\pi}\frac{1}{N}\left|\frac{dN}{dt}\right|R_w = -\gamma, \tag{1.8}$$

with a solution of linear algebraic damping $D(t) = D(0) - \gamma t$.

This simple result captures the experimental observations that the mode amplitude decays as a linear function of time and that the magnitude of the damping

rate is proportional to the flux of halo particles through the resonant layer. The predicted magnitude of the damping rate is about half the measured rate.

Although this simple derivation has the advantage of brevity, it leaves questions unanswered. For example, given that the resonant particles cause mode damping, do they also cause a mode frequency shift? Also, why focus exclusively on the thin ribbon of electrons beyond the critical contour, when there are many more resonant electrons? Is it really true that the mode transfers zero net angular angular momentum to these other resonant electrons?

A conceptual issue is the use of angular momentum balance. In fact, the total angular momentum for the plasma core and halo is not conserved. Transport continually changes the angular momentum of the halo particles as these electrons move out radially.

Also, the simple theory is implicitly based on a zero-diffusion model; the transport is assumed to be due exclusively to mobility. Unfortunately, the zero-diffusion model leads to an infinite density gradient at the leading edge of the halo, and such a gradient cannot be maintained in the presence of even a small diffusion coefficient. For the experimental conditions, diffusion affects the orbits of all the particles deemed responsible for damping in the simple theory. Indeed the whole idea of well-defined orbits looses meaning in the face of such diffusion. The orbits are diffusively broadened.

What is needed is a new, more rigorous theory based on a solution of the coupled Poisson and transport equations. Such a theory talks about an evolving density, rather the particle orbits, and makes no assumption about conservation of angular momentum.

We note at the outset, however, that despite the problems listed above, the damping rate given in Eq. (1.8) will survive in the new theory, provided that the diffusion coefficient is sufficiently small, as defined by inequalities given later. The simple theory needs a more rigorous backup, indeed is wrong in detail, but captures the essence of the physics. The new theory does predict a frequency shift

$$\Delta\omega = \frac{32}{3}\frac{ecD}{BR_w}n^{(0)}(R_1),\qquad(1.9)$$

where $n^{(0)}(R_1)$ is the unperturbed density in the resonant region of the halo.

The new theory preserves an important simplification of the traditional linear theory for an $m = 1$ diocotron mode[21]. For any unperturbed density perturbation $n^{(0)}(r)$ that is monotonically decreasing in r and goes to zero for some $r > R_w$, the mode perturbation results from a uniform displacement D of the plasma column off the trap axis. The displaced column produces an image in the conducting wall, and in the linear limit (i.e. $D/R_w \ll 1$), the electric field from the image is uniform over the whole column, producing a uniform $\mathbf{E} \times \mathbf{B}$ drift of the whole column transverse to the displacement $\mathbf{D}$. This uniform motion of the column around the trap axis is the mode.

In the traditional theory, there are no resonant particles near the wall, but the theory presented here must include such particles. Moreover, the perturbed charge density of the resonant particles produces an electric field that acts back on the plasma core, and one might worry that this field would spoil the picture of uniform core displacement. However, that is not the case.

The resonant particles are well outside the plasma core, so the field from the resonant particles is a vacuum field in the region of the core. The dipole portion of

this field is the portion that drives the mode resonantly, and a dipole vacuum field is uniform. Recall that a dipole vacuum potential can be written in the form

$$\delta\phi(r,\theta,t) = -\delta E_x(t)r\cos\bar\theta - \delta E_y(t)r\sin\bar\theta, \qquad (1.10)$$

where $\delta E_x(t)$ is the uniform field along the direction $\bar\theta = 0$ and $\delta E_y(t)$ is the uniform field along $\bar\theta = \pi/2$. We assume that the halo density is small, so the uniform field $\delta E_x(t)\hat{x} + \delta E_y\hat{y}$ is a small increment to the uniform field from the image in the wall and produces only a small increment in the uniform drift velocity of the core. Thus, the core perturbation is still a uniform displacement.

In Section 3.3, the damping rate $\dot{D}$ and the frequency shift $\Delta\omega$ are obtained as Green's function integrals over the perturbed charge density in the resonant region. To obtain these integral expressions, the perturbed charge density of the core is taken to be of the form arising from a uniform displacement.

The integral expressions can be rewritten in the form

$$\dot{D} = \frac{c}{B}\delta E_y(t),\, D\Delta\omega = -\frac{c}{B}\delta E_x(t), \qquad (1.11)$$

which yields a simple physical interpretation. The component of the uniform field from the resonant particles that is transverse to the displacement (δE_y) cause an $\mathbf{E}\times\mathbf{B}$ drift motion of the core back toward the trap axis, that is, a damping of the mode. Likewise, the component of the field along the displacement (δE_x) causes an increment to the $\mathbf{E}\times\mathbf{B}$ drift velocity around the trap axis, that is, a mode frequency shift.

A second re-writing of the integral expression for $\dot{D}$ clarifies the issue of angular

momentum conservation. The equation can be re-written as a statement that the torque exerted by the core on the resonant particles is equal and opposite to the torque exerted by the resonant particles back on the core. Two opposing torques are equal and opposite even if a third torque (say, due to the transport) acts. The treatment based on Poisson's equation correctly, and automatically, focuses on torque balance, rather than angular momentum balance.

For the conditions of the experiment, we will see that the transport caused change in angular momentum of electrons being swept to the wall is small compared to the change caused by the mode field, so the angular momentum balance is approximately correct. Nevertheless, the calculation of the damping rate should at least start from a rigorous foundation based on torque balance.

To obtain explicit expressions for the damping rate and frequency shift, the transport equation must be solved for the halo density distribution in the resonant region and the result substituted into the Green's function integrals. As a first step, the transport equation is discussed and simplified in Section 3.4.

Note that the halo evolution takes place in two stages. First the halo extends radially outward until it reaches to the wall. At the wall, the electrons are continuously absorbed, and a quasi-steady state density distribution is established. We calculate the damping rate and frequency shift for this density distribution.

Section 3.5 obtains simple analytic expressions for the density distribution, damping rate and frequency shift by using an idealized transport model: zero diffusion coefficient and constant coefficient of mobility. The $\mathbf{E} \times \mathbf{B}$ drift flow and mobility flow are then both incompressible and can be incorporated in a Hamiltonian description of the electron orbits. This idealized model implicitly underlies the simple theory[2, 3],

but leads to an infinite density gradient at the leading edge of the halo, which is untenable.

Section 3.6 includes the effect of diffusive broadening at the leading edge gradient. For the conditions of the experiments, the broadening substantially modifies the density distribution and the orbits in the region that determines the damping rate, so one might expect that the answer for the damping rate would be substantially changed. However, the Green's function integral for the damping rate can be rewritten in an approximate form that involves only the flux entering the broadening layer, and this form again yields the zero-diffusion damping rate in Eq. (3.2). The approximation requires that the diffusion coefficient be sufficiently small, as will be specified by inequalities in Section 3.6. Subject to these inequalities the frequency shift is also relatively unchanged.

Numerical solutions for the diffusively broadened density distribution are obtained in Appendix B and are used in the Green's function integral to obtain numerical results for the damping rate. The numerical results are in good agreement with the approximate analytic result of Section 3.6.

Section 3.7 obtains a perturbative correction to the damping rate to account for the slow time dependence in $D(t)$. This time dependence causes the contours themselves to move, and the corrected damping rate is proportional to the flux through the moving contour. For the conditions of the experiment the correction is small.

At the end of Chapter 3, Section 3.8 is a discussion on the general applicability of this flux-driven damping mechanism.

1.2.2 Azimuthal mode number $m = 2$

Subsequent to the experimental discovery of the damping for an $m = 1$ diocotron mode, similar damping was observed for an $m = 2$ mode[2, i.e. paper 3 in publication list]. Again, algebraic damping began when the halo particles reached the resonant layer, which for the $m = 2$ mode is well separated from the wall. The resonant radius[3, i.e. paper 4 in publication list] for an $m = 2$ mode is $R_{c2} = \sqrt{2}R_p$, where R_p is the core radius.
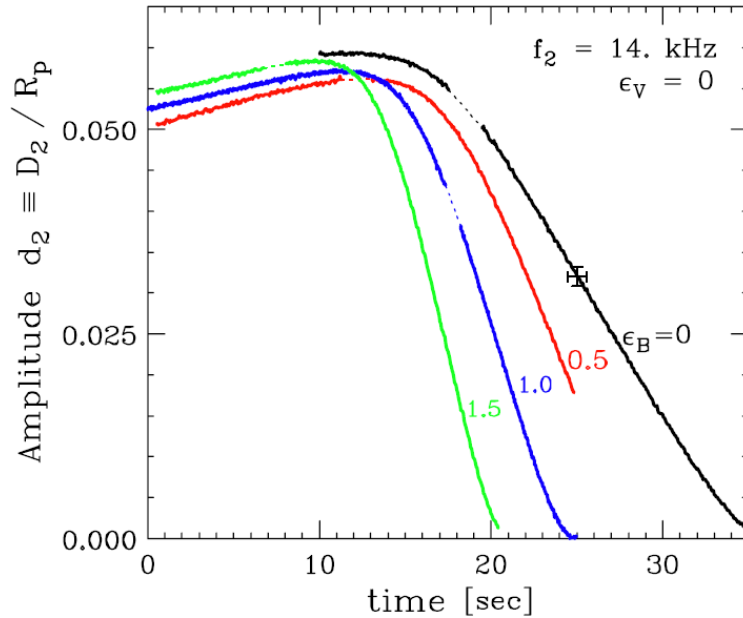
Figure 1.4: Normalized amplitude of $m = 2$ mode vs time for several values of transport flux. The flux is controlled by quadrupole wall voltage ϵ_v in Volts and magnetic field tilt angle ϵ_B in radians. This figure is taken from Ref. 2 (paper 3 in publication list).

Fig. (1.1), taken from Ref. 2 (paper 3 in publication list), shows the normalized amplitudes of an $m = 2$ mode versus time for several values of the transport flux. The amplitudes of an $m = 2$ mode is characterized by the surface ripple Δ (D_2 in the figure) of the core from the core radius R_p, and in Fig. (1.4), this surface ripple is normalized to the core radius R_p. In the experiments, the algebraic damping begins

when the radially expanding halo reaches the resonant radius R_{c2}. Fig. (1.5), using data taken from Fig. 5 of Ref. 2 (paper 3 in the publication list), shows that the algebraic damping rate $\gamma_2 = \dot{\Delta}/R_p$ is proportional to the normalized rate $|\dot{N}|/N$ at which particles are crossing the resonant radius. $|\dot{N}|$ is the number of particles per unit length crossing the resonant radius per unit time for the $m = 2$ mode.
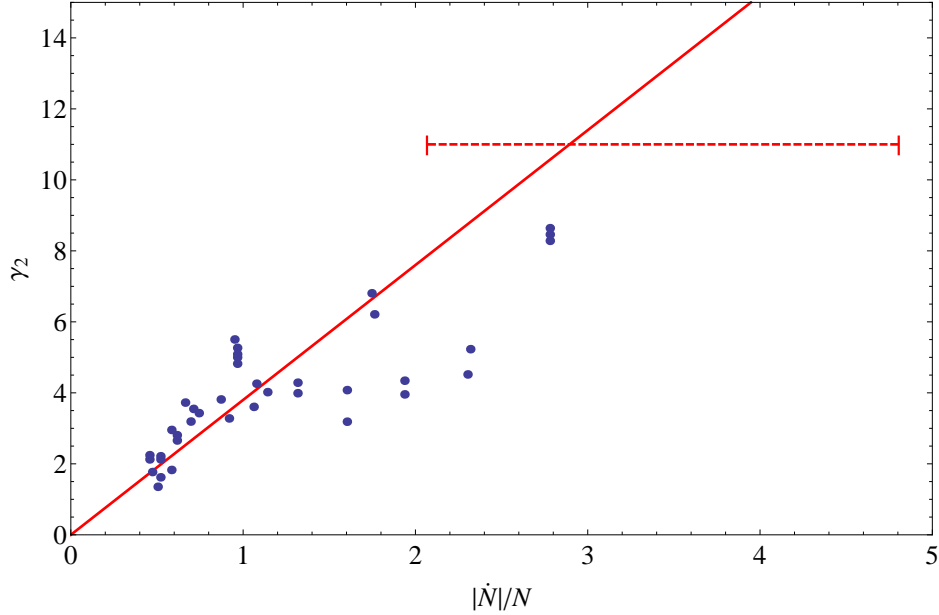
Figure 1.5: Damping rate of $m = 2$ mode vs normalized rate at which particles cross $r = R_{c2}$. The data used in this figure is taken from Fig. 5 of Ref. 2 (paper 3 in publication list).

Because the resonant layer for the $m = 2$ mode is well separated from the wall, one may ask what plays the role of the wall in truncating particle orbits? Put another way, what prevents the resonant particles from giving back angular momentum that they have received from the mode? We believe that the answer is simply passage of the particles through the "cat's-eye" orbits in the resonant layer. Because of transport, the particles cannot come back through these structures, and in the one-way passage, the particles pick up significant angular momentum from the mode, causing the damping. In principle, this mechanism also would apply for $m = 3$ and

higher, but the resonant layer is closer to and even inside the core for higher m modes, and such modes typically suffer large ordinary Landau damping.

Ref. 3 (paper 4 in the publication list) provides parallel calculations of the damping rate for both the $m = 1$ and $m = 2$ modes using the simple, but heuristic, argument of angular momentum balance in the zero-diffusion limit. A complication for the case of the $m = 2$ mode is that the slow damping of the mode is not negligible and must be included in an ad hoc manner. For the $m = 2$ mode, this calculation yields an implicit expression for the mode amplitude

$$\frac{2}{3}\left[\frac{\Delta(t)}{R_p}\right]^{3/2} + 4\frac{n^{(0)}(R_1)}{n^{(0)}(0)}\left[\frac{\Delta(t)}{R_p}\right]^{1/2} = \frac{2}{3}\left[\frac{\Delta(0)}{R_p}\right]^{3/2} + 4\frac{n^{(0)}(R_1)}{n^{(0)}(0)}\left[\frac{\Delta(0)}{R_p}\right]^{1/2} - \frac{4\sqrt{2}|\dot{N}|t}{\pi N},$$

$$(1.12)$$

where $\Delta(t)$ is the displacement of the surface ripple characterizing the mode amplitude.
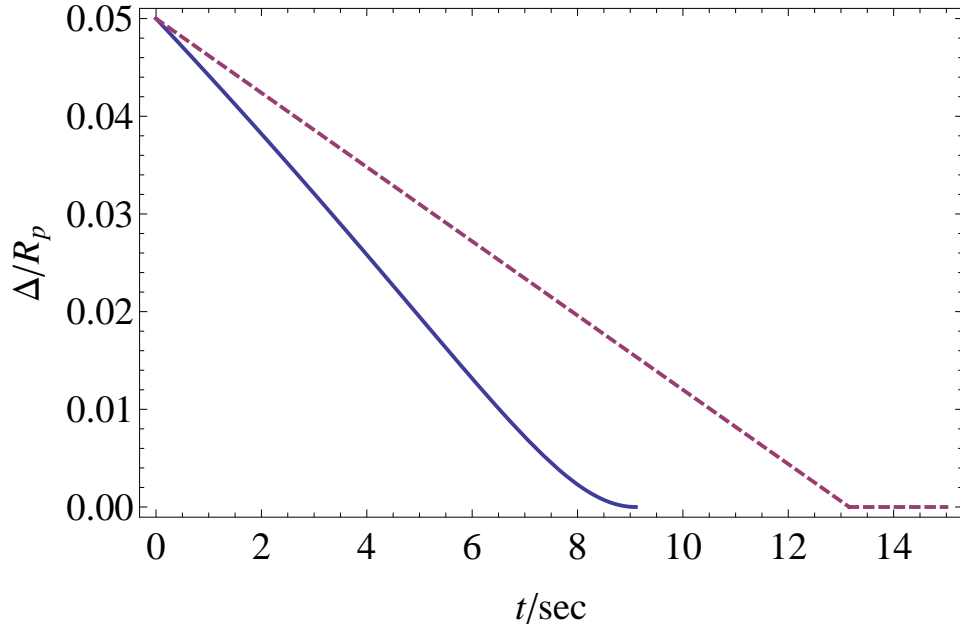
Figure 1.6: Damping curve of the $m = 2$ mode amplitude $\Delta(t)/R_p$. The solid curve is the theoretical curve following Eq. (1.12), and the dashed curve is the curve following the experimental damping rate.

Fig. (1.6) shows the time-dependence of the $m = 2$ mode amplitude $\Delta(t)/R_p$, using the values $n^{(0)}(R_1)/n^{(0)}(0) = 10^{-2}$ and $|\dot{N}|/N = 10^{-3}$. The solid curve is the theoretical curve that follows Eq. (1.12), and the dashed curve is the linear curve that follows the experimentally observed value of damping rate in Ref. 2 (paper 3 in the publication list). The figure shows that this simple theory in Eq. (1.12) gives a damping time of the same order of magnitude as, but shorter than, in the experiment.

In Chapter 3 we do not provide a more rigorous treatment of the damping of the $m = 2$ mode in parallel with the damping of the $m = 1$ mode, because there are technical differences between the $m = 1$ and $m = 2$ cases. The $m = 1$ mode admits an analytic solution for a general monotonically decreasing density profile, while the $m = 2$ mode does not. The structure of the "cat's-eye" orbits differ, since the potential goes to zero at the resonant radius for an $m = 1$ mode (i.e. at the wall), but not for the $m = 2$ mode. Also, the truncation of the orbits by the wall is different than simply passing through the "cats eye orbits. In the case of $m = 2$ mode, as the halo particles are swept and pushed to the other side of the separatrix, and continue to deviate outward from the $\mathbf{E} \times \mathbf{B}$-drift orbits, filamentation occurs and the evolution of the halo is complex. The theory for the $m = 2$ mode must wait for a later paper.

1.3 A mechanistic interpretation of the resonant wave-particle interaction

Chapter 4 provides a re-interpretation of the resonant wave-particle interaction of Landau[30]. There are two halves to this interaction: first there is the influence of

the wave on the resonant particles and second the influence of the resonant particles back on the wave. The mechanisms for the two halves of the interaction are usually described differently. For the first half, the mechanism is obvious; the wave electric field acts on the resonant particles and produces a perturbation in the resonant particle charge density. The mechanism for the second half of the interaction is usually described through Poisson's equation, or equivalently, a dispersion relation that follows from Poisson's equation; the perturbed charge density from the resonant particles makes a small correction to the dispersion relation, and this correction yields a small imaginary frequency shift, which is the damping decrement for the wave. In contrast, here we provide a mechanical interpretation of the second half of the interaction that is similar to the interpretation of the first half.

Consider the simple case of a Langmuir wave that is excited in a collisionless, Maxwellian plasma, with the wave phase velocity well out on the tail of the velocity distribution. We will see that the wave induced displacement of the non-resonant electrons, that is, the electrons in the main part of the Maxwellian, satisfies an oscillator equation that is driven by the bare electric field from the perturbed charge density of the resonant electrons. This field drives the oscillator resonantly, since the resonant electrons travel at the phase velocity of the wave. From this perspective, the wave damping simply results from the action of the driver field from the resonant electrons back on the oscillator.

The interpretation does not specify the perturbed charge density of the resonant particles, so the interpretation applies equally well to the cases of linear Landau damping and growth and to the case of a large amplitude wave with nonlinear, trapped particle orbits. In general, the portion of the drive field that is 90° out of phase with

the oscillator produces damping or growth and the portion that is in phase produces a frequency shift.

Because Landau's analysis of the damping was rather formal and did not offer a physical interpretation, other authors have provided physical interpretations[31, 32, 33, 34]. Here, we find a particularly simple interpretation by focusing on only half of the wave-particle interaction: namely, the influence of the resonant particles back on the wave.

One usually thinks of Landau resonances in connection with waves in a collisionless plasma, that is, waves that are described by Vlasov dynamics, but such resonances also occur for waves that are described by 2D $\mathbf{E} \times \mathbf{B}$ drift dynamics. A simple example is a diocotron wave that is excited on a nonneutral plasma column in a Penning-Malmberg trap[14, 15, 35, 23]. The analysis is simplest for the case where the plasma column consists of a high-density core surrounded by a relatively low-density halo. The diocotron wave can be thought of as a surface wave that propagates azimuthally around the core. At some critical radius in the halo, the azimuthal $\mathbf{E} \times \mathbf{B}$ drift rotation velocity of the halo fluid elements matches the phase velocity of the wave potential, and the resonant interaction of the wave potential and fluid elements gives rise to Landau damping.

In the standard analysis, the linearized continuity equation for the $\mathbf{E} \times \mathbf{B}$ drift flow is combined with Poisson's equation to obtain a dispersion relation. When the resonant region is in the low density halo, the perturbed charge density of the resonant electrons makes a small correction to the dispersion relation, yielding a small imaginary frequency shift, which is the wave damping decrement. To understand more clearly how the resonant particles act back on the wave, we focus on the equation of

motion for the surface ripple on the plasma core. As we will see, the bare electric field from the perturbed charge density of the resonant electrons acts back on the core, causing $\mathbf{E} \times \mathbf{B}$ drifts that reduce the amplitude of the surface ripple, that is, damp the wave. Again, we find a simple mechanistic description of the manner in which the resonant electrons act back on the wave.

Chapter 1, in parts, is taken from the papers appearing in Physics of Plasmas as C.Y. Chim, T.M. O'Neil, D.H.E. Dubin, *Physics of Plasmas* **21**, 042115 (2014), C.Y. Chim, T.M. O'Neil, *Physics of Plasmas* **23**, 072113 (2016), and C.Y. Chim, T.M. O'Neil, *Physics of Plasmas* **23**, 050801 (2016). The dissertation author was the primary investigator and author of these papers.

Chapter 2

Collisional relaxation of a strongly magnetized two-species pure ion plasma

2.1 Abstract

The collisional relaxation of a strongly magnetized pure ion plasma that is composed of two species with slightly different masses is discussed. We have in mind two isotopes of the same singly ionized atom. Parameters are assumed to be ordered as $\Omega_1, \Omega_2 \gg |\Omega_1 - \Omega_2| \gg \bar{v}_{ij}/\bar{b}$ and $\bar{v}_{\perp j}/\Omega_j \ll \bar{b}$, where Ω_1 and Ω_2 are two cyclotron frequencies, $\bar{v}_{ij} = \sqrt{T_\parallel/\mu_{ij}}$ is the relative parallel thermal velocity characterizing collisions between particles of species i and j, and $\bar{b} = 2e^2/T_\parallel$ is the classical distance of closest approach for such collisions, and $\bar{v}_{\perp j}/\Omega_j = \sqrt{2T_{\perp j}/m_j}/\Omega_j$ is the characteristic cyclotron radius for particles of species j. Here, μ_{ij} is the reduced mass for the two particles, and $T_\parallel$ and $T_{\perp j}$ are temperatures that characterize velocity components

parallel and perpendicular to the magnetic field. For this ordering, the total cyclotron action for the two species, $\mathcal{I}_1 = \sum_{i \in 1} m_1 v_{\perp i}^2/(2\Omega_1)$ and $\mathcal{I}_2 = \sum_{i \in 2} m_2 v_{\perp i}^2/(2\Omega_2)$ are adiabatic invariants that constrain the collisional dynamics. On the timescale of a few collisions, entropy is maximized subject to the constancy of the total Hamiltonian H and the two actions $\mathcal{I}_1$ and $\mathcal{I}_2$, yielding a modified Gibbs distribution of the form $\exp[-H/T_\parallel - \alpha_1 \mathcal{I}_1 - \alpha_2 \mathcal{I}_2]$. Here, the α_j's are related to $T_\parallel$ and $T_{\perp j}$ through $T_{\perp j} = (1/T_\parallel + \alpha_j/\Omega_j)^{-1}$. Collisional relaxation to the usual Gibbs distribution, $\exp[-H/T_\parallel]$, takes place on two timescales. On a timescale longer than the collisional timescale by a factor of $(\bar{b}^2 \Omega_1^2/\bar{v}_{11}^2) \exp\{5[3\pi(\bar{b}|\Omega_1 - \Omega_2|/\bar{v}_{12})]^{2/5}/6\}$, the two species share action so that α_1 and α_2 relax to a common value α. On an even longer timescale, longer than the collisional timescale by a factor of the order $\exp\{5[3\pi(\bar{b}\Omega_1/\bar{v}_{11})]^{2/5}/6\}$, the total action ceases to be a good constant of the motion and α relaxes to zero.

2.2   Introduction

There is good agreement between theory and experiment for the collisional relaxation of strongly magnetized single species plasmas[6, 7, 8, 9, 10]. The relaxation is novel because the collisional dynamics is constrained by adiabatic invariants associated with the cyclotron motion. Here we extend the theory to the case of a two-species plasma, where the charges of the two species are the same ($e_1 = e_2$) and the masses differ only slightly (i.e., $|m_1 - m_2| \ll m_1, m_2$). We have in mind a pure ion plasma that is composed of two isotopes. Such isotopically impure ion plasmas are often used in experiments[11, 12].

In Section 2.3, we begin with an analysis of a collision between two isotopically different ions that move in the uniform magnetic field $\mathbf{B} = B\hat{z}$. For sufficiently strong

magnetic field, the collision looks very different from Rutherford scattering; the two ions approach and move away from one another in tight helical orbits that follow magnetic field lines.

We will find that the sum of the cyclotron actions for the two ions, $I_1 + I_2 = m_1 v_{\perp 1}^2/(2\Omega_1) + m_2 v_{\perp 2}^2/(2\Omega_2)$, is an adiabatic invariant that is nearly conserved in the collision. Here, $m_j v_{\perp j}^2/2$ and $\Omega_j = eB/(m_j c)$ are the cyclotron kinetic energy and cyclotron frequency for the two ions ($j = 1, 2$). More specifically, the change in the total action is of order $\Delta(I_1 + I_2) \sim \exp[-\Omega_c \tau]$, where $\Omega_1 \simeq \Omega_2 \equiv \Omega_c$ and τ is a time that characterizes the duration of the collision. The time is shortest, and the change $\Delta(I_1 + I_2)$ largest, for nearly head-on collisions, where $\tau \simeq (\pi/2)(b/v_\parallel)$. Here $v_\parallel$ is the initial relative velocity of the ions parallel to the magnetic field, $b = 2e^2/(\mu v_\parallel^2)$ is the minimum separation between the ions allowed on energetic grounds, and $\mu \equiv m_1 m_2/(m_1 + m_2)$ is the reduced mass. This estimate of τ uses guiding center drift dynamics as a zeroth order approximation to the orbits and so assumes that the cyclotron radii for the two ions are small compared to the ion separation [i.e., $v_{\perp j}/\Omega_j \ll b$]. For sufficiently large B, the product $\Omega_c \tau = (\pi/2)(\Omega_c b/v_\parallel)$ is large compared to unity and the change $\Delta(I_1 + I_2) \sim \exp[-(\pi/2)(\Omega_c b/v_\parallel)]$ is exponentially small.

The same analysis shows that the change in the individual actions is of order $\Delta I_1 \simeq -\Delta I_2 \sim \exp[-|\Omega_1 - \Omega_2|\tau]$, which also is exponentially small if $|\Omega_1 - \Omega_2|[\pi b/(2v_\parallel)]$ is large. By assumption, the ion masses, and therefore the ion cyclotron frequencies, differ only slightly, so we have the ordering $\Omega_1, \Omega_2 \gg |\Omega_1 - \Omega_2| \gg v_\parallel/b$,

which implies the conclusion

$$I_1, I_2 \gg |\Delta I_1| \simeq |\Delta I_2| \gg |\Delta(I_1 + I_2)|. \tag{2.1}$$

The individual actions are well conserved, and the sum of the two actions is conserved even better.

In Section 2.4, we determine how these adiabatic invariants constrain the collisional relaxation of a strongly magnetized plasma composed of such ions. We say that the plasma is strongly magnetized when

$$\bar{b} \gg \frac{\bar{v}_{\perp,jk}}{\Omega_j} \text{ and } |\Omega_1 - \Omega_2| \gg \frac{\bar{v}_{jk}}{\bar{b}}, \tag{2.2}$$

where $\bar{v}_{ij} = \sqrt{T_\parallel/\mu_{ij}}$ is the relative parallel thermal velocity, $\bar{b} = 2e^2/(\mu_{jk}\bar{v}_{jk}^2) = 2e^2/T_\parallel$ is the distance of closest approach, $\bar{v}_{\perp j} = \sqrt{2T_{\perp j}/m_j}$ is the perpendicular thermal velocity for species j, and μ_{jk} is the reduced mass of two interacting particles from species j and k. As we will see, the temperatures $T_\parallel$, $T_{\perp 1}$ and $T_{\perp 2}$ need not be equal during the evolution to thermal equilibrium. The condition $\Omega_1, \Omega_2 \gg |\Omega_1 - \Omega_2|$ plus inequalities (2.2) imply that all collisions between unlike ions are in the strongly magnetized parameter regime.

Note that this definition of strong magnetization is more restrictive than that used previously for the case of single-species plasmas[8, 9]. The requirement $|\Omega_1 - \Omega_2| \gg \bar{v}_{jk}/\bar{b}$ has replaced the less restrictive requirement $\Omega_1, \Omega_2 \gg \bar{v}_{jk}/\bar{b}$.

As a first step in determining the influence of the adiabatic invariants on the evolution, we note that the difference between the cyclotron frequencies of like ions is zero, so the change in the individual actions is not exponentially small. Of course,

the change in the sum of the two actions for the like ions is exponentially small.

Thus, on the timescale of a few collisions, one expects that like ions will interchange cyclotron action with each other, but not with unlike ions. On this timescale, the total cyclotron action of species 1 (i.e., $\mathcal{I}_1 = \sum_{j=1}^{N_1} I_{1j}$) and the total cyclotron action of species 2 (i.e., $\mathcal{I}_2 = \sum_{j=1}^{N_2} I_{2j}$) along with the total Hamiltonian $\mathcal{H}$ are constants of the motion, and a modified Gibbs distribution, $\exp[-\mathcal{H}/T_\parallel - \alpha_1\mathcal{I}_1 - \alpha_2\mathcal{I}_2]$ is established[13]. Here $T_\parallel$, α_1 and α_2 are thermodynamic variables. From the velocity dependence in $\mathcal{H}$, $\mathcal{I}_1$ and $\mathcal{I}_2$, one can see that $T_\parallel$ is the temperature that characterizes velocity components parallel to the magnetic field and that $T_{\perp 1} = [1/T_\parallel + \alpha_1/\Omega_1]^{-1}$ and $T_{\perp 2} = [1/T_\parallel + \alpha_2/\Omega_2]^{-1}$ are the temperatures that characterize the perpendicular velocity components for species 1 and 2.

Inequalities (2.2) imply that on a longer timescale particles of the two species interchange action with each other conserving the sum $\mathcal{I}_1 + \mathcal{I}_2$. On this timescale, the variables α_1 and α_2 evolve to a common value, yielding the distribution $\exp[-\mathcal{H}/T_\parallel - \alpha(\mathcal{I}_1 + \mathcal{I}_2)]$, where α is that common value. On a still longer timescale, $\mathcal{I}_1 + \mathcal{I}_2$ is not conserved, and α evolves to zero, yielding the usual Gibbs distribution $\exp[-\mathcal{H}/T_\parallel]$.

The purpose of this chapter is to calculate the rate at which α_1 and α_2 evolve to the common value α and the much slower rate at which α evolves to zero. We will find that $\alpha_1 - \alpha_2$ satisfies the equation

$$\frac{d}{dt}(\alpha_1 - \alpha_2) = -\nu_a(\alpha_1 - \alpha_2) \tag{2.3}$$

and that α satisfies the equation

$$\frac{d}{dt}\alpha = -\nu_b\alpha, \tag{2.4}$$

where ν_a is of the order $\mathcal{O}[n\bar{b}_0^2\bar{v}_{11,0}\Lambda_2(\bar{b}|\Omega_1-\Omega_2|/\bar{v}_{12})(\bar{v}_{11}/(\bar{b}\Omega_1))^2]$ and ν_b is of the order $\mathcal{O}[n\bar{b}_0^2\bar{v}_{11,0}\Lambda_1(\bar{b}\Omega_1/\bar{v}_{11})]$, and subscript 0 refers to initial values before equilibration. $\Lambda_1(\bar{\kappa})$ and $\Lambda_2(\bar{\kappa})$ decrease exponentially with increasing $\bar{\kappa}$. In the limit of $\bar{\kappa} \gg 1$, $\Lambda_1(\bar{\kappa})$ and $\Lambda_2(\bar{\kappa})$ are approximated by the asymptotic expressions

$$\Lambda_1(\bar{\kappa}) \simeq 3.10\bar{\kappa}^{-7/15}e^{-5(3\pi\bar{\kappa})^{2/5}/6}, \tag{2.5}$$

$$\Lambda_2(\bar{\kappa}) \simeq 3.87\bar{\kappa}^{13/15}e^{-5(3\pi\bar{\kappa})^{2/5}/6}. \tag{2.6}$$

In $\Lambda_1(\bar{\kappa})$, $\bar{\kappa}$ is the magnetization $\bar{\kappa}_{ij} = \bar{b}\Omega_i/\bar{v}_{ij}$, whereas in $\Lambda_2(\bar{\kappa})$, $\bar{\kappa}$ is the magnetization difference $|\bar{\kappa}_{12} - \bar{\kappa}_{21}|$, when Λ_1 and Λ_2 are used to describe the equipartition rates.

2.3 Two-particle collision

In this section, we consider the isolated collision of two ions that have equal charges ($e_1 = e_2 \equiv e$), slightly different masses ($|m_1 - m_2| \ll m_1, m_2$), and move in the uniform magnetic field $\mathbf{B} = B\hat{z}$. The Hamiltonian for the two interacting charges can be written as

$$H = \sum_{k=1}^{2}[\frac{p_{zk}^2}{2m_k} + \frac{p_{xk}^2}{2m_k} + \frac{(p_{yk} - eBx/c)^2}{2m_k}] + \frac{e^2}{[(x_1 - x_2)^2 + (y_1 - y_2)^2 + (z_1 - z_2)^2]^{1/2}}, \tag{2.7}$$

where we have used the vector potential $\mathbf{A} = Bx\hat{y}$, and the quantities (x_k, p_{xk}), (y_k, p_{yk}), (z_k, p_{zk}) are canonically conjugate coordinates and momenta[36].

We assume that the magnetic field strength and initial velocities satisfy the conditions for strong magnetization as defined in Section I (i.e., $v_{\perp j}/\Omega_j \ll b$ and

$|\Omega_1 - \Omega_2| \gg v_{\parallel}/b)$. In this limit, the following transformation[37] is useful:

$$Y_k = y_k - \frac{c}{eB}p_{xk}, \tag{2.8}$$

$$X_k = \frac{c}{eB}p_{yk}, \tag{2.9}$$

$$\psi_k = -\tan^{-1}(\frac{y_k - Y_k}{x_k - X_k}), \tag{2.10}$$

$$I_k = \frac{p_{xk}^2 + (p_{yk} - eBx_k/c)^2}{2m_k\Omega_k}. \tag{2.11}$$

One can check that (z_k, p_{zk}), $(Y_k, P_{Y_k} \equiv \frac{eB}{c}X_k)$ and (ψ_k, I_k) satisfy the usual Poisson brackets required of canonically conjugate coordinates and momenta, i.e. $\{q_i, p_j\} = \delta_{ij}$. Here (X_k, Y_k) are the coordinates of the guiding center for the k-th particle, and (ψ_k, I_k) are the gyro-angle and cyclotron action for the k-th particle. In terms of these new canonical variables, the Hamiltonian takes the form

$$H = \sum_{k=1}^{2}(\frac{p_{zk}^2}{2m_k} + \Omega_k I_k) + \frac{e^2}{|\mathbf{r}_1 - \mathbf{r}_2|}, \tag{2.12}$$

where

$$|\mathbf{r}_1 - \mathbf{r}_2|^2 = (z_1 - z_2)^2 + (X_1 + \rho_1 \cos\psi_1 - X_2 - \rho_2 \cos\psi_2)^2$$

$$+(Y_1 - \rho_1 \sin\psi_1 - Y_2 + \rho_2 \sin\psi_2)^2. \tag{2.13}$$

Here $\rho_k = \sqrt{2I_k/(m_k\Omega_k)}$ is the cyclotron radius of the k-th particle.

Since $|\mathbf{r}_1 - \mathbf{r}_2|$ is periodic in ψ_1 and ψ_2, the Hamiltonian can be written in the form

$$H = \sum_{k=1}^{2}(\frac{p_{zk}^2}{2m_k} + \Omega_k I_k) + \sum_{\mu,\nu} g_{\mu\nu}e^{i(\mu\psi_1 + \nu\psi_2)}, \tag{2.14}$$

where $g_{\mu\nu} = g_{\mu\nu}(I_1, I_2, z_1 - z_2, X_1 - X_2, Y_1 - Y_2)$, and μ and ν run over all integer values from $-\infty$ to $+\infty$.

We will find it instructive to calculate the change over the course of the collision in the sum and difference of the cyclotron actions, $\Delta(I_1 + I_2)$ and $\Delta(I_1 - I_2)$. Hamilton's equations yield the time derivatives

$$\frac{d}{dt}(I_1 + I_2) = -(\frac{\partial}{\partial\psi_1} + \frac{\partial}{\partial\psi_2})H = -\sum_{\mu\nu} i(\mu + \nu)g_{\mu\nu}e^{i(\mu\psi_1 + \nu\psi_2)} \tag{2.15}$$

and

$$\frac{d}{dt}(I_1 - I_2) = -(\frac{\partial}{\partial\psi_1} - \frac{\partial}{\partial\psi_2})H = -\sum_{\mu\nu} i(\mu - \nu)g_{\mu\nu}e^{i(\mu\psi_1 + \nu\psi_2)} \tag{2.16}$$

For strong magnetization, one expects guiding center drift theory to provide a good zeroth order approximation to the particle orbits. Moreover, the guiding center variables are slowly varying in time compared to the rapidly varying gyro-angles ψ_1 and ψ_2. In this approximation, the arguments of $g_{\mu\nu} = g_{\mu\nu}(I_1, I_2, z_1 - z_2, X_1 - X_2, Y_1 - Y_2)$ are slowly varying and the exponentials $e^{i(\mu\psi_1 + \nu\psi_2)}$ are rapidly oscillating, and the time integral of such a product phase mixes to a small value. We will find that the value is exponentially small in the ratio of the rapid to the slow timescales.

At this point, we can anticipate the main result of the calculation. The smallest frequency for the exponentials is $|\Omega_1 - \Omega_2|$, corresponding to the choice $\mu = -\nu = \pm 1$. Since the coefficient for this term vanishes identically in Eq. (2.15) but not in Eq. (2.16), the change $|\Delta(I_1 + I_2)|$ is much smaller than the change $|\Delta(I_1 - I_2)|$. Equivalently, one may say that the total action is conserved to much better accuracy than either of the two actions independently, i.e. $|\Delta(I_1 + I_2)| \ll |\Delta I_1|, |\Delta I_2|$.

The guiding center Hamiltonian[38, 39] is obtained simply by setting $\rho_1 =$

$\rho_2 = 0$ in Eq. (2.13), yielding

$$H_{\mathrm{GC}} = \sum_{k=1}^{2} (\frac{p_{zk}^2}{2m_k} + \Omega_k I_k) + \frac{e^2}{[(z_1 - z_2)^2 + (X_1 - X_2)^2 + (Y_1 - Y_2)^2]^{1/2}}, \qquad (2.17)$$

where $P_{Y_k} = \frac{c}{eB}X_k$. Making the canonical transformation to center-of-mass and relative coordinates

$$
\begin{aligned}
z &= z_1 - z_2, & (2.18)\\
Z &= \frac{m_1 z_1 + m_2 z_2}{m_1 + m_2}, & (2.19)\\
p_z &= \frac{m_2 p_{z1} - m_1 p_{z2}}{m_1 + m_2}, & (2.20)\\
P_Z &= p_{z1} + p_{z2} & (2.21)
\end{aligned}
$$

yields the Hamiltonian

$$H_{\mathrm{GC}} = \frac{P_Z^2}{2M} + \frac{p_z^2}{2\mu} + I_1\Omega_1 + I_2\Omega_2 + \frac{e^2}{[(z_1 - z_2)^2 + (X_1 - X_2)^2 + (Y_1 - Y_2)^2]^{1/2}}, \quad (2.22)$$

where $M = m_1 + m_2$ and $\mu = m_1 m_2/(m_1 + m_2)$.

Thus, with guiding center dynamics, the quantities H_{GC}, P_Z, I_1, I_2, and $(X_1 - X_2)^2 + (Y_1 - Y_2)^2 \equiv |\Delta \mathbf{R}_\perp|^2$ are constants of the motion, and the relative coordinate $z(t)$ is governed by the equation

$$\frac{\mu \dot{z}^2(t)}{2} + \frac{e^2}{(|\Delta \mathbf{R}_\perp|^2 + z^2(t))^{1/2}} = \frac{\mu v_\parallel^2}{2}, \qquad (2.23)$$

where $v_\parallel \equiv \dot{z}(t = -\infty)$ is the initial relative velocity. From this equation, one sees that the minimum allowed separation between the guiding centers is given by

$b = \sqrt{|\Delta\mathbf{R}_\perp|^2 + z^2}|_{\min} = 2e^2/(\mu v_\parallel^2)$. We choose $t = 0$ so that $z^2(t)$ is an even function of t. For the case where $|\Delta\mathbf{R}_\perp| < b$, there is no reflection and we choose $z(0) = 0$, and for the case where $|\Delta\mathbf{R}_\perp| > b$, we choose $t = 0$ to be at the point of reflection, that is, $z^2(0) = b^2 - (\Delta\mathbf{R}_\perp^2)$.

In the guiding center drift approximation, the most rapidly varying variable in the argument of $g_{\mu\nu}(I_1, I_2, z_1 - z_2, X_1 - X_2, Y_1 - Y_2)$ is the relative coordinate $z(t) = z_1(t) - z_2(t)$, and the timescale associated with this variation is of order $b/v_\parallel$ or larger. By comparison, the timescale for the oscillatory variation of the exponential $\exp(i\mu\psi_1 + i\nu\psi_2)$ is $|\mu\Omega_1 + \nu\Omega_2|^{-1} < |\Omega_1 - \Omega_2|^{-1}$. Thus, the strong magnetization ordering $v_\parallel/b \ll |\Omega_1 - \Omega_2| \ll \Omega_1, \Omega_2$ is simply a statement of the needed separation of timescales.

We Taylor expand $g_{\mu\nu}$ in powers of $\rho_k/\sqrt{|\Delta\mathbf{R}_\perp|^2 + z^2} \leq \rho_k/b \ll 1$. As one would expect, each term in the expansion of $g_{\mu\nu}$ is of order $(\rho/b)^{|\mu|+|\nu|}$, and for simplicity we retain only the lowest order term. An equivalent way to do so is to expand H in powers of ρ_k and collect terms of the right Fourier dependence $\exp(i\mu\psi_1 + i\nu\psi_2)$, so as to obtain the Taylor-approximated $g_{\mu\nu}$. Expressions of $g_{\mu\nu}$ that are used in the calculation are the following:

$$g_{10} = -\frac{e^{i(\Omega_1 t + \phi_1)}}{2}\frac{e^2 v_{\perp 1}/\Omega_1}{|\Delta\mathbf{R}_\perp|^2 + z^2} = g^*_{-1,0}, \tag{2.24}$$

$$g_{01} = \frac{e^{i(\Omega_2 t + \phi_2)}}{2}\frac{e^2 v_{\perp 2}/\Omega_2}{|\Delta\mathbf{R}_\perp|^2 + z^2} = g^*_{0,-1}, \tag{2.25}$$

$$g_{1,-1} = -\frac{e^{i(\Omega_1 - \Omega_2)t + i(\phi_1 - \phi_2)}}{2}\frac{e^2}{(|\Delta\mathbf{R}|^2 + z^2)^{3/2}}\left(1 - \frac{3|\Delta\mathbf{R}_\perp|^2}{2(|\Delta\mathbf{R}_\perp|^2 + z^2)}\right)\frac{v_{\perp 1}v_{\perp 2}}{\Omega_1\Omega_2} = g^*_{-1,1}, \tag{2.26}$$

where $v_{\perp k} = \rho_k\Omega_k$ is the cyclotron velocity, $\phi_k = \psi_k(t = 0)$ is the gyroangle at $t = 0$,

and as mentioned earlier we choose $t = 0$ so that $z^2(t)$ is an even function of time. Also we note that $|g_{10}|$ and $|g_{01}|$ are of the order $\rho_k \propto \Omega_k^{-1} \propto B^{-1}$, but $|g_{1,-1}|$ is of the order $\rho_k^2 \propto \Omega_k^{-2} \propto B^{-2}$.

Since the time integrals $\int_{-\infty}^{\infty} dt g_{\mu\nu} \exp(i\mu\psi_1 + i\nu\psi_2)$ turn out to be exponentially small in the ratio of the slow to rapid timescales we need only to retain the lowest frequency terms in the sum over μ and ν. Specifically, we retain the terms with frequencies $|\Omega_1 - \Omega_2|$, Ω_1, and Ω_2, using Eqns. (2.24) to (2.26) to obtain the results

$$
\begin{aligned}
&\Delta(I_1 - I_2) \\
= \ &-\int_{-\infty}^{\infty} e^2 \frac{v_{\perp 2}}{\Omega_2} \sin\phi_2 \frac{|\Delta\mathbf{R}_\perp|}{(|\Delta\mathbf{R}_\perp|^2 + z^2)^{3/2}} \cos(\Omega_2 t) dt \\
&-\int_{-\infty}^{\infty} e^2 \frac{v_{\perp 1}}{\Omega_1} \sin\phi_1 \frac{|\Delta\mathbf{R}_\perp|}{(|\Delta\mathbf{R}_\perp|^2 + z^2)^{3/2}} \cos(\Omega_1 t) dt \\
&+\int_{-\infty}^{\infty} \frac{e^2 v_{\perp 1} v_{\perp 2}}{(|\Delta\mathbf{R}_\perp|^2 + z^2)^{3/2}} \frac{2}{\Omega_1 \Omega_2} \cos[(\Omega_1 - \Omega_2)t] \\
&\cdot \sin(\phi_1 - \phi_2)(1 - \frac{3|\Delta\mathbf{R}_\perp|^2}{2(|\Delta\mathbf{R}_\perp|^2 + z^2)}) dt, \quad (2.27)
\end{aligned}
$$

and

$$
\begin{aligned}
&\Delta(I_1 + I_2) \\
= \ &\int_{-\infty}^{\infty} e^2 \frac{v_{\perp 2}}{\Omega_2} \sin\phi_2 \frac{|\Delta\mathbf{R}_\perp|}{(|\Delta\mathbf{R}_\perp|^2 + z^2)^{3/2}} \cos(\Omega_2 t) dt \\
&-\int_{-\infty}^{\infty} e^2 \frac{v_{\perp 1}}{\Omega_1} \sin\phi_1 \frac{|\Delta\mathbf{R}_\perp|}{(|\Delta\mathbf{R}_\perp|^2 + z^2)^{3/2}} \cos(\Omega_1 t) dt. \quad (2.28)
\end{aligned}
$$

The integrals carrying $\cos(\Omega_i t)$ are proportional to

$$
f_1(\kappa_i, \eta) = \int_{-\infty}^{\infty} \frac{d\xi \cos(\kappa_i \xi)}{(\eta^2 + \zeta^2(\xi))^{3/2}}, \quad (2.29)
$$

while the integral carrying $\cos[(\Omega_1 - \Omega_2)t]$ is proportional to

$$f_2(\kappa_1 - \kappa_2, \eta) = \int_{-\infty}^{\infty} \frac{d\xi \cos[(\kappa_1 - \kappa_2)\xi]}{(\eta^2 + \zeta^2(\xi))^{3/2}}(1 - \frac{3\eta^2}{2[\eta^2 + \zeta^2(\xi)]}),$$ (2.30)

where $\xi = v_{\parallel}t/b$, $\kappa_i = b\Omega_i/v_{\parallel}$, $\eta = |\Delta \mathbf{R}_{\perp}|/b$ and $\zeta = z/b$. In terms of these variables, differential equation (2.23) takes the form

$$(\frac{d\zeta}{d\xi})^2 + \frac{1}{\sqrt{\eta^2 + \zeta^2(\xi)}} = 1,$$ (2.31)

where $\zeta^2(0) = \max(0, 1 - \eta^2)$. In the next section, we will need the results

$$\Delta(I_1 + I_2) = -\frac{e^2}{b\Omega_1}(\frac{v_{\perp 1}}{v_{\parallel}} \sin \phi_1)\eta f_1(\kappa_1, \eta) + \frac{e^2}{b\Omega_2}(\frac{v_{\perp 2}}{v_{\parallel}} \sin \phi_2)\eta f_1(\kappa_2, \eta),$$ (2.32)

$$\Delta I_1 = -\frac{e^2}{b\Omega_1}(\frac{v_{\perp 1}}{v_{\parallel}} \sin \phi_1)\eta f_1(\kappa_1, \eta)$$

$$+ \frac{e^2}{b\Omega_1\Omega_2}\frac{v_{\perp 1}v_{\perp 2}}{v_{\parallel}b}f_2(\kappa_1 - \kappa_2, \eta) \sin(\phi_1 - \phi_2),$$ (2.33)

$$\Delta I_2 = \frac{e^2}{b\Omega_2}(\frac{v_{\perp 2}}{v_{\parallel}} \sin \phi_2)\eta f_1(\kappa_2, \eta) + \frac{e^2}{b\Omega_1\Omega_2}\frac{v_{\perp 1}v_{\perp 2}}{v_{\parallel}b}f_2(\kappa_1 - \kappa_2, \eta) \sin(\phi_2 - \phi_1).$$

(2.34)

In the regime of strong magnetization (i.e., $1 \ll |\kappa_1 - \kappa_2| \ll \kappa_1, \kappa_2$), the integrals f_1 and f_2 are exponentially small, since the integrands are the product of a rapidly oscillating cosine and a slowly varying function. The rapid oscillation makes a direct evaluation of such integrals difficult.

In Appendix A, we analytically continue the integrals into the complex ξ-plane, making the exponentially small value of the integrals manifest in the integrands themselves. This facilitates numerical evaluation of the integrals and yields the asymptotic

forms

$$f_1(\kappa_j, \eta) \;=\; h_1(\kappa_j, \eta)\exp[-g(\eta)\kappa_j], \qquad (2.35)$$

$$f_2(|\kappa_1 - \kappa_2|, \eta) \;=\; h_2(|\kappa_1 - \kappa_2|, \eta)\exp[-g(\eta)|\kappa_1 - \kappa_2|], \qquad (2.36)$$

where

$$g(\eta) = \left|\int_1^\eta \frac{x^{3/2}dx}{\sqrt{(x-1)(\eta^2 - x^2)}}\right| \qquad (2.37)$$

is shown in Fig. (2.1). From the numerical evaluations one can see that the quantities $h_j(\kappa, \eta)$ are neither exponentially small nor large. Also for $\eta = 0$, one can show that $h_j(\kappa, 0) = h_2(\kappa, 0) \simeq 8\pi\kappa/9$. In the next section, we will need the asymptotic forms only for small η. Fig. (2.2) shows a comparison of the numerical solution for $f_1(\kappa, 0) = f_2(\kappa, 0) \equiv f(\kappa)$ (solid curve) with the asymptotic solution (dashed curve).
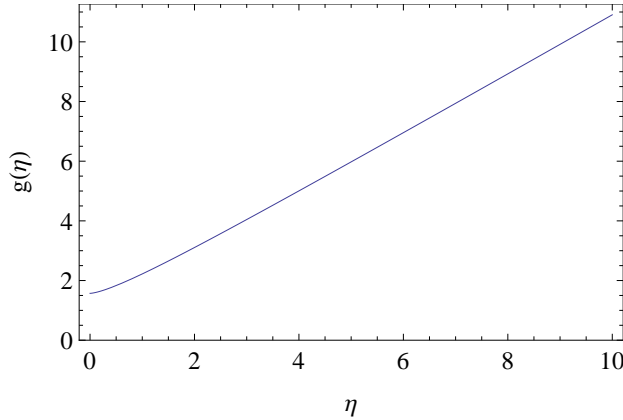
Figure 2.1: Graph of $g(\eta)$.

As expected, the asymptotic forms are exponentially small in the ratio of the slow to fast timescales. For example, for f_1 the fast timescale is $\tau_f = \Omega_j^{-1}$ and the slow timescale is $\tau_s \simeq (\pi/2)(b/v_\parallel)$ for $\eta = |\mathbf{R}_\perp|/b < 1$ and $\tau_s \simeq |\mathbf{R}_\perp|/v_\parallel$ for $\eta > 1$. Note from Fig. (2.1) that $g(0) = \pi/2$ and that $g(\eta) \approx \eta$ for $\eta \gg 1$. For f_2, the only
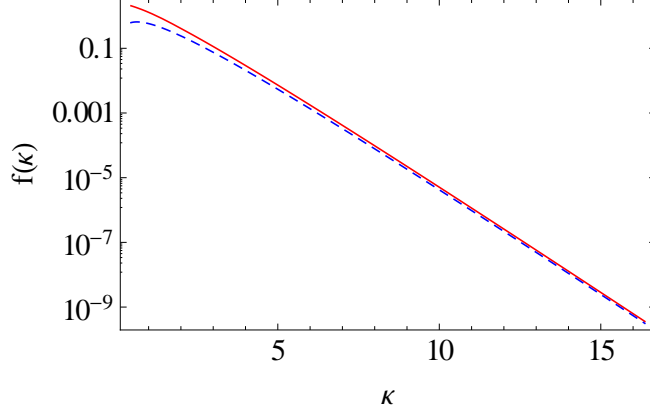
Figure 2.2: Values of $f(\kappa)$. Solid line: numerical integration of $f(\kappa)$. Dashed line: asymptotic expression for large κ.

difference is that the fast timescale is $|\Omega_1 - \Omega_2|^{-1}$.

For strong magnetization (i.e., $1 \ll |\kappa_1 - \kappa_2| \ll \kappa_1, \kappa_2$), the asymptotic forms verify the expected ordering for the changes in the actions (i.e., $|\Delta(I_1 + I_2)| \ll |\Delta I_1|, |\Delta I_2| \ll 1$).

As a check on the accuracy of Eqs. (2.32), (2.33) and (2.34), we compare the predictions for $\Delta(I_1 - I_2)$ and $\Delta(I_1 + I_2)$ with results obtained by direction numerical integrations of the equations of motion for some sample collisions. For these comparisons, we choose $m_2 = m_1 + 0.1m_1$ and $v_{\perp 1} = v_{\perp 2} = 0.01v_{\parallel}$. The two particles are initially separated by the distance $d = 100b$ and given the initial relative velocity $v_z = v_{\parallel}\sqrt{1 - b/\sqrt{|\Delta\mathbf{R}|^2 + d^2}}$. The collision ends when the particles are again separated in the z-direction by the distance d. The motion is followed with a sixth-order Runge-Kutta algorithm[40], using a timestep that is sufficiently small for the error in the total energy to be small compared to the change $\Delta(E_{\perp 1} + E_{\perp 2})$. The phase angles ϕ_j are varied to obtain the peak-to-peak variation in $\Delta(I_1 - I_2)$ and $\Delta(I_1 + I_2)$. The solid curves in Figs. (2.3) and (2.4) are the predictions of Eqs. (2.32), (2.33) and (2.34), with numerical evaluation of integrals (2.29) and (2.30), for

the scaled changes $\Delta(I_1 - I_2)/(m_1 v_{\perp 1}^2/\Omega_1)$ and $\Delta(I_1 + I_2)/(m_1 v_{\perp 1}^2/\Omega_1)$, respectively. The points result from integrating the particle equations of motion. For the collisions in these figures, η is near zero, and κ_2 is varied over a range of values. Of course, $\kappa_1 = 1.1\kappa_2$ and $|\kappa_2 - \kappa_1| = 0.1\kappa_2$. In Fig. (2.5), κ_1 is fixed at the value 21.0, and η is varied. We can see from the figures that our theory matches with the simulation results as long as magnetization is strong, i.e. $\kappa_1 \gg 1$. Particularly from Fig. (2.4), it is evident that the theory breaks down when κ_1 goes lower than around 2.
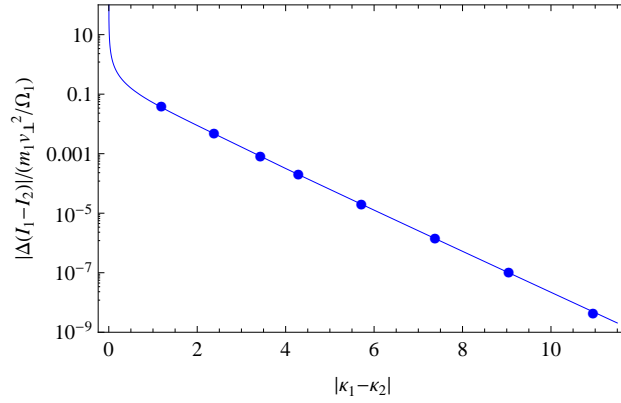
Figure 2.3: Change in cyclotron action difference vs $|\kappa_1 - \kappa_2| = \kappa_1/11$. Here $v_{\perp 1} = v_{\perp 2} = 0.5 v_\parallel$ and $m_2 = 1.1 m_1$.
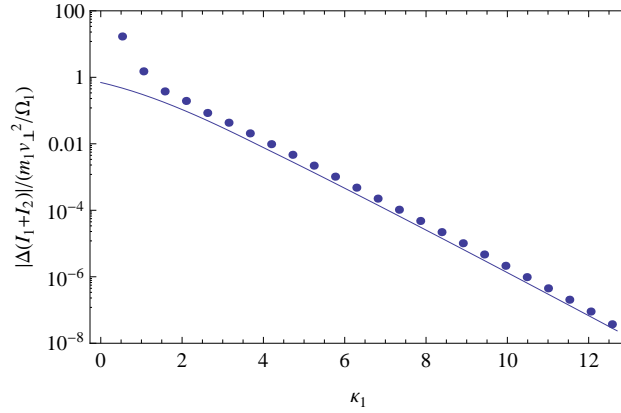
Figure 2.4: Change in cyclotron action sum vs magnetization κ_1. Dots: simulation results. Line: values using numerical integration of $f_1(\kappa_1, \eta = 0)$.
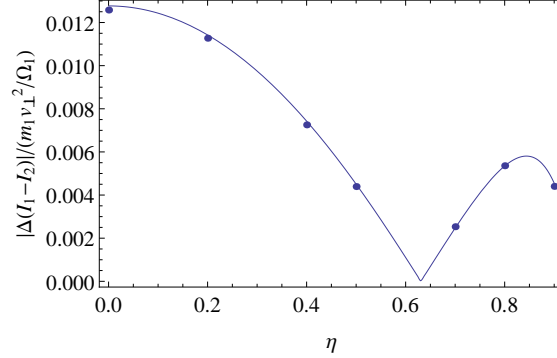
Figure 2.5: Change in cyclotron action difference vs rescaled transverse separation η, for $\kappa_1 = 21$ and $|\kappa_1 - \kappa_2| = 1.9$. Dots: simulation results. Line: values using exact numerical integration of $f_2(|\kappa_1 - \kappa_2|, \eta)$.

2.4   Collisional evolution of a plasma

This section discusses the collisional evolution of a two species, strongly magnetized, pure ion plasma. Species 1 consists of N_1 singly ionized atoms of mass m_1 and species 2 of N_2 singly ionized atoms of mass m_2, where $|m_1 - m_2| \ll m_1, m_2$. For simplicity, the plasma is assumed to be uniform and immersed in a continuous neutralizing background charge. A laboratory realization of such a plasma is a thermal equilibrium, pure ion plasma that is confined in a Malmberg-Penning trap. Plasma rotation in the uniform axial magnetic field of the trap is equivalent to neutralization by a continuous background charge.

The plasma is assumed to be in the weakly correlated parameter regime, $e^2 n^{1/3}/T_\parallel \ll 1$, where n is the density[41, 42]. The inequality can be written as $\bar{b} \ll n^{-1/3}$, so close collisions, which are primarily responsible for changes in the cyclotron actions, are well separated binary interactions of the kind considered in the previous section. Furthermore, the plasma is assumed to satisfy the strong magnetization ordering in Eq. (2.2), so all collisions between unlike ions are of the kind considered in the previous section.

To understand the final assumption, first recall from Eqs. (2.32)-(2.34) of the previous section that the change in actions during a collision depends sinusoidally on the initial gyroangles $\phi_{kj} = \phi_{kj}(t = 0)$. The time between close collisions is much larger than a cyclotron period, so we assume that the particles enter each collision with random gyroangles.

Thus, the N-particle dynamics consists of many statistically independent, binary interactions of the kind considered in the previous section. In this section, we simply establish a statistical framework to understand the cumulative effect of these collisions. The derivation follows an approach similar to the Green-Kubo relations[43].

For a collision between unlike particles, we found in the previous section that the changes in the individual actions are exponentially small, $|\Delta I_1| \simeq |\Delta I_2| \sim \mathcal{O}(\exp[-\pi|\kappa_1 - \kappa_2|/2])$, and that the change in the sum of the actions is even smaller $|\Delta(I_1 + I_2)| \sim \mathcal{O}(\exp[-\pi\kappa/2])$. However, for a collision between like particles, the change in the individual actions is not exponentially small since $\Omega_1 = \Omega_2$ and $\exp[-\pi/2|\kappa_1 - \kappa_2|] = 1$. Of course, the change in the sum of the actions is exponentially small since $\kappa = \kappa_1 \simeq \kappa_2 \gg 1$.

Thus, on the timescale of a few collisions, one expects the like particles to interchange action with each other nearly preserving the sums $\mathcal{I}_1 = \sum_{j=1}^{N_1} I(j_1)$ and $\mathcal{I}_2 = \sum_{j=2}^{N_2} I(j_2)$, where $I(j_k)$ is the action of the j-th particle of species k ($k = 1, 2$). Maximizing entropy subject to the constancy of the total Hamiltonian $\mathcal{H}$ and the total actions $\mathcal{I}_1$ and $\mathcal{I}_2$ yields a modified Gibbs distribution of the form[13]

$$D_0 = \frac{1}{Z} \exp[-\frac{\mathcal{H}}{T_\parallel} - \alpha_1\mathcal{I}_1 - \alpha_2\mathcal{I}_2], \qquad (2.38)$$

where Z and the thermodynamic variables $T_\parallel$, α_1 and α_2 are determined by the

normalization $1 = \int d\Gamma D_0(\Gamma)$ and the expectation values

$$\langle \mathcal{I}_k \rangle = \int d\Gamma D_0(\Gamma) \mathcal{I}_k = \frac{N_k}{\alpha_k + \Omega_k/T_\parallel}, \tag{2.39}$$

$$\langle \mathcal{H} \rangle = \int d\Gamma D_0(\Gamma) \mathcal{H} = (N_1 + N_2)T_\parallel + \langle \mathcal{I}_1 \rangle \Omega_1 + \langle \mathcal{I}_2 \rangle \Omega_2 + \mathcal{U}_{\text{corr}}. \tag{2.40}$$

Here, $d\Gamma$ is a volume element in the N-particle phase space ($N = N_1 + N_2$). The first three terms in the expression for $\langle \mathcal{H} \rangle$ are kinetic energy terms, whose form can be understood from the velocity dependence in $\mathcal{H}$ [i.e., $\sum_{j=1}^{N_1} m_1(v_{\parallel j}^2 + v_{\perp j}^2)/2 + \sum_{j=1}^{N_2} m_2(v_{\parallel j}^2 + v_{\perp j}^2)/2$] and in $\mathcal{I}_k$ [i.e., $\sum_{j=1}^{N_k} m_k v_{\perp j}^2/(2\Omega_k)$]. The last term, $\mathcal{U}_{\text{corr}}$, is the correlation energy due to the interaction potentials in $\mathcal{H}$. For a weakly correlated and neutralized plasma, this latter term is small compared to the kinetic energy terms[41], so we drop this term and use

$$\langle \mathcal{H} \rangle \simeq \frac{(N_1 + N_2)T_\parallel}{2} + \langle \mathcal{I}_1 \rangle \Omega_1 + \langle \mathcal{I}_2 \rangle \Omega_2. \tag{2.41}$$

Because the $\mathcal{I}_k$'s are not exact constants of the motion, the Liouville distribution, D, is not given exactly by D_0. We set $D = D_0 + D_1$, where D_1 is a small correction due to the time variation of the $\mathcal{I}_k$. Also, the thermodynamic variables, $T_\parallel$, α_1 and α_2 vary slowly in time, and the purpose of this section is to determine that variation.

To that end, we must evaluate the rates of change

$$\frac{d\langle \mathcal{I}_k \rangle}{dt} = \int d\Gamma \frac{\partial D}{\partial t} \mathcal{I}_k = \int d\Gamma D\{\mathcal{I}_k, \mathcal{H}\}, \tag{2.42}$$

$$\frac{d\langle \mathcal{H} \rangle}{dt} = \int d\Gamma \frac{\partial D}{\partial t} \mathcal{H} = \int d\Gamma D\{\mathcal{H}, \mathcal{H}\} = 0, \tag{2.43}$$

where $\{,\}$ is the Poisson bracket, and use has been made of the Liouville equation, $0 = \frac{dD}{dt} = \frac{\partial D}{\partial t} + \{D, \mathcal{H}\}$, and of integration by parts.

There is a subtle point in the evaluation of the Right Hand Side of Eq. (2.42). If one were to approximate D by D_0, the resulting integral would be zero

$$\int d\Gamma\, D_0\{\mathcal{I}_k, \mathcal{H}\} = \int d\Gamma \sum_{j=1}^{N_k} (-T_\| \frac{\partial D_0}{\partial \psi_{kj}}) = 0, \tag{2.44}$$

where ψ_{kj} is the gyroangle conjugate to I_{kj} and use has been made of the facts that the only dependence on ψ_{kj} is in $\mathcal{H}$ and that dependence is periodic. The non-zero contribution to the Right Hand Side of Eq. (2.42) comes exclusively from D_1, and to know D_1 one must solve the Liouville equation.

We suppose that at some time $t - \tau$, the correction D_1 is zero and let D_1 develop through the collisional dynamics. From the Liouville equation, $dD/dt = 0$, one finds that $D(t, \Gamma) = D_0[t - \tau, \Gamma'(\Gamma, -\tau)]$ where the phase point $\Gamma' = \Gamma'(\Gamma, t' - t)$ evolves to the phase point Γ as the time evolves from t' to t. In evaluating $D_0[t - \tau, \Gamma']$, we use $\mathcal{H}(\Gamma') = \mathcal{H}(\Gamma)$ and $\mathcal{I}_k(\Gamma') = \mathcal{I}_k(\Gamma) - \delta\mathcal{I}_k$, where

$$\delta\mathcal{I}_k = \int_{t-\tau}^{t} dt' \{\mathcal{I}_k, \mathcal{H}\}|_{\Gamma'(\Gamma, t'-t)}. \tag{2.45}$$

By hypothesis, $\mathcal{I}_k$ changes through a sequence of close collisions entered with randomly phased initial gyroangles. Thus, one can think of $\mathcal{I}_k(t)$ as a stochastic variable that suffers a sequence of many small and random changes. The correlation time for $\dot{\mathcal{I}}_k(t)$ is about the duration of a close collision, and the change in $\mathcal{I}_k(t)$ during that time is small. We choose the time interval τ to be longer than the correlation time but still small enough that $\delta\mathcal{I}_k$ is a small change.

Taylor expanding $D_0[t - \tau, \Gamma']$ with respect to the $\delta\mathcal{I}_k$'s yields the distribution

$$D(t,\Gamma) \simeq D_0(t - \tau, \Gamma) + \sum_{h=1}^{2} \alpha_h D_0(t - \tau, \Gamma) \int_{t-\tau}^{t} dt' \{\mathcal{I}_h, \mathcal{H}\}|_{\Gamma'(\Gamma, t'-t)}. \qquad (2.46)$$

When this distribution is substituted into integrand (2.42), the first term integrates to zero according to Eq.(2.44). Since the thermodynamic variables change only by a small amount during the time τ, $D_0(t - \tau, \Gamma)$ may be approximated by $D_0(t, \Gamma)$ in the second term yielding the result

$$\frac{d\langle \mathcal{I}_k \rangle}{dt} = \sum_{h=1}^{2} \alpha_h \int_{t-\tau}^{t} dt' \int d\Gamma D_0(t, \Gamma)\{\mathcal{I}_k, \mathcal{H}\}|_{\Gamma}\{\mathcal{I}_h, \mathcal{H}\}|_{\Gamma'(\Gamma, t'-t)}. \qquad (2.47)$$

The Poisson brackets in Eq. (2.47) are non-zero only in regions of Γ-space corresponding to close, well-separated, binary collisions. In those regions the Poisson brackets depend primarily on the coordinates and velocities of the two colliding particles. Thus, the coordinates of all the other particles may be integrated out, reducing Eq. (2.47) to the form

$$
\begin{aligned}
\frac{d\langle \mathcal{I}_k \rangle}{dt} \\
= \quad & \alpha_k \frac{N_k(N_k - 1)}{2} \int_{t-\tau}^{t} dt' \int d\gamma \mathcal{F}(1_k, 2_k)\{I(1_k) + I(2_k), H(1_k, 2_k)\}|_{\gamma} \\
& \cdot \{I(1_k) + I(2_k), H(1_k, 2_k)\}|_{\gamma'=\gamma'(\gamma, t'-t)} \\
& + \alpha_k N_k N_{k'} \int_{t-\tau}^{t} dt' \int d\gamma \mathcal{F}(1_k, 1_{k'})\{I(1_k), H(1_k, 1_{k'})\}|_{\gamma} \\
& \cdot \{I(1_k), H(1_k, 1_{k'})\}|_{\gamma'=\gamma'(\gamma, t'-t)} \\
& + \alpha_{k'} N_k N_{k'} \int_{t-\tau}^{t} dt' \int d\gamma \mathcal{F}(1_k, 1_{k'})\{I(1_k), H(1_k, 1_{k'})\}|_{\gamma} \\
& \cdot \{I(1_{k'}), H(1_k, 1_{k'})\}|_{\gamma'=\gamma'(\gamma, t'-t)}.
\end{aligned}
\qquad (2.48)
$$

Here $k' = 2$ if $k = 1$ and $k' = 1$ if $k = 2$. The two-particle function $\mathcal{F}(i_k, j_q)$ is obtained by integrating $D(\Gamma)$ over coordinates and velocities for all particles except i_k and j_q, and $H(i_k, j_q)$ is the two-particle Hamiltonian governing the collisions between i_k and j_q (see Eq.(2.12) of the previous section). The first term in Eq.(2.48) describes a collision between particles 1 and 2 of species k, and there are $N_k(N_k - 1)/2$ such collisions. The next two terms describe a collision between particle 1 of species k and particle 1 of species k', and there are $N_k N_{k'}$ such collisions. If for brevity we refer to particles i_k and j_q as particles 1 and 2, the two-particle phase-space volume element $d\gamma$ is given by

$$
\begin{aligned}
d\gamma &= dz_1 dp_1 dz_2 dp_2 d\psi_1 dI_1 d\psi_2 dI_2 dY_1 dP_{Y_1} dY_2 dP_{Y_2} \\
&= (m_k m_q)^3 dz dv_z dZ dV_z d\psi_1 d\psi_2 v_{\perp 1} dv_{\perp 1} v_{\perp 2} dv_{\perp 2} \cdot dX_1 dY_1 dX_2 dY_2, \quad (2.49)
\end{aligned}
$$

where use has been made of the definitions $I_j = m_j v_{\perp j}^2/(2\Omega_j)$ and $P_{Y_j} = m_j \Omega_j X_j$, and where (z, v_z) are the relative position and velocity in z and (Z, V_z) are the center of mass position and velocity. These latter two variables do not enter the Poisson brackets.

Next we argue that the $t' - t$ dependence in the $d\gamma$-integrals of Eq.(2.48) is even in $t' - t$. From Hamiltonian (2.14), we see that the Poisson brackets in Eq.(2.48) involve terms of the form $g_{\mu\nu} \exp[i\mu\psi_1 + i\nu\psi_2]$. The dependence on $t' - t$ enters because the second bracket in each product of brackets is evaluated at the primed phase point $\Gamma' = \Gamma'(\Gamma, t' - t)$. When the products of brackets are averaged over the random initial phases of the gyroangles, the resulting time dependence from the gygroangles is of the form $\cos[\mu(\psi_1' - \psi_1) + \nu(\psi_2' - \psi_2)] = \cos[(\mu\Omega_1 + \nu\Omega_2)(t' - t)]$,

which is even in $(t' - t)$. The remaining time dependence comes from the relative coordinate $z' = z'(z, t' - t)$, which enters $g_{\mu\nu}(\gamma')$. From Eq.(2.23), one can see that z' is unchanged for $(t' - t) \to -(t' - t)$ and $v_\| \to -v_\|$, where $v_\|$ is the value of the relative velocity v_z before the interaction. This is seen most simply for the simple case where the particles stream without interaction and $z' = z + v_z(t' - t)$. Of course, $f(\gamma)$ is invariant under the interchange $v_z \to -v_z$, so the $d\gamma$-integrals are even in $(t' - t)$.

Thus, the integral $\int_{t-\tau}^{t} dt'$ in Eq.(2.48), can be replaced by the integral $\frac{1}{2}\int_{t-\tau}^{t+\tau} dt'$. The dt' integral then extends over the full duration of a collision, and Eq.(2.48) can be rewritten as

$$
\begin{aligned}
\frac{d\langle \mathcal{I}_k \rangle}{dt} \\
= \frac{1}{2}\{ \alpha_k \frac{N_k(N_k - 1)}{2} \int d\gamma \mathcal{F}(1_k, 2_k)\{I(1_k) + I(2_k), H(1_k, 2_k)\}\Delta(I(1_k) + I(2_k))_{(1_k, 2_k)} \\
+ \alpha_k N_k N_{k'} \int d\gamma \mathcal{F}(1_k, 1_{k'})\{I(1_k), H((1_k, 1_{k'}))\}\Delta(I(1_k))_{(1_k, 1_{k'})} \\
+ \alpha_{k'} N_k N_{k'} \int d\gamma \mathcal{F}(1_k, 1_{k'})\{I(1_k), H((1_k, 1_{k'}))\}\Delta(I(1_{k'}))_{(1_k, 1_{k'})} \},
\end{aligned}
\tag{2.50}
$$

where

$$
\Delta(I(1_k) + I(2_k))_{(1_k, 2_k)} \equiv \int_{t-\tau}^{t+\tau} dt'\{I(1_k) + I(2_k), H(1_k, 2_k)\}|_{\gamma'=\gamma'(\gamma, t'-t)},
\tag{2.51}
$$

is the change in $(I(1_k) + I(2_k))$ during a collision between particles 1_k and 2_k. The quantities $\Delta(I(1_k))_{(1_k, 1_{k'})}$ and $\Delta(I(1_{k'}))_{(1_k, 1_{k'})}$ follow the same notation. These changes were evaluated in Section II.

Next we note that one coordinate in the $d\gamma$-integral can be written as a time
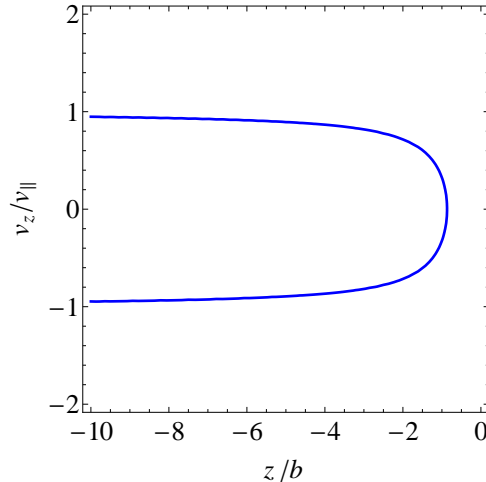
Figure 2.6: A typical trajectory for a collision in the (z, v_z) plane. Here b is the distance of closest approach, and $v_\parallel$ is the velocity at $t = \pm\infty$.

integral. Figure (2.6) shows the (z, v_z) phase space with a typical trajectory for a collision. Such a trajectory is described by Eq.(2.23). The $d\gamma$-integral includes an integral over the $dzdv_z$ plane, and we propose to carry out the integral by arranging area elements in a sequence along each phase in the trajectory using the incompressible nature of the flow, $dz'dv'_z = dzdv_z$. Along the trajectory, the two-particle distribution $\mathcal{F}$ is a constant, so it may be evaluated at some starting area element before the interaction, say at $dzdv_z$. At this starting element we set $dz = |v_z|dt$, where $|v_z|$ is the initial relative velocity defined in Eq.(2.23). Thus for each element along the trajectory, we have the integration element $dz'dv'_z = |v_z|dtdv_z$. The time integral dt is an integral of the Poisson bracket along the trajectory, that is, over the course of the collision, and yields the change in the actions during the collision. Thus, Eq. (2.50)

reduces to the form

$$\frac{d\langle \mathcal{I}_k \rangle}{dt} = \frac{1}{2}\{\alpha_k \frac{N_k(N_k-1)}{2}\int d\tilde{\gamma}\mathcal{F}^{(0)}[\Delta(I(1_k)+I(2_k))_{(1_k,2_k)}]^2$$

$$+\alpha_k N_k N_{k'}\int d\tilde{\gamma}\mathcal{F}^{(0)}[\Delta(I(1_k))_{(1_k,1_{k'})}]^2$$

$$+\alpha_{k'} N_k N_{k'}\int d\tilde{\gamma}\mathcal{F}^{(0)}[\Delta(I(1_k))_{(1_k,1_{k'})}][\Delta(I(1_{k'}))_{(1_k,1_{k'})}]\}. \quad (2.52)$$

where $\mathcal{F}^{(0)}$ is the distribution evaluated at a phase point before the interaction and

$$d\tilde{\gamma} = \frac{d\gamma}{dt}$$

$$= (m_k m_q)^3 |v_z| dv_z dZ dV_z d\psi_1 d\psi_2 v_{\perp 1} dv_{\perp 1} v_{\perp 2} dv_{\perp 2} \cdot dX_1 dY_1 dX_2 dY_2. \quad (2.53)$$

Here the subscripts 1 and 2 stand for i_k and j_q as in Eq. (2.48).

In this same notation, the distribution before the interaction is given by

$$\mathcal{F}^{(0)} = C\exp[-\frac{H(1,2)}{T_{\parallel}} - \alpha_1 I_1 - \alpha_2 I_2], \quad (2.54)$$

where C is a normalization constant and

$$H(1,2) = \frac{m_k}{2}(v_{z1}^2 + v_{\perp 1}^2) + \frac{m_q}{2}(v_{z2}^2 + v_{\perp 2}^2)$$

$$= \frac{\mu_{kq}v_z^2}{2} + \frac{M_{kq}V_z^2}{2} + \frac{m_k v_{\perp 1}^2}{2} + \frac{m_q v_{\perp 2}^2}{2}. \quad (2.55)$$

Here $\mu_{kq} = m_k m_q/(m_k+m_q)$ is the reduced mass and $M_{kq} = m_k+m_q$ is the total mass

of the two particles. From the normalization $\int d\gamma \mathcal{F}^{(0)} = 1$, we find the distribution

$$
\begin{aligned}
\mathcal{F}^{(0)} \;=\;& \frac{1}{L^6 (m_k m_q)^3 (2\pi)^2} \frac{\sqrt{m_k m_q}}{2\pi T_\parallel} \frac{m_k m_q}{T_{\perp k} T_{\perp q}} \\
& \cdot \exp\Big(-\frac{\mu_{kq} v_z^2}{2T_\parallel} - \frac{M_{kq} V_z^2}{2T_\parallel} - \frac{m_k v_{\perp 1}^2}{2T_{\perp k}} - \frac{m_q v_{\perp 2}^2}{2T_{\perp q}}\Big),
\end{aligned}
\tag{2.56}
$$

where L^3 is the volume of the plasma and $T_{\perp k} = T_\parallel / (1 + \alpha_k T_\parallel / \Omega_k)$.

It is convenient to define the relative, parallel thermal velocity of a species i particle and a species j particle as

$$
\bar{v}_{ij} = \sqrt{\frac{T_\parallel}{\mu_{ij}}},
\tag{2.57}
$$

and the magnetization of a species-i particle in interaction with a species-j particle as

$$
\bar{\kappa}_{ij} = \frac{\bar{b}\Omega_i}{\bar{v}_{ij}},
\tag{2.58}
$$

where the distance of closest approach is $\bar{b} = 2e^2 / T_\parallel$.

Note that because of this definition the $\bar{\kappa}_{ij}$'s are related to $\bar{\kappa}_{11}$ by ratios of masses:

$$
\bar{\kappa}_{ij} \;=\; \bar{\kappa}_{11} \frac{m_1}{m_i} \sqrt{\frac{2m_i/m_1}{(1 + m_i/m_j)}}.
\tag{2.59}
$$

Specifically,

$$\bar{\kappa}_{22} = \bar{\kappa}_{11}(\frac{m_1}{m_2})^{1/2}, \tag{2.60}$$

$$\bar{\kappa}_{12} = \bar{\kappa}_{11}\sqrt{\frac{2}{(1 + m_1/m_2)}}, \tag{2.61}$$

$$\text{and } \bar{\kappa}_{21} = \bar{\kappa}_{11}\frac{m_1}{m_2}\sqrt{\frac{2}{(1 + m_1/m_2)}}. \tag{2.62}$$

According to Eq. (2.32)-(2.34), the change in actions depend on the initial gyroangles ϕ_1 and ϕ_2. Along any trajectory of the kind shown in Fig. (2.6), the gyroangle ϕ_j differs from the ψ_j in the differential for $d\tilde{\gamma}$ only by a constant, so we can replace $d\psi_1 d\psi_2$ in the differential with $d\phi_1 d\phi_2$. Also, the change in actions depend on X_1, Y_1, X_2, Y_2 only through $\eta = |\Delta \mathbf{R}_\perp|/b$, where $|\Delta \mathbf{R}_\perp|^2 = (X_1 - X_2)^2 + (Y_1 - Y_2)^2$, so in the differential $d\tilde{\gamma}$ we set $dX_1 dY_1 dX_2 dY_2 = 2\pi b^2 \eta d\eta dX_2 dY_2$. The integral over $dZ dX_2 dY_2$ then trivially gives a factor of L^3. The change in actions does not depend on V_z, so the V_z integral yields $\sqrt{2\pi T_z/M_{kq}}$. When substituting Eq.(2.56) for $\mathcal{F}^{(0)}(1,2)$, one must be careful to identify the species of particles 1 and 2. For example, in the first term of Eq. (2.52) both 1 and 2 are of species k, and in the second and third terms, particles 1 and 2 are of species k and k'. Making these substitutions and using the relations $\mathcal{I}_k = N_k T_{\perp k}/\Omega_k$ and $\alpha_k/\Omega_k = (1/T_{\perp k} - 1/T_\parallel)$ yields the result

$$
\begin{aligned}
\frac{dT_{\perp k}}{dt} &= (T_\parallel - T_{\perp k})[n_k \bar{b}^2 \bar{v}_{kk} \cdot \frac{\sqrt{2\pi}}{8}\Lambda_1(\bar{\kappa}_{kk}) + n_{k'} \bar{b}^2 \bar{v}_{kk'} \cdot \frac{\sqrt{2\pi}}{4}\frac{\mu_{kk'}}{m_k}\Lambda_1(\bar{\kappa}_{kk'})] \\
&\quad + \frac{(\alpha_k - \alpha_{k'})T_{\perp k}T_{\perp k'}}{\Omega_{k'}} \cdot \frac{\mu_{kk'}^2}{m_k m_{k'}} \cdot \frac{n_{k'} \bar{b}^2 \bar{v}_{kk'}}{\bar{\kappa}_{kk'}\bar{\kappa}_{k'k}}\frac{\sqrt{2\pi}}{2}\Lambda_2(|\bar{\kappa}_{kk'} - \bar{\kappa}_{k'k}|), \tag{2.63}
\end{aligned}
$$

where

$$\Lambda_1(\bar{\kappa}) = \int_0^\infty \frac{d\sigma}{\sigma} \int_0^\infty \eta^3 d\eta f_1^2(\frac{\bar{\kappa}}{\sigma^3}, \eta) e^{-\sigma^2/2} \tag{2.64}$$

$$\Lambda_2(\bar{\kappa}) = \int_0^\infty d\sigma \sigma^3 \int_0^\infty \eta d\eta f_2^2(\frac{\bar{\kappa}}{\sigma^3}, \eta) e^{-\sigma^2/2}. \tag{2.65}$$

In Appendix A, we obtain the large $\bar{\kappa}$ asymptotic limits

$$\Lambda_1(\bar{\kappa}) = 3.10 \bar{\kappa}^{-7/15} e^{-5(3\pi\bar{\kappa})^{2/5}/6}, \tag{2.66}$$

$$\Lambda_2(\bar{\kappa}) = 3.87 \bar{\kappa}^{13/15} e^{-5(3\pi\bar{\kappa})^{2/5}/6}. \tag{2.67}$$

For the strong magnetization ordering $\bar{\kappa}_{ij} \gg |\bar{\kappa}_{12} - \bar{\kappa}_{21}| \gg 1$, we note that $\Lambda_1(\bar{\kappa}_{ij}) \ll \Lambda_2(|\bar{\kappa}_{12} - \bar{\kappa}_{21}|)$.

Here, the last term on the Right Hand Side of Eq. (2.63) describes the rapid relaxation where particles of species k collide with particles of species k' and exchange cyclotron actions. As one would expect, this term is proportional to $(\alpha_k - \alpha_{k'})$ and vanishes when $\alpha_k = \alpha_{k'}$. The first term describes the slow relaxation where the total cyclotron action is broken and liberated (or absorbed) cyclotron energy is exchanged with parallel energy. As one would expect, this term is proportional to $T_\parallel - T_{\perp k}$, and vanishes when $T_\parallel = T_{\perp k}$. Note here that $(T_\parallel - T_{\perp k})$ is proportional to α_k, so one may equally say that the term vanishes when $\alpha_k = 0$. Also, note that when the two species are the same (i.e. when $k = k'$) and when $\alpha_k = \alpha_{k'}$, the rate equation reduces to that obtained in the work of O'Neil and Hjorth[9]. Finally, we will argue in the next section that Eq. (2.63) is an easy place to generalize the treatment to more than two species. One simply sums k' over all species except $k' = k$.

Next we introduce scaled variables. The thermodynamic variables $T_\parallel$, α_1 and

α_2 are the three unknowns, which we scale as $\hat{T}_\parallel = T_\parallel/T_{\parallel 0}$ and $\hat{\alpha}_k = \alpha_k T_{\parallel 0}/\Omega_1$, where $T_{\parallel 0} = T_\parallel(0)$ is the initial value of $T_\parallel$. An equivalent set of thermodynamic variables is the three temperatures $T_\parallel$, $T_{\perp 1}$ and $T_{\perp 2}$; we scale the perpendicular temperatures as $\hat{T}_{\perp k} = T_{\perp k}/T_{\parallel 0}$. $\hat{\alpha}_k$ and $\hat{T}_{\perp k}$ are related by $\hat{\alpha}_k = (m_1/m_k)(1/\hat{T}_{\perp k} - 1/\hat{T}_\parallel)$. The actions are scaled as $\langle \hat{\mathcal{I}}_k \rangle = \langle \mathcal{I}_k \rangle (\Omega_1/T_{\parallel 0})$. We introduce a scaled time $\hat{t} = t n \bar{b}_0^2 \bar{v}_{11,0}$, where again subscripts zero refer to initial values and $n\bar{b}^2\bar{v}_{11} = n\bar{b}_0^2\bar{v}_{11,0}(T_{\parallel 0}/T_\parallel)^{3/2}$. The magnetization parameter $\bar{\kappa}_{ij}$ is already dimensionless, but does have a temperature dependence $\bar{\kappa}_{ij} = \bar{\kappa}_{ij,0}(T_{\parallel 0}/T_\parallel)^{3/2}$. Following the same notation, we write density ratios as $\hat{n}_k = n_k/n$ The scaling removes dependence on the total density n, and dependence on B enters only in the combination with $T_{\parallel 0}$ through the magnetization parameter $\bar{\kappa}_{11,0}$. As we will see, the solution depends only on the initial values of the scaled thermodynamic variables, the initial magnetization strength $\bar{\kappa}_{11,0} = \Omega_1\bar{b}_0/\bar{v}_{11,0}$, the mass ratio m_1/m_2, and the density ratios $\hat{n}_k = n_k/n$.

In terms of these scaled variables Eq.(2.63) takes the form

$$\frac{d\hat{T}_{\perp k}}{d\hat{t}} = [\hat{\alpha}_k \frac{\hat{G}_k}{\hat{n}_k} + (\hat{\alpha}_k - \hat{\alpha}_{k'})\frac{\hat{K}_k}{\hat{n}_k}]\frac{m_1}{m_k}, \qquad (2.68)$$

where

$$\hat{G}_k = \frac{\hat{T}_{\perp k}}{\hat{T}_\parallel^{1/2}} \cdot (\frac{m_k}{m_1})^{3/2}\frac{\sqrt{2\pi}}{8}[\hat{n}_k^2\Lambda_1(\bar{\kappa}_{kk}) + \hat{n}_k\hat{n}_{k'}\sqrt{\frac{2}{1 + m_k/m_{k'}}}\Lambda_1(\bar{\kappa}_{kk'})] \quad (2.69)$$

regulates equipartition of $\hat{T}_{\perp k}$ with $\hat{T}_\parallel$ on the slower timescale, and

$$\hat{K}_k = \frac{\hat{T}_{\perp k}\hat{T}_{k'}}{\hat{T}_\parallel^{3/2}} \cdot \hat{n}_k\hat{n}_{k'}\frac{\sqrt{2\pi}}{8} \cdot \sqrt{(\frac{m_k}{m_1}\frac{m_{k'}}{m_1})^3\frac{2m_1}{m_k + m_{k'}}} \cdot \frac{\Lambda_2(|\bar{\kappa}_{kk'} - \bar{\kappa}_{k'k}|)}{\bar{\kappa}_{11}^2} \quad (2.70)$$

regulates equipartition of α_k with $\alpha_{k'}$ on the faster timescale. The statement of conservation of energy in Eq.(2.41) can be rewritten as the relation

$$\hat{T}_\parallel(t) = 1 + 2\{\hat{n}_1[\hat{T}_{\perp 1}(0) - \hat{T}_{\perp 1}(t)] + \hat{n}_2[\hat{T}_{\perp 2}(0) - \hat{T}_{\perp 2}(t)]\}. \tag{2.71}$$

This equation plus Eq.(2.68) for $k = 1$ and 2 and the relation $\hat{\alpha}_k = (m_1/m_k)(1/\hat{T}_{\perp k} - 1/\hat{T}_\parallel)$ determine the evolution of the three unknowns $T_\parallel$, $T_{\perp 1}$ and $T_{\perp 2}$ (or equivalently $T_\parallel$, α_1 and α_2).

To obtain equations for $\hat{\alpha}_1(t)$ and $\hat{\alpha}_2(t)$ alone, we combine Eq. (2.68) with the relations

$$\frac{d\hat{\alpha}_k}{d\hat{t}} = \frac{m_1}{m_k}\left(\frac{1}{\hat{T}_\parallel^2}\frac{d\hat{T}_\parallel}{d\hat{t}} - \frac{1}{\hat{T}_{\perp k}^2}\frac{d\hat{T}_{\perp k}}{d\hat{t}}\right), \tag{2.72}$$

$$0 = \frac{1}{2}\frac{d\hat{T}_\parallel}{d\hat{t}} + \hat{n}_1\frac{d\hat{T}_{\perp 1}}{d\hat{t}} + \hat{n}_2\frac{d\hat{T}_{\perp 2}}{d\hat{t}}. \tag{2.73}$$

The result is

$$\frac{d\hat{\alpha}_1}{d\hat{t}} = -\hat{\nu}_{11}\hat{\alpha}_1 - \hat{\nu}_{12}\hat{\alpha}_2 - \hat{\Gamma}_1(\hat{\alpha}_1 - \hat{\alpha}_2), \tag{2.74}$$

$$\frac{d\hat{\alpha}_2}{d\hat{t}} = -\hat{\nu}_{21}\hat{\alpha}_1 - \hat{\nu}_{22}\hat{\alpha}_2 - \hat{\Gamma}_2(\hat{\alpha}_2 - \hat{\alpha}_1), \tag{2.75}$$

where the $\hat{\nu}_{ij}$'s and the $\hat{\Gamma}_k$'s are given by

$$\hat{\nu}_{ij} = \left(\frac{\delta_{ij}m_1^2}{\hat{T}_{\perp i}^2\hat{n}_i m_i^2} + \frac{2m_1^2}{\hat{T}_\parallel^2 m_i m_j}\right)\hat{G}_j, \tag{2.76}$$

$$\hat{\Gamma}_k = \left[\frac{m_1^2}{\hat{T}_{\perp k}^2\hat{n}_k m_k^2} + \frac{2(1 - m_k/m_{k'})}{\hat{T}_\parallel^2 m_k^2/m_1^2}\right]\hat{K}_k, \tag{2.77}$$

and $\hat{T}_{\perp k} = \hat{T}_{\parallel}/(1+\hat{\alpha}_k\hat{T}_{\parallel}m_k/m_1)$. In these coefficients, $\hat{T}_{\parallel}(t)$ and $\hat{T}_{\perp k}(t)$ are determined by Eq. (2.71) and the relation $\hat{T}_{\perp k} = \hat{T}_{\parallel}/(1 + \hat{\alpha}_k\hat{T}_{\parallel}m_k/m_1)$.

Analytic progress in solving Eqs. (2.74) and (2.75) is possible in two separate limits. We first discuss the solutions in these limits and then solve the equations numerically for various values of the parameters, verifying the limiting behaviors expected from the analytic solutions.

For sufficiently strong magnetization, the $\hat{K}_k$ and $\hat{G}_j$ integrals satisfy the inequality $\hat{K}_1, \hat{K}_2 \gg \hat{G}_1, \hat{G}_2$, and the collisional relaxation takes place on two timescales. By subtracting Eq. (2.75) from Eq. (2.74) and neglecting $\hat{G}_1$ and $\hat{G}_2$ compared to $\hat{K}_1, \hat{K}_2$, we obtain the equation

$$\frac{d}{d\hat{t}}(\hat{\alpha}_1 - \hat{\alpha}_2) = -\hat{\nu}_a(\hat{\alpha}_1 - \hat{\alpha}_2), \tag{2.78}$$

where

$$
\begin{aligned}
\hat{\nu}_a &= \hat{\Gamma}_1 + \hat{\Gamma}_2 \\
&= \hat{K}_1 \cdot [\frac{1}{\hat{T}_{\perp 1}^2 \hat{n}_1} + \frac{1}{\hat{T}_{\perp 2}^2 \hat{n}_2}\frac{m_1^2}{m_2^2} + \frac{2(1 - m_1/m_2)^2}{\hat{T}_{\parallel}^2}]
\end{aligned}
\tag{2.79}
$$

is the rate at which $\hat{\alpha}_1$ and $\hat{\alpha}_2$ relax to a common value $\hat{\alpha}$.

At a slower rate, $\hat{\alpha}$ relaxes to zero. To obtain this rate, we multiply Eq. (2.74) by $\hat{\Gamma}_2$ and Eq. (2.75) by $\hat{\Gamma}_1$ and add to obtain the result

$$\hat{\Gamma}_2\frac{d\hat{\alpha}_1}{d\hat{t}} + \hat{\Gamma}_1\frac{d\hat{\alpha}_2}{d\hat{t}} = -\hat{\Gamma}_2(\hat{\nu}_{11}\hat{\alpha}_1 + \hat{\nu}_{12}\hat{\alpha}_2) - \hat{\Gamma}_1(\hat{\nu}_{21}\hat{\alpha}_1 + \hat{\nu}_{22}\hat{\alpha}_2). \tag{2.80}$$

The large quantity $\hat{K}_1$ enters the $\hat{\Gamma}_j$ on both sides of this equation and cancels, leaving

a slow rate of order $\hat{G}_j$. Setting $\hat{\alpha}_1 = \hat{\alpha}_2 = \hat{\alpha}$ then yields the equation

$$\frac{d\hat{\alpha}}{d\hat{t}} = -\hat{\nu}_b \hat{\alpha}, \qquad (2.81)$$

where

$$
\begin{aligned}
\hat{\nu}_b &= \frac{\hat{\Gamma}_2(\hat{\nu}_{11} + \hat{\nu}_{12})}{\hat{\Gamma}_1 + \hat{\Gamma}_2} + \frac{\hat{\Gamma}_1(\hat{\nu}_{21} + \hat{\nu}_{22})}{\hat{\Gamma}_1 + \hat{\Gamma}_2} \\
&= \{\sum_{k=1}^{2}[\frac{m_1^2/m_{k'}^2}{\hat{T}_{\perp k'}^2 \hat{n}_{k'}} + \frac{2m_1/m_{k'}(m_1/m_{k'} - 1)}{\hat{T}_\parallel^2}] \cdot [\frac{2m_1/m_k(1 + m_1/m_k)}{\hat{T}_\parallel^2} + \frac{m_1^2/m_k^2}{\hat{T}_{\perp k}^2 \hat{n}_k}]\hat{G}_k\} \\
&\quad \cdot [\frac{1}{\hat{T}_{\perp 1}^2 \hat{n}_1} + \frac{m_1^2/m_2^2}{\hat{T}_{\perp 2}^2 \hat{n}_2} + \frac{2(1 - m_1/m_2)^2}{\hat{T}_\parallel^2}]^{-1} \qquad (2.82)
\end{aligned}
$$

is the rate at which $\hat{\alpha}$ decays to zero, and hence from the relation $\hat{\alpha}_k = (m_1/m_k)(1/\hat{T}_{\perp k} - 1/\hat{T}_\parallel)$, the rate at which $\hat{T}_{\perp 1}$ and $\hat{T}_{\perp 2}$ approaches $\hat{T}_\parallel$.

Of course, this approximate solution is only accurate to order $|\hat{G}_j/\hat{K}_k| \ll 1$. For example, $\hat{\alpha}_1(t) - \hat{\alpha}_2(t)$ does not decay to exactly zero during the first phase of the evolution but rather to the small value $(\hat{\alpha}_1 - \hat{\alpha}_2) \simeq [(\hat{\nu}_{22} + \hat{\nu}_{21} - \hat{\nu}_{11} - \hat{\nu}_{12})/(\hat{\Gamma}_1 + \hat{\Gamma}_2)]\hat{\alpha} \sim \mathcal{O}(\hat{G}_j/\hat{K}_k)\hat{\alpha} \ll \hat{\alpha}$. One can understand this by setting $d\hat{\alpha}_1/d\hat{t}, d\hat{\alpha}_2/d\hat{t} \approx 0$ in Eqs. (2.74) and (2.75) and solving for $\hat{\alpha}_1 - \hat{\alpha}_2$.

Another analytic solution is possible when $\hat{\alpha}_1$ and $\hat{\alpha}_2$ are small, and Eqs. (2.74) and (2.75) may be treated as linear coupled equations with constant coefficients $\hat{\nu}_{ij}$ and $\hat{\Gamma}_j$. In these coefficients, one must set $\hat{T}_\parallel = \hat{T}_{\perp 1} = \hat{T}_{\perp 2} = \hat{T}$. A normal mode analysis[36] then yields the solution

$$\begin{pmatrix} \hat{\alpha}_1(t) \\ \hat{\alpha}_2(t) \end{pmatrix} = C_+ \begin{pmatrix} \hat{\alpha}_{1+} \\ \hat{\alpha}_{2+} \end{pmatrix} e^{\hat{S}_+ \hat{t}} + C_- \begin{pmatrix} \hat{\alpha}_{1-} \\ \hat{\alpha}_{2-} \end{pmatrix} e^{\hat{S}_- \hat{t}}, \qquad (2.83)$$

where C_+ and C_- are constants determined by the initial values $\hat{\alpha}_1(0)$ and $\hat{\alpha}_2(0)$, the damping decrements $\hat{S}_+$ and $\hat{S}_-$ are given by

$$\hat{S}_{\pm} = \frac{1}{2}\{-(\hat{\nu}_{22} + \hat{\nu}_{11} + \hat{\Gamma}_1 + \hat{\Gamma}_2) \pm [(\hat{\nu}_{22} + \hat{\nu}_{11} + \hat{\Gamma}_1 + \hat{\Gamma}_2)^2$$
$$-4[(\hat{\nu}_{11}\hat{\nu}_{22} - \hat{\nu}_{12}\hat{\nu}_{21} + (\hat{\nu}_{11} + \hat{\nu}_{12})\hat{\Gamma}_2 + (\hat{\nu}_{22} + \hat{\nu}_{21})\hat{\Gamma}_1)]]^{1/2}\}, \quad (2.84)$$

and the eigenvectors by

$$\begin{pmatrix} \hat{\alpha}_{1+} \\ \hat{\alpha}_{2+} \end{pmatrix} = \begin{pmatrix} \hat{\Gamma}_1 - \hat{\nu}_{12} \\ \hat{S}_+ + \hat{\nu}_{11} + \hat{\Gamma}_1 \end{pmatrix}, \begin{pmatrix} \hat{\alpha}_{1-} \\ \hat{\alpha}_{2-} \end{pmatrix} = \begin{pmatrix} \hat{\Gamma}_1 - \hat{\nu}_{12} \\ \hat{S}_- + \hat{\nu}_{11} + \hat{\Gamma}_1 \end{pmatrix}. \quad (2.85)$$

In the strongly magnetized limit where $\hat{\Gamma}_j \gg \hat{\nu}_{ij}$, we recover the previous solution. The damping decrements are approximately

$$\hat{S}_- \simeq -(\hat{\Gamma}_1 + \hat{\Gamma}_2), \hat{S}_+ \simeq -\frac{(\hat{\nu}_{11} + \hat{\nu}_{12})\hat{\Gamma}_2 + (\hat{\nu}_{22} + \hat{\nu}_{21})\hat{\Gamma}_1}{\hat{\Gamma}_1 + \hat{\Gamma}_2}, \quad (2.86)$$

in agreement with Eqs. (2.79) and (2.82). In this limit, the $|+\rangle$ eigenvector is proportional to

$$\begin{pmatrix} \hat{\alpha}_{1+} \\ \hat{\alpha}_{2+} \end{pmatrix} = \begin{pmatrix} 1 \\ 1 + \frac{(\hat{\nu}_{11} + \hat{\nu}_{12} - \hat{\nu}_{21} - \hat{\nu}_{22})}{\hat{\Gamma}_1 + \hat{\Gamma}_2} \end{pmatrix}, \quad (2.87)$$

and $[\hat{\alpha}_1(t) - \hat{\alpha}_2(t)]$ evolves to near zero on the timescale $S_-^{-1} \simeq 1/(\Gamma_1 + \Gamma_2)$. As mentioned earlier, the correction is of order $(\hat{\nu}_{11} + \hat{\nu}_{12} - \hat{\nu}_{21} - \hat{\nu}_{22})/(\hat{\Gamma}_1 + \hat{\Gamma}_2) \sim \mathcal{O}(\hat{G}_j/\hat{K}_k) \ll 1$.

When the $\hat{\Gamma}_k$'s are comparable to the $\hat{\nu}_{ij}$, the separation in timescales between $\hat{S}_+$ and $\hat{S}_-$ no longer exists. This is the case when magnetization is low or the ion mass difference between the two species is large. However, we note again that our

rates only apply to the strong magnetization regime $|\bar{\kappa}_{12} - \bar{\kappa}_{21}| \gg 1$. If magnetization is low and $|\bar{\kappa}_{12} - \bar{\kappa}_{21}| \lesssim 1$, the timescale in which particles of different species exchange cyclotron action is comparable to the timescale of a few collisions. Over this timescale, the distribution would not be cast into the modified Maxwellian in Eq. (2.38) as assumed.

We convert the rate equations back to unscaled version for easier reference, using the definitions of the scaled physical quantities. The unscaled version of Eqn. (2.74) and (2.75) is

$$\frac{d\alpha_k}{dt} = -\nu_{kk}\alpha_k - \nu_{kk'}\alpha_{k'} - \Gamma_k(\alpha_k - \alpha_{k'}), \tag{2.88}$$

where

$$\nu_{kl} = \left(\frac{2\Omega_k\Omega_l}{nT_{\parallel}^2} + \frac{\Omega_k^2\delta_{kl}}{n_kT_{\perp k}^2}\right)G_k, \tag{2.89}$$

$$\Gamma_k = \left[\frac{\Omega_k^2}{n_kT_{\perp k}^2} + \frac{2\Omega_k(\Omega_k - \Omega_{k'})}{nT_{\parallel}^2}\right]K_k, \tag{2.90}$$

and

$$G_k = \frac{T_{\parallel}T_{\perp k}}{\Omega_k^2}\left[n_k^2\bar{b}\bar{v}_{kk}\frac{\sqrt{2\pi}}{8}\Lambda_1(\bar{\kappa}_{kk}) + n_kn_{k'}\bar{b}\bar{v}_{kk'}\frac{\sqrt{2\pi}}{4}\frac{\mu_{kk'}}{m_k}\Lambda_1(\bar{\kappa}_{kk'})\right], \tag{2.91}$$

$$K_k = \frac{T_{\perp k}T_{\perp k'}}{\Omega_k\Omega_{k'}}\frac{\mu_{kk'}^2}{m_km_{k'}}\frac{n_kn_{k'}\bar{b}^2\bar{v}_{kk'}}{\bar{\kappa}_{kk'}\bar{\kappa}_{k'k}}\frac{\sqrt{2\pi}}{2}\Lambda_2(|\bar{\kappa}_{kk'} - \bar{\kappa}_{k'k}|). \tag{2.92}$$

Then in the first stage of equilibration,

$$\frac{d}{dt}(\alpha_1 - \alpha_2) = -\nu_a(\alpha_1 - \alpha_2), \tag{2.93}$$

where

$$\nu_a = [\frac{\Omega_1^2}{n_1 T_{\perp 1}^2} + \frac{\Omega_2^2}{n_2 T_{\perp 2}^2} + \frac{2(\Omega_1 - \Omega_2)^2}{n T_{\parallel}^2}]K_1. \tag{2.94}$$

And then in the next stage of equilibration, where $\alpha_1 = \alpha = \alpha_2$,

$$\frac{d\alpha}{dt} = -\nu_b \alpha, \tag{2.95}$$

where

$$\begin{aligned}
\nu_b &= \frac{\Gamma_2(\nu_{11} + \nu_{12}) + \Gamma_1(\nu_{21} + \nu_{22})}{\Gamma_1 + \Gamma_2} \\
&= [\sum_{k=1}^{2}(\frac{2\Omega_{k'}(\Omega_{k'} - \Omega_k)}{n T_{\parallel}^2} + \frac{\Omega_{k'}^2}{n_{k'} T_{\perp k'}^2})(\frac{2\Omega_k(\Omega_k + \Omega_{k'})}{n T_{\parallel}^2} + \frac{\Omega_k^2}{n_k T_{\perp k}^2})G_k] \\
&\quad \cdot [\frac{\Omega_1^2}{n_1 T_{\perp 1}^2} + \frac{\Omega_2^2}{n_2 T_{\perp 2}^2} + \frac{2(\Omega_1 - \Omega_2)^2}{n T_{\parallel}}]^{-1}. \tag{2.96}
\end{aligned}$$

Next we consider three numerical integrations of (2.74) and (2.75). For both the first and the second integrations, we choose $\hat{n}_1 = \hat{n}_2 = 1/2$ for convenience, and $m_2/m_1 = 25/24$, as that is the mass ratio of two common constituent ions in a pure ion plasma, namely Mg_{25}^+ and Mg_{24}^+[11, 12]. For all the cases, the lighter ion has a mass of $m_1 = 24m_p$, where m_p is the proton mass. We choose the total density to be $n = 10^5$ cm^{-3}. The parallel temperature $T_{\parallel}$ is assumed to be in the range where the plasma is weakly correlated, i.e., $\Gamma_{corr} < 1$, where $\Gamma_{corr} = (4\pi n/3)^{1/3}e^2/T_{\parallel}$ is the coupling parameter[41]. This requires $T_{\parallel} > 1.1 \times 10^{-5}$ eV. We also choose the magnetic field to be $B = 60$ kG, a value that was realized in past experiments[7, 6].

The first integration is for a case of strong magnetization $\bar{\kappa}_{11,0} = 80.0$ and correspondingly $\bar{\kappa}_{12,0} - \bar{\kappa}_{21,0} = 3.2$. The initial parallel temperature $T_{\parallel 0}$ under this value of $\bar{\kappa}_{11,0}$ is 4.5×10^{-5} eV. With this temperature, the system has a weak cor-

relation of $\Gamma_{\text{corr}} = 0.24$. For such a density and temperature, the collision rate is $n\bar{b}_0^2\bar{v}_{11,0} = 7.7 \times 10^3 \text{ s}^{-1}$. Also, the initial scaled perpendicular temperatures are taken to be $\hat{T}_{\perp 1,0} = 0.5$ and $\hat{T}_{\perp 2,0} = 0.25$. The evolution of $\hat{\alpha}_1$ and $\hat{\alpha}_2$ is shown in Fig. (2.7) and of $\hat{T}_{\perp 1}, \hat{T}_{\perp 1}$ and $\hat{T}_{\parallel}$ in Fig. (2.8). In this case, the separation of timescales is clearly apparent. $\hat{\alpha}_1$ and $\hat{\alpha}_2$ evolve to a common value in a time of 10 s and then evolve to zero in the longer time of 1000 s, or 17 minutes. Note in both figures that the abscissa is a logarithmic scale. As $T_{\parallel}$ decreases during the final relaxation, the magnetization $\bar{\kappa}_{11} \propto T_{\parallel}^{-3/2}$ rises and the equipartition rate, which has the $\exp[-5(3\pi\bar{\kappa}_{11}^{2/5})/6]$ dependence, is exponentially suppressed. This accounts for the fact that the final equipartition takes place over a long three decades of time. In Fig. (2.8), the temperatures $\hat{T}_{\perp 1}$ and $\hat{T}_{\perp 2}$ have slightly different values even after $\hat{\alpha}_1$ and $\hat{\alpha}_2$ have reached common value because of the mass dependence in the relation $\hat{T}_{\perp k} = \hat{T}_{\parallel}(1 + \hat{\alpha}_k\hat{T}_{\parallel}m_k/m_1)$. Note that the correction in Eq. (2.87) is not visible on the scale of the figures.

The second case, as shown in Fig. (2.9) and (2.10), is for a case where the initial parallel temperature is lower than the perpendicular temperatures, but the magnetization and ion masses stay the same as in the first case. The first equipartition, when $\hat{\alpha}_1$ and $\hat{\alpha}_2$ are approaching to the same value, has similar duration as in the previous case, but the final equipartition occurs over an exponentially much shorter duration of 20 s than in that previous case, as the increase in parallel temperature speeds up equipartition exponentially.

The third integration is for a case of strong magnetization, but large ion mass difference between the two species. $\bar{\kappa}_{11,0} = 80.0$ and $\bar{\kappa}_{12,0} - \bar{\kappa}_{21,0} = 24.7$, with a choice of $m_2/m_1 = 1.4$. The values of n and $T_{\parallel,0}$ are the same as in the previous

cases. In this case, the rate $\hat{\nu}_a \sim \mathcal{O}(\exp[-5(3\pi|\bar{\kappa}_{12} - \bar{\kappa}_{21}|^{2/5})/6]/\bar{\kappa}_{11}^2)$ of the first equipartition is comparable to the rate $\hat{\nu}_b \sim \mathcal{O}(\exp[-5(3\pi\bar{\kappa}_{11}^{2/5})/6])$ of the second stage. The thermodynamic variables $\hat{\alpha}_1$ and $\hat{\alpha}_2$ decay to zero without equilibrating first to a common value, and the temperatures $\hat{T}_{\parallel}$, $\hat{T}_{\perp 1}$ and $\hat{T}_{\perp 2}$ converge to the same value, as in Fig. (2.11) and (2.12).
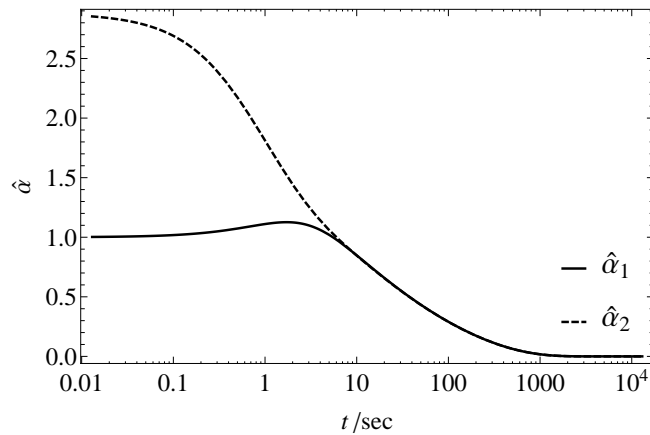
Figure 2.7: The time evolution of $\hat{\alpha}_1$ and $\hat{\alpha}_2$ for the case of $\bar{\kappa}_{11,0} = 80.0$, $m_2/m_1 = 25/24$ and $\hat{n}_1 = \hat{n}_2 = .5$. Here $n\bar{b}_0^2\bar{v}_{11,0} = 7.7 \times 10^3$ s^{-1} and $T_{\parallel 0} = 4.5 \times 10^{-5}$ eV.
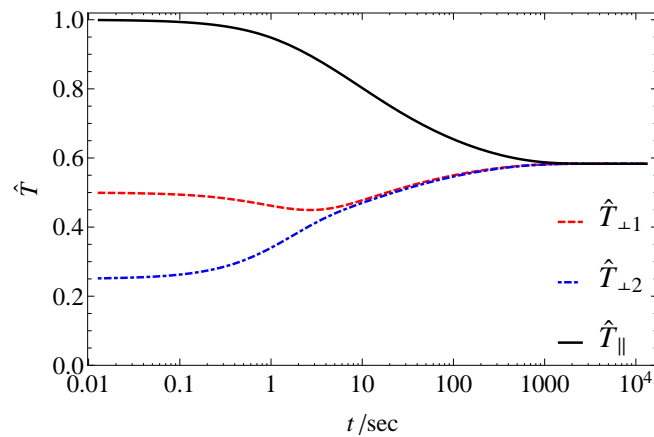
Figure 2.8: The time evolution of $\hat{T}_{\perp 1}$, $\hat{T}_{\perp 2}$ and $\hat{T}_{\parallel}$ for the case of $\bar{\kappa}_{11,0} = 80.0$, $m_2/m_1 = 25/24$ and $\hat{n}_1 = \hat{n}_2 = .5$. Here $n\bar{b}_0^2\bar{v}_{11,0} = 7.7 \times 10^3$ s^{-1} and $T_{\parallel 0} = 4.5 \times 10^{-5}$ eV.
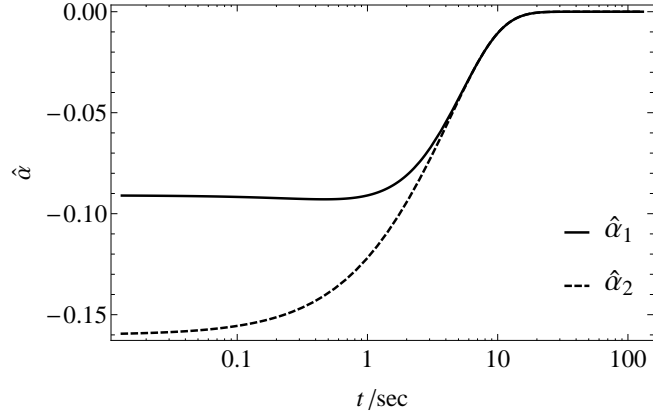
Figure 2.9: The time evolution of $\hat{\alpha}_1$ and $\hat{\alpha}_2$ for the case of $\bar{\kappa}_{11,0} = 80.0$, $m_2/m_1 = 25/24$ and $\hat{n}_1 = \hat{n}_2 = .5$. Here $n\bar{b}_0^2\bar{v}_{11,0} = 7.7 \times 10^3$ s^{-1} and $T_{\|0} = 4.5 \times 10^{-5}$ eV.
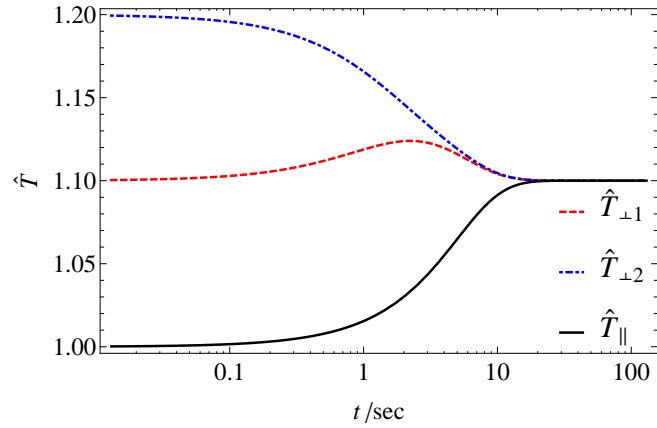
Figure 2.10: The time evolution of $\hat{T}_{\perp 1}, \hat{T}_{\perp 2}$ and $\hat{T}_{\|}$ for the case of $\bar{\kappa}_{11,0} = 80.0$, $m_2/m_1 = 25/24$, and $\hat{n}_1 = \hat{n}_2 = .5$. Here $n\bar{b}_0^2\bar{v}_{11,0} = 7.7 \times 10^3$ s^{-1} and $T_{\|0} = 4.5 \times 10^{-5}$ eV.
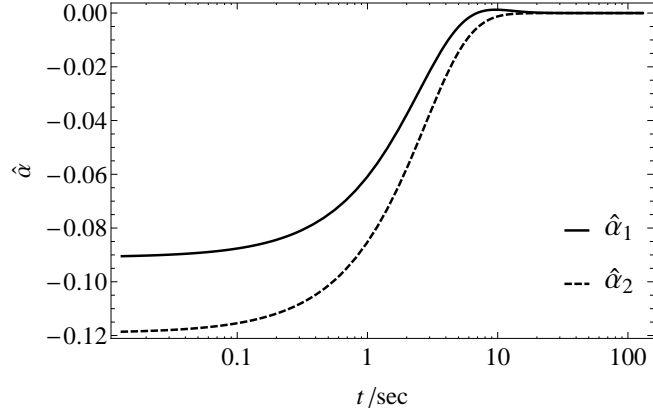
Figure 2.11: The time evolution of $\hat{\alpha}_1$ and $\hat{\alpha}_2$ for the case of $\bar{\kappa}_{11,0} = 80.0$ and $|\bar{\kappa}_{21,0} - \bar{\kappa}_{12,0}| = 24.7$. Here $m_2/m_1 = 1.4$, $\hat{n}_1 = \hat{n}_2 = .5$, $n\bar{b}_0^2\bar{v}_{11,0} = 7.7 \times 10^3$ s^{-1} and $T_{\|0} = 4.5 \times 10^{-5}$ eV.
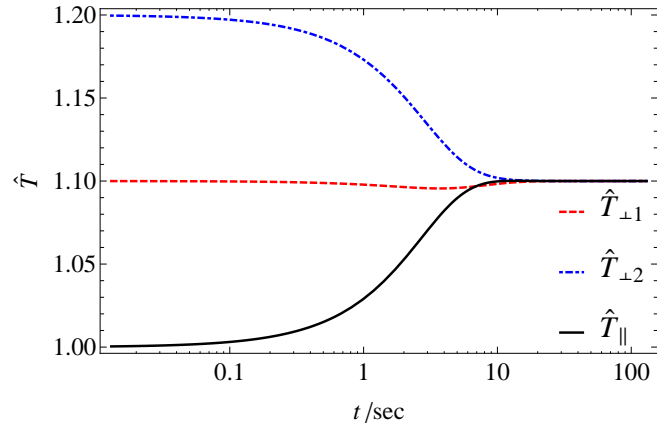
Figure 2.12: The time evolution of $\hat{T}_{\perp 1}, \hat{T}_{\perp 2}$ and $\hat{T}_\|$ for the case of $\bar{\kappa}_{11,0} = 80.0$ and $|\bar{\kappa}_{21,0} - \bar{\kappa}_{12,0}| = 24.7$. Here $m_2/m_1 = 1.4$, $\hat{n}_1 = \hat{n}_2 = .5$, $n\bar{b}_0^2\bar{v}_{11,0} = 7.7 \times 10^3$ s^{-1} and $T_{\|0} = 4.5 \times 10^{-5}$ eV.

2.5   Discussion

The analysis of Section III assumes that the ion plasma is immersed in a uniform neutralizing background charge. For the case of a single species ion plasma, a laboratory realization of this simple theoretical model is a pure ion plasma in a

Malmberg-Penning trap[44]. Rotation of the plasma in the uniform axial magnetic field of the trap induces a radial electric field and a radial centrifugal force that can be thought of as arising from an imaginary cylinder of uniform neutralizing background charge[41, 45]. The Gibb's distribution for the magnetically confined single-species plasma differs only by rigid rotation from that for a plasma confined by a cylinder of neutralizing charge[41, 45].

However, there is a caveat to this equivalence for the case of a pure ion plasma with different mass species. The rotation can give rise to centrifugal separation of the species[11, 46, 47]. A parameter that determines the degree of separation is the quantity $\omega^2 |m_2 - m_1| r_p^2 / T_\parallel$, where ω is the plasma rotation frequency and r_p is the radius of the cylindrical plasma column. We assume that this quantity is small compared to unity so that centrifugal separation is negligible and the equivalence is preserved. Note that ω varies inversely with magnetic field strength[41], so small $\omega^2 |m_2 - m_1| r_p^2 / T_\parallel$ can be consistent with strong magnetization.

For a plasma in a Malmberg-Penning trap, the Hamiltonian $\mathcal{H}$ and the actions $\mathcal{I}_k$ are to be interpreted as the Hamiltonian and actions in the rotating frame of the plasma. To be precise, the actions are defined in the local drift frame[48], but for the plasmas of interest, the difference between the local drift velocity and the local plasma velocity (i.e. $r\omega$) is negligibly small, that is, small compared to the thermal velocity.

Another caveat concerns the statement of conservation of kinetic energy in Eq. (2.63). In some experiments heating processes have rates that are comparable to the rate at which the α_k's relax. If the heating process is understood and the rate can be quantified in a formula, the heating rate should replace the zero on the Left Hand

Side of Eq. (2.73). Alternatively, one can proceed empirically and measure $T_{\parallel}(t)$, say using Laser Induced Fluorescence[44], and then use Eq. (2.63) to determine the evolution of $T_{\perp 1}(t)$ and $T_{\perp 2}(t)$, or equivalently of $\alpha_1(t)$ and $\alpha_2(t)$. Of course, the relaxation of the α's can occur on two timescales, and it may be that the heating is negligible for the relatively rapid relaxation of $\alpha_1(t)$ and $\alpha_2(t)$ to a common value, but not negligible on the longer timescale where that common value relaxes to zero.

Finally, there is the question of how the theory should be generalized for the case of three or more isotopic ions. In the discussion following Eq. (2.63), we noted that this can accomplished by summing the Right Hand Side over k' for $k' \neq k$. In terms of scaled variables, one can sum over k' for subscript $k' \neq k$ on the Right Hand Side of Eq. (2.68). Note that subscript k' is also implicitly hidden in the expressions (2.69) and (2.70) for G_k and K_k. Eq. (2.68) then provides k equations for the $T_{\perp k}$. Also, Eq. (2.73) for conservation of energy must be modified by summing over terms for each $T_{\perp k}$. This generalization is valid because we keep the assumption of the dominance of uncorrelated binary collisions, among particles of all the k species.

Chapter 2, in full, is a reprint of the material as it appears in Physics of Plasmas. C.Y. Chim, T.M. O'Neil, D.H.E. Dubin, *Physics of Plasmas* **21**, 042115 (2014). The dissertation author was the primary investigator and author of this paper.

Chapter 3

Flux-driven algebraic damping of $m = 1$ diocotron mode

3.1 Abstract

Recent experiments with pure electron plasmas in a Malmberg-Penning trap have observed the algebraic damping of $m = 1$ diocotron modes. Transport due to small field asymmetries produces a low density halo of electrons moving radially outward from the plasma core, and the mode damping begins when the halo reaches the resonant radius $r = R_w$ at the wall of the trap. The damping rate is proportional to the flux of halo particles through the resonant layer. The damping is related to, but distinct from spatial Landau damping, in which a linear wave-particle resonance produces exponential damping. This paper explains with analytic theory the new algebraic damping due to particle transport by both mobility and diffusion. As electrons are swept around the "cat's eye" orbits of the resonant wave-particle interaction, they form a dipole ($m = 1$) density distribution. From this distribution, the electric field

component perpendicular to the core displacement produces $\mathbf{E} \times \mathbf{B}$-drift of the core back to the axis, that is, damps the $m = 1$ mode. The parallel component produces drift in the azimuthal direction, that is, causes a shift in the mode frequency.

3.2 Introduction

Diocotron modes are dominant features in the low frequency dynamics of non-neutral plasmas confined in Malmberg-Penning traps[14, 15, 16, 17]. In an ideal limit, these modes involve only cross magnetic field $\mathbf{E} \times \mathbf{B}$ drift motion and are described by the drift-Poisson equations[14]. These equations are isomorphic to Euler's equations for the ideal (i.e., incompressible and inviscid) flow of a neutral fluid, and the diocotron modes are analogues of a Kelvin modes on a fluid vortex[18, 19].

There has been much previous work on diocotron mode instabilities[15, 20, 21, 22] and on diocotron mode damping[18, 19, 23, 24, 25, 26]. This paper focuses on damping.

Previously identified damping mechanisms include a spatial version of the Landau resonance[18, 23], the rotational pumping of bulk viscosity[24, 25], axial velocity dissipation on a separatrix for plasma columns with trapped and passing particles[27], and a strong damping mechanism when the radial magnetron field from end cylinders dominates over the radial space charge field[26]. The Landau mechanism fits into the ideal 2D $\mathbf{E} \times \mathbf{B}$ drift framework, but others, such as rotational pumping, involve physics beyond the ideal model.

This chapter discusses a damping mechanism that is a close cousin of Landau damping, so we begin with a review of the spatial Landau resonance.

The nonneutral plasma column is immersed in a uniform axial magnetic field

$B\hat{z}$, has a radial space charge electric field $E(r)\hat{r}$, and consequently undergoes an azimuthal $\mathbf{E} \times \mathbf{B}$ drift rotation. Here, (r, θ, z) is a cylindrical coordinate system with the z-axis coincident with the axis of the trap. We consider the plasma column to be a pure electron plasma in this paper.

A diocotron mode of azimuthal mode number m can experience a resonant interaction with the rotating plasma flow at a critical plasma radius $R_{\text{res}}(m)$, where $\omega_m = m\omega_E[R_{\text{res}}(m)]$. Here, m is the azimuthal mode number, ω_m is the mode frequency, and $\omega_E(r) = -cE(r)/Br$ is the local rotation frequency of the plasma.

Linear mode theory[18, 19, 23] predicts that this spatial Landau resonance produces exponential mode damping when the slope of the radial density distribution is negative at the critical radius, and this damping has been observed experimentally for low order azimuthal modes with $m > 1$[23].

The $m = 1$ mode is special in that the resonant radius is at the wall where typically there are no particles. It was long thought that an $m = 1$ mode would not experience damping due to a Landau resonance[18].

However, recent experiments[2] have observed a novel algebraic damping of the $m = 1$ mode, which we believe is a close cousin of Landau damping. In these experiments, transport produces a low density halo of particles that gradually extends out from the plasma core until it reaches the wall. The algebraic damping begins when the halo reaches the resonant region (the wall for $m = 1$), and the damping rate is proportional to the flux of particles through the resonance.

The theoretical picture that we envision for this flux driven algebraic damping is similar to, but distinct from, spatial Landau damping. In both cases, the damping results from an interaction of the mode field with resonant particles, but the particu-

lars of the interactions are very different in the two cases. In spatial Landau damping, the resonant particles are present before the mode is excited, and the damping results from a mode-driven rearrangement of particles near the resonant radius. The analysis is linear and leads to exponential damping.

In contrast, for the new flux-driven algebraic damping, there are no particles initially at the resonant radius. The transport gradually brings particles to the resonant radius, and the mode field then sweeps the particles around the nonlinear cat's eye orbits to a scrape-off layer, causing the damping.

As will be discussed later, the scrape-off layer is a thin region adjacent to the wall where guiding center drift theory breaks down and particles (electrons) are rapidly absorbed by the wall. The scrape-off layer is at least as thick as a cyclotron radius. We will assume that the thickness of the layer is much smaller than the mode amplitude.

While the new theory can be described within a 2D flow framework, the transport and the truncation of particle orbits by the wall are non-ideal elements beyond the $\mathbf{E} \times \mathbf{B}$ drift description.

The paper that reported the experimental results on the new damping also included a short theoretical explanation[2, 3]. To help understand this theory consider Fig. 3.1, which shows the cross section of an electron plasma column that has been displaced off the trap axis through the excitation of an $m = 1$ diocotron mode. The displacement is of magnitude D and direction $\bar{\theta} = 0$. The gray lines are equipotential contours as seen in the mode frame. In this frame the $\mathbf{E} \times \mathbf{B}$ drift flow is along the equipotential contours. The orange shaded region represents the relatively high density plasma core. In this region, the mode potential can be described by linear

theory, and the equipotential curves are simply displaced circles. The resonant region is near the wall, and there nonlinear effects distort the circles. Near the left side of the figure are the "cat's eye" orbits, which describe the motion of particles that are trapped in the wave trough. In order to make the "cat's eye" orbits easier to see in Fig. 3.1, the ratio of the displacement to the wall radius (i.e. D/R_w) was taken to be the largest of experiment values at 0.1.

In addition to the $\mathbf{E} \times \mathbf{B}$ drift flow, there is a slow transport flow. The transport produces a low density halo that gradually extends out from the plasma core. A given particle slowly spirals out, moving successively from one contour to another of larger radius.

The green dot-dashed equipotential contours in Fig. 3.1 is the critical contour that just misses the blue dashed scrape-off layer at $\bar{\theta} = 0$. When transport moves an electron through this critical contour, the electron hits the scrape-off layer and is absorbed by the wall before returning to $\bar{\theta} = 0$. The red solid curve in Fig. 3.1 shows the trajectory of such an electron.

The previous theory focuses on the transfer of canonical angular momenta from the plasma core to such electrons. In the guiding center drift approximation, the canonical angular momentum for an electron in the uniform magnetic field of the trap is simply $P_\theta = eBr^2/2c$, where the radial position r is measured from the center of the trap, B is the magnetic field strength and $e = -|e|$ is the electron charge[28, 29]. When an $m = 1$ diocotron mode is excited, the plasma core is displaced off the trap axis by a small amount D, and the core canonical angular momentum per unit length is changed by $N(eB/2c)D^2$, where N is the number of core particles per unit length[23]. This change in angular momentum is called the canonical angular
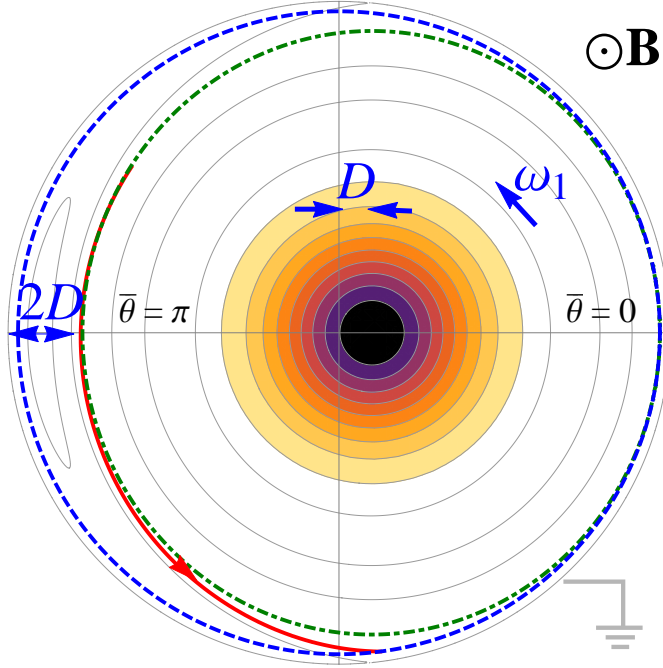
Figure 3.1: Cross section of the electron plasma column in a $m = 1$ mode. The orange shaded region is the plasma core. The gray lines are equipotential contours in the mode frame. The blue dashed curve is the scrape-off layer. The green dot-dashed curve is the critical contour. The red solid curve is a particle trajectory.

momentum of the mode.

When an individual electron $\mathbf{E} \times \mathbf{B}$ drifts in a nearly circular orbit around the displaced center of the plasma core, the radius of the electron measured from the center of the trap oscillates by order $\Delta r \sim D \cos[\bar{\theta}(t)]$. Thus, the electron continually trades angular momentum back and forth with the core, or equivalently with mode. However, the orbit for an electron that crosses the critical contour is truncated by the wall, so there is a net change in angular momentum. Since the thickness of the "cat's eye" orbit is of order D, the net change in angular momentum is of order $\Delta P_\theta \sim (eB/2c)[R_w^2 - (R_w - D)^2] \sim (eB/c)R_w D$. More precisely, the previous derivation[2] obtained the average change in canonical angular momentum

$\langle \Delta P_\theta \rangle = (2/\pi)(eB/c)R_w D.$

Balancing the rate of change of the mode angular momentum against the rate of change of halo particle angular momentum yields the equation

$$\frac{d}{dt} N \frac{eB}{2c} D^2 + \left| \frac{dN}{dt} \right| \langle \Delta P_\theta \rangle = 0, \tag{3.1}$$

where $|dN/dt|$ is the rate per unit length at which halo particles pass through the resonance to the wall. Substituting for $\langle \Delta P_\theta \rangle$ yields the damping rate equation

$$\frac{dD}{dt} = -\frac{2}{\pi} \frac{1}{N} \left| \frac{dN}{dt} \right| R_w = -\gamma, \tag{3.2}$$

with a solution of linear algebraic damping $D(t) = D(0) - \gamma t$.

This simple result captures the experimental observations that the mode amplitude decays as a linear function of time and that the magnitude of the damping rate is proportional to the flux of halo particles through the resonant layer. The predicted magnitude of the damping rate is about half the measured rate.

Although this simple derivation has the advantage of brevity, it leaves questions unanswered. For example, given that the resonant particles cause mode damping, do they also cause a mode frequency shift? Also, why focus exclusively on the thin ribbon of electrons beyond the critical contour, when there are many more resonant electrons? Is it really true that the mode transfers zero net angular angular momentum to these other resonant electrons?

A conceptual issue is the use of angular momentum balance. In fact, the total angular momentum for the plasma core and halo is not conserved. Transport continually changes the angular momentum of the halo particles as these electrons

move out radially.

Also, the simple theory is implicitly based on a zero-diffusion model; the transport is assumed to be due exclusively to mobility. Unfortunately, the zero-diffusion model leads to an infinite density gradient at the leading edge of the halo, and such a gradient cannot be maintained in the presence of even a small diffusion coefficient. For the experimental conditions, diffusion affects the orbits of all the particles deemed responsible for damping in the simple theory. Indeed the whole idea of well-defined orbits looses meaning in the face of such diffusion. The orbits are diffusively broadened.

What is needed is a new, more rigorous theory based on a solution of the coupled Poisson and transport equations. Such a theory talks about an evolving density, rather the particle orbits, and makes no assumption about conservation of angular momentum.

We note at the outset, however, despite the problems listed above, the damping rate given in Eq. (3.2) will survive in the new theory, provided that the diffusion coefficient is sufficiently small, as defined by inequalities given later. The simple theory needs a more rigorous backup, indeed is wrong in detail, but captures the essence of the physics. The new theory does predict a frequency shift

$$\Delta\omega = \frac{32}{3}\frac{ecD}{BR_w}n^{(0)}(R_1),\tag{3.3}$$

where $n^{(0)}(R_1)$ is the unperturbed density in the resonant region of the halo.

The new theory preserves an important simplification of the traditional linear theory for an $m = 1$ diocotron mode[21]. For any unperturbed density perturbation $n^{(0)}(r)$ that is monotonically decreasing in r and goes to zero for some $r > R_w$, the

mode perturbation results from a uniform displacement D of the plasma column off the trap axis. The displaced column produces an image in the conducting wall, and in the linear limit (i.e. $D/R_w \ll 1$), the electric field from the image is uniform over the whole column, producing a uniform $\mathbf{E} \times \mathbf{B}$ drift of the whole column transverse to the displacement $\mathbf{D}$. This uniform motion of the column around the trap axis is the mode.

In the traditional theory, there are no resonant particles near the wall, but the theory presented here must include such particles. Moreover, the perturbed charge density of the resonant particles produces an electric field that acts back on the plasma core, and one might worry that this field would spoil the picture of uniform core displacement. However, that is not the case.

The resonant particles are well outside the plasma core, so the field from the resonant particles is a vacuum field in the region of the core. The dipole portion of this field is the portion that drives the mode resonantly, and a dipole vacuum field is uniform. Recall that a dipole vacuum potential can be written in the form

$$\delta\phi(r, \theta, t) = -\delta E_x(t) r \cos\bar{\theta} - \delta E_y(t) r \sin\bar{\theta}, \tag{3.4}$$

where $\delta E_x(t)$ is the uniform field along the direction $\bar{\theta} = 0$ and $\delta E_y(t)$ is the uniform field along $\bar{\theta} = \pi/2$. We assume that the halo density is small, so the uniform field $\delta E_x(t)\hat{x} + \delta E_y\hat{y}$ is a small increment to the uniform field from the image in the wall and produces only a small increment in the uniform drift velocity of the core. Thus, the core perturbation is still a uniform displacement.

In Section 3.3, the damping rate $\dot{D}$ and the frequency shift $\Delta\omega$ are obtained as Green's function integrals over the perturbed charge density in the resonant region.

To obtain these integral expressions, the perturbed charge density of the core is taken to be of the form arising from a uniform displacement.

The integral expressions can be rewritten in the form

$$\dot{D} = \frac{c}{B}\delta E_y(t), \, D\Delta\omega = -\frac{c}{B}\delta E_x(t), \tag{3.5}$$

which yields a simple physical interpretation. The component of the uniform field from the resonant particles that is transverse to the displacement (δE_y) cause an $\mathbf{E} \times \mathbf{B}$ drift motion of the core back toward the trap axis, that is, a damping of the mode. Likewise, the component of the field along the displacement (δE_x) causes an increment to the $\mathbf{E} \times \mathbf{B}$ drift velocity around the trap axis, that is, a mode frequency shift.

A second re-writing of the integral expression for $\dot{D}$ clarifies the issue of angular momentum conservation. The equation can be re-written as a statement that the torque exerted by the core on the resonant particles is equal and opposite to the torque exerted by the resonant particles back on the core. Two opposing torques are equal and opposite even if a third torque (say, due to the transport) acts. The treatment based on Poisson's equation correctly, and automatically, focuses on torque balance, rather than angular momentum balance.

For the conditions of the experiment, we will see that the transport caused change in angular momentum of electrons being swept to the wall is small compared to the change caused by the mode field, so the angular momentum balance is approximately correct. Nevertheless, the calculation of the damping rate should at least start from a rigorous foundation based on torque balance.

To obtain explicit expressions for the damping rate and frequency shift, the

transport equation must be solved for the halo density distribution in the resonant region and the result substituted into the Green's function integrals. As a first step, the transport equation is discussed and simplified in Section 3.4.

Note that the halo evolution takes place in two stages. First the halo extends radially outward until it reaches to the wall. At the wall, the electrons are continuously absorbed, and a quasi-steady state density distribution is established. We calculate the damping rate and frequency shift for this density distribution.

Section 3.5 obtains simple analytic expressions for the density distribution, damping rate and frequency shift by using an idealized transport model: zero diffusion coefficient and constant coefficient of mobility. The $\mathbf{E} \times \mathbf{B}$ drift flow and mobility flow are then both incompressible and can be incorporated in a Hamiltonian description of the electron orbits. This idealized model implicitly underlies the simple theory[2, 3], but leads to an infinite density gradient at the leading edge of the halo, which is untenable.

Section 3.6 includes the effect of diffusive broadening at the leading edge gradient. For the conditions of the experiments, the broadening substantially modifies the density distribution and the orbits in the region that determines the damping rate, so one might expect that the answer for the damping rate would be substantially changed. However, the Green's function integral for the damping rate can be rewritten in an approximate form that involves only the flux entering the broadening layer, and this form again yields the zero-diffusion damping rate in Eq. (3.2). The approximation requires that the diffusion coefficient be sufficiently small, as will be specified by inequalities in Section 3.6. Subject to these inequalities the frequency shift is also relatively unchanged.

Numerical solutions for the diffusively broadened density distribution are obtained in Appendix B and are used in the Green's function integral to obtain numerical results for the damping rate. The numerical results are in good agreement with the approximate analytic result of Section 3.6.

Section 3.7 obtains a perturbative correction to the damping rate to account for the slow time dependence in $D(t)$. This time dependence causes the contours themselves to move, and the corrected damping rate is proportional to the flux through the moving contour. For the conditions of the experiment the correction is small.

Finally, Section 3.8 is a discussion on the general applicability of this flux-driven damping mechanism.

3.3   Green's function solution for the mode damping rate and frequency shift

In this section, we obtain expressions for the mode damping rate and frequency shift as Green's function integrals over the perturbed charge density in the resonant region of the halo. To complete the calculation and obtain explicit expressions for the damping rate and frequency shift, one must solve for the perturbed charge density in the resonant region and substitute into the Green's function integrals. This second part of the calculation is deferred to later sections.

The linear $m = 1$ diocotron mode has the happy property[14, 49, 21] that the self-consistent density perturbation, mode potential and mode frequency are known analytically for any unperturbed density profile $n^{(0)}(r)$ that is monotonically decreasing in r and goes to zero for some $r < R_w$. The self-consistent density perturbation

and mode potential are given by the expressions

$$\delta n(r, \theta, t) = -\frac{\partial n^{(0)}}{\partial r} D \cos(\theta - \omega_1 t - \alpha), \tag{3.6}$$

$$\delta \phi(r, \theta, t) = -\frac{rB}{c}[-\omega_1 + \omega_E(r)]D \cos[\theta - \omega_1 t - \alpha], \tag{3.7}$$

where $\omega_1 \equiv \omega_E(R_w)$ is the mode frequency. As mentioned above, the mode can be understood as a uniform displacement of the plasma column off the trap axis. From Eq. (3.6), one can see that the displacement is of magnitude D and in the instantaneous direction $\theta = \omega_1 t + \alpha$, where α is a phase shift. In Fig. (3.1), the angle in the wave frame is simply $\bar{\theta} = \theta - \omega_1 t - \alpha$.

The term $(rB/c)\omega_1 D \cos(\theta - \omega_1 t - \alpha)$ in the potential represents a uniform electric field due to the image of the displaced plasma in the conducting wall. Recall that the image is located far outside the wall in the linear theory limit where $D \ll R_w$. The uniform field produces a uniform $\mathbf{E} \times \mathbf{B}$ drift of the plasma as a whole. The direction of the image field is always along the direction of the instantaneous displacement, so the uniform drift velocity moves the plasma around the trap axis. The other term in the mode potential, $(-rB/c)\omega_E(r)D \cos(\theta - \omega_1 t - \alpha)$, simply accounts for a shift in the origin of the radial space charge field of the plasma column itself.

In this theory, there are no particles in the resonant region near the wall. However, here such particles must be included. As we will see, the mode potential acting on the resonant particles produces a perturbed resonant particle charge density, and this charge density produces a correction to the mode potential. This correction acts back on the particles in the non-resonant region causing a correction to the $\mathbf{E} \times \mathbf{B}$ drift motion. Nevertheless, we will postulate that the perturbed charge density in the

non-resonant region continues to be of the form given by Eq. (3.6). Physically, the perturbation in the non-resonant region is still a uniform displacement.

Why is this the case? The resonant particles near the wall are all outside the non-resonant region, so the correction potential is a vacuum potential in the non-resonant region. Moreover, the dipole component of such potential represents a uniform electric field. Thus, the $\mathbf{E} \times \mathbf{B}$ drift velocity from this field is uniform over the whole non-resonant region and provides a small correction to the uniform drift velocity produced by the linear mode potential in Eq. (3.7). As we will see, the correction can be accounted for simply by allowing D and α in Eq. (3.6) to be time-dependent.

What is omitted in this description? First, the nonlinear orbits in the resonant region create density perturbations with azimuthal mode number greater than 1, and these harmonic perturbations produce fields in the non-resonant region that are not uniform. However, these harmonic fields do not drive the $m = 1$ diocotron mode resonantly, and the density perturbations produced are negligibly small.

Also neglected is an even smaller correction to the perturbed density in the non-resonant region that is caused by the transport. This correction is linear in mode amplitude and can lead to the kind of exponential damping or growth discussed earlier by Davidson and Chao[21]. We neglect this effect and focus on the interaction of the mode with resonant particles. This choice is motivated by the experimental observation that the damping begins only when the halo particles reach the resonant region. The present theory is complementary to the earlier theory of Davidson and Chao[21].

The $m = 1$ Fourier components of the potential and density are related through

the Green's function solution[23]

$$\delta\phi_1(r,t) = -4\pi e \int_0^{R_w} 2\pi r'dr'G_1(r|r')\delta n_1(r',t), \qquad (3.8)$$

where

$$G_1(r|r') = \frac{1}{4\pi}\begin{cases} \dfrac{r}{r'}\left(\dfrac{r'^2}{R_w^2}-1\right) & r < r' \\ \dfrac{r'}{r}\left(\dfrac{r^2}{R_w^2}-1\right) & r' < r \end{cases} \qquad (3.9)$$

is the Green's function and

$$\delta\phi_1(r,t) = \int_0^{2\pi}\frac{d\theta}{2\pi}e^{-i\theta}\delta\phi(r,\theta,t) \qquad (3.10)$$

$$\delta n_1(r,t) = \int_0^{2\pi}\frac{d\theta}{2\pi}e^{-i\theta}\delta n(r,\theta,t) \qquad (3.11)$$

are the Fourier components of the perturbed potential and density. Note that the Green's function satisfies the required boundary condition $G_1(R_w|r') = 0$. Also, note that Eq. (3.8) is valid whether or not linear theory can be used to find the density perturbation.

We postulate that the perturbed density can be written as

$$\delta n(r,\theta,t) = -D\cos(\theta-\omega_1 t-\alpha)\frac{\partial n^{(0)}}{\partial r}\mathcal{U}(R_1-r) + \delta n'(r,\theta,t), \qquad (3.12)$$

where $\mathcal{U}(R_1-r)$ is a step-function and R_1 is the outer limit of the non-resonant region, that is, the region where linear theory may be used. The quantity $\delta n'(r,\theta,t)$ is the perturbed charge density in the resonant region (i.e., for $R_1 < r < R_w$). The postulated functional form for the non-resonant region $(r < R_1)$ assumes that the perturbation is still a uniform displacement, even when the field from the resonant

particles is taken into account, as explained in earlier.

Substituting Eq. (3.12) into Eq. (3.8) yields the relation

$$
\begin{aligned}
\delta\phi_1(r,t) &= 4\pi e \frac{D}{2} e^{-i\omega_1 t - i\alpha} \int_0^{R_1} 2\pi r' dr' G_1(r|r') \frac{\partial n^{(0)}}{\partial r'} \\
&\quad -4\pi e \int_{R_1}^{R_w} 2\pi r' dr' G_1(r|r') \delta n_1'(r,t),
\end{aligned}
\tag{3.13}
$$

where

$$
\delta n_1'(r,t) = \int_0^{2\pi} \frac{d\theta}{2\pi} \delta n'(r',\theta,t) e^{-i\theta}
\tag{3.14}
$$

is the Fourier component of $\delta n'(r,\theta,t)$. In evaluating the Green's function integrals, one must be careful to use the correct form of $G_1(r|r')$ depending on whether $r > r'$ or $r < r'$.

For the non-resonant region $r < R_1$, the Green's function integral in the first term yields the result

$$
\begin{aligned}
4\pi e \int_0^{R_1} 2\pi r' dr' G_1(r|r') \frac{\partial n^{(0)}}{\partial r'} &= 4\pi e \left[\int_0^r 2\pi r' dr' G_1(r|r') \frac{\partial n^{(0)}}{\partial r'} \right. \\
&\quad \left. + \int_r^{R_1} 2\pi r' dr' G_1(r|r') \frac{\partial n^{(0)}}{\partial r'} \right] \\
&= 2er \left[\frac{N(r)}{r^2} - \frac{N(R_1) + \pi n^{(0)}(R_1)(R_w^2 - R_1^2)}{R_w^2} \right],
\end{aligned}
\tag{3.15}
$$

where both integrals on the Right Hand Side have been integrated by parts and $N(r) \equiv \int_0^r 2\pi r' dr' n^{(0)}(r')$. For the resonant region $R_1 < r < R_w$, the Green's function

integral in the first term yields the result

$$4\pi e \int_0^{R_1} 2\pi r' dr' G_1(r|r') \frac{\partial n^{(0)}}{\partial r'} = -2er\left(\frac{1}{R_w^2} - \frac{1}{r^2}\right)[N(R_1) - \pi R_1^2 n^{(0)}(R_1)], \quad (3.16)$$

where again integration by parts has been used.

We will need the potential in the resonant region later; here we focus on the potential in the non-resonant region, where Eq. (3.13) reduces to the form

$$\frac{c}{B}\delta\phi_1(r,t)e^{i\omega_1 t + i\alpha} = [\omega_1 - \omega_E(r)]\frac{D}{2}r - \frac{4\pi ec}{B}\int_{R_1}^{R_w} 2\pi r' dr' G_1(r|r')\delta n_1'(r',t)e^{i\omega_1 t + i\alpha}.$$

$$(3.17)$$

Here, $\omega_E(r) = -2ecN(r)/Br^2$ is the rotation frequency, and ω_1 is given by $\omega_E(R_w)$, assuming that the density takes the constant value $n^{(0)}(R_1)$ in the resonant region $R_1 < r < R_w$. Note that the first term on the Right Hand Side of Eq. (3.17) has the same form as the coefficient of $\cos(\theta - \omega_1 t - \alpha)$ in Eq. (3.7) for the linear diocotron mode.

We will see that the density is not in fact constant in the resonant region; particles are excluded from the closed cat's eye orbits, and the frequency shift $\Delta\omega$ accounts for this fact.

The linearized continuity equation[14] in the non-resonant region takes the form

$$\left[\frac{\partial}{\partial t} + i\omega_E(r)\right]\delta n_1(r,t) = \frac{ic}{Br}\delta\phi_1(r,t)\frac{\partial n^{(0)}}{\partial r}, \quad (3.18)$$

where a small correction to $\delta n_1(r,t)$ due to transport has been neglected.

Solving for $\delta\phi_1(r,t)$ in Eq. (3.17) and substituting into Eq. (3.18) yields the

relation

$$
re^{i\omega_1 t + i\alpha} \left[\frac{1}{i} \frac{\partial}{\partial t} + \omega_E(r) \right] \frac{\delta n_1(r,t)}{\partial n^{(0)}/\partial r}
$$

$$
= -[\omega_E(r) - \omega_1] \frac{D}{2} r - \frac{4\pi ec}{B} \int_0^{R_w} 2\pi r' dr' G_1(r|r') \delta n_1'(r',t) e^{i\omega_1 t + i\alpha}. \quad (3.19)
$$

For a self-consistent solution, this equation must be satisfied when the non-resonant density perturbation postulated as the first term in Eq. (3.12) is substituted for $\delta n(r,t)$. Substituting and carrying out the time derivatives yield the equation

$$
-\frac{r}{2} \left\{ \frac{1}{i} \frac{\partial D}{\partial t} - \frac{\partial \alpha}{\partial t} D + [\omega_E(r) - \omega_1] D \right\}
$$

$$
= -[\omega_E(r) - \omega_1] \frac{D}{2} r - \frac{4\pi ec}{B} \int_0^{R_w} 2\pi r' dr' G_1(r|r') \delta n_1'(r',t) e^{i\omega_1 t + i\alpha}.
$$

$$
(3.20)
$$

The two terms in square brackets cancel, leaving the result

$$
-i\frac{\partial D}{\partial t} - \frac{\partial \alpha}{\partial t} D = \frac{8\pi ec}{Br} \int_{R_1}^{R_w} 2\pi r' dr' G_1(r|r') \delta n_1'(r',t) e^{i\omega_1 t + i\alpha}. \quad (3.21)
$$

In the non-resonant region ($r < R_1$), the upper form for the Green's function in Eq. (3.9) must be used, and this form is proportional to r. Thus, the r-dependence on the Right Hand Side of Eq. (3.21) cancels. When $D\partial\alpha/\partial t$ and $i\partial D/\partial t$ are chosen to match the real and imaginary time-dependence of the Right Hand Side, we have a self-consistent solution.

Using Eq. (3.14) and taking the real and imaginary parts of Eq. (3.21) yields

the desired integral expressions for the damping rate and frequency shift

$$\frac{\partial D}{\partial t} = \frac{8\pi ec}{Br} \int_{R_1}^{R_w} r' dr' \int_0^{2\pi} d\theta G_1(r|r') \delta n'(r', \theta, t) \sin[\theta - \omega t - \alpha], \qquad (3.22)$$

$$D\frac{\partial \alpha}{\partial t} = D\Delta\omega = -\frac{8\pi ec}{Br} \int_{R_1}^{R_w} r' dr' \int_0^{2\pi} d\theta G_1(r|r') \delta n'(r', \theta, t) \cos[\theta - \omega t - \alpha],$$

$$(3.23)$$

where $\Delta\omega \equiv \partial\alpha/\partial t$ is the frequency shift.

The argument of the sine and cosine functions in Eqs. (3.22) and (3.23) [i.e., $\bar{\theta} = \theta - \omega_1 t - \alpha$] is the angle measured in the instantaneous rotating frame of the wave, and the $\bar{\theta}$-integrals in these equations are simply the dipole Fourier components of $\delta n'(r, \theta, t)$ evaluated in the rotating frame. In subsequent sections, we will evaluate $\delta n'$ in this rotating frame.

A simple interpretation of Eqs. (3.22) and (3.23) provides a more mechanistic explanation of the damping and frequency shift. The interpretation starts from the observation that the Left Hand Side of the equations [i.e., $\partial D/\partial t$ and $\Delta\omega D$] both have the dimensions of velocity. As mentioned above, the charge density $e\delta n'(r, \theta, t)$ is zero for $r < R_1$, so the corresponding dipole potential produced in the region $r < R_1$ is of the vacuum form

$$\delta\phi'(r, \bar{\theta}, t) = -r\delta E_x \cos\bar{\theta} - r\delta E_y \sin\bar{\theta}, \qquad (3.24)$$

where δE_x and δE_y are independent of $\bar{\theta}$ and r. The Right Hand Sides of Eqs. (3.22) and (3.23) are simply expressions for $(c/B)\delta E_y$ and $-(c/B)\delta E_x$ respectively. Thus, Eq. (3.22) is simply a statement that the field δE_y, from the resonant particle charge density, produces an $\mathbf{E} \times \mathbf{B}$ drift motion of the plasma along the direction

of instantaneous displacement $\mathbf{D}$, that is, a growth or damping of the displacement depending on the sign of δE_y. Likewise, Eqs. (3.23) is a statement that δE_x causes an $\mathbf{E} \times \mathbf{B}$ drift increment to the velocity of the plasma transverse to $\mathbf{D}$, and such an increment causes a frequency shift in the rate of rotation of the plasma around the trap axis, that is, an increment in the mode frequency.

Finally, how does the Green's function solution clarify the issues associated with the angular momentum balance argument[2, 3]? Let $e\delta n_a(r, \bar{\theta})$ and $e\delta n_b(r, \bar{\theta})$ be two perturbed charge densities in a Penning trap. The torque exerted on $e\delta n_a(r, \bar{\theta})$ by the field from $e\delta n_b(r, \bar{\theta})$ is given by the integral

$$
\begin{aligned}
\tau_{a,b} &= -e^2 \int_0^{R_w} r'dr' \int_0^{2\pi} d\bar{\theta}' \int_0^{R_w} rdr \int_0^{2\pi} d\bar{\theta} \\
&\quad \cdot \left\{ \frac{1}{r} \left[\frac{\partial}{\partial \bar{\theta}} G(r, \bar{\theta}, r', \bar{\theta}') \right] \cdot r\delta n_a(r, \bar{\theta}) \delta n_b(r', \bar{\theta}') \right\}.
\end{aligned}
\tag{3.25}
$$

Because the trap has cylindrical symmetry, the Green's function has the functional form $G(r, \bar{\theta}, r', \bar{\theta}') = G(r, r', \bar{\theta} - \bar{\theta}')$. Thus the opposing torques are equal and opposite [i.e., $\tau_{a,b} + \tau_{b,a} = 0$], even if a third torque, such as that due to transport, acts.

Eq. (3.22) for the damping rate is equivalent to such a statement of torque balance. Let $\delta n_a(r, \bar{\theta})$ be the perturbed charge density of the non-resonant region [i.e., $-D\partial n^{(0)}/\partial r \cos \bar{\theta}$], and let $\delta n_b(r, \bar{\theta})$ be the dipole component of the perturbed charge density of the resonant region [i.e., the dipole component of $\delta n'(r, \bar{\theta})$]. The torque $\tau_{a,b}$ is given by the integral

$$
\tau_{a,b} = \int_0^{R_1} rdr \int_0^{2\pi} d\bar{\theta} (-D \frac{\partial n^{(0)}}{\partial r} \cos \bar{\theta}) \left(-\frac{e}{r} \frac{\partial \delta \phi_b}{\partial \bar{\theta}} \right) r.
\tag{3.26}
$$

Using orthogonality of the sinusoidal functions in the harmonic expansion of $\delta \phi_b(r, \bar{\theta})$,

the $\bar{\theta}$-integral in Eq. (3.26) picks out the term $-rE_y \sin \bar{\theta}$ in the dipole portion of $\delta\phi_b(r, \bar{\theta})$, as given by Eq. (3.24), yielding the result

$$\tau_{a,b} = -\pi D e E_y \int_0^{R_1} r^2 dr \frac{\partial n^{(0)}}{\partial r} = -\pi D \frac{\partial D}{\partial t} \frac{eB}{c} \int_0^{R_1} r^2 dr \frac{\partial n^{(0)}}{\partial r}. \qquad (3.27)$$

Multiplying Eq. (3.22) by $-\pi D (eB/c) r^2 \partial n^{(0)}/\partial r$ and integrating over dr from $r = 0$ to $r = R_1$ yields the equation

$$\tau_{a,b} = -8\pi^2 e^2 \int_{R_1}^{R_w} r' dr' \int_0^{2\pi} d\bar{\theta} \delta n_b(r', \bar{\theta}) \int_0^{R_1} r dr G_1(r|r') \frac{\partial n^{(0)}}{\partial r} D \sin \bar{\theta}, \qquad (3.28)$$

where $\delta n_b(r', \bar{\theta})$ has been substituted for $\delta n'(r', \bar{\theta})$. The potential $\delta\phi_a(r', \bar{\theta})$ is given by the expression

$$\delta\phi_a(r', \bar{\theta}) = -4\pi e \int_0^{R_1} 2\pi r dr G_1(r', r)[-D \frac{\partial n^{(0)}}{\partial r} \cos \bar{\theta}], \qquad (3.29)$$

where $r' > R_1 \geq r$. Using the relation $G_1(r', r) = G_1(r, r')$ for $r' > r$ yields the result

$$\delta\phi_a(r', \bar{\theta}) = 8\pi^2 e D \int_0^{R_1} r dr G_1(r, r') \frac{\partial n^{(0)}}{\partial r} \cos \bar{\theta}, \qquad (3.30)$$

so Eq. (3.26) can be rewritten as the result

$$\tau_{a,b} = -\int_{R_1}^{R_w} r' dr' \int_0^{2\pi} d\bar{\theta} \delta n_b(r', \bar{\theta}) \left(-\frac{e}{r} \frac{\partial \delta\phi_a}{\partial \bar{\theta}} \right) r = -\tau_{b,a}. \qquad (3.31)$$

3.4 Transport equation

The particles move under the combined influence of an $\mathbf{E} \times \mathbf{B}$ drift flow and a radial transport flow, so the density evolves according to the equation

$$\frac{\partial n}{\partial t} + \frac{c}{B}\hat{z} \times \nabla_\perp \phi \cdot \nabla_\perp n + \frac{1}{r}\frac{\partial}{\partial r}r\Gamma_r(r) = 0, \tag{3.32}$$

where $\phi(r, \theta, t)$ is the electric potential and $\Gamma_r(r)$ is the radial transport flux.

We employ a Hamiltonian description of the drift dynamics, where $H(\theta, P_\theta, t) = e\phi[r(P_\theta), \theta, t]$ is the drift Hamiltonian and $(\theta, P_\theta = eBr^2/2c)$ are a canonically conjugate coordinate and momentum pair[50, 29, 51]. One can easily check that the Hamilton's equations of motion[52] are the same as the $\mathbf{E} \times \mathbf{B}$ drift equations in a uniform magnetic field $\mathbf{B} = B\hat{z}$. The Left Hand Side of Eq. (3.32) then can be written in the form

$$\frac{\partial n}{\partial t} + \frac{c}{B}\hat{z} \times \nabla_\perp \phi \cdot \nabla_\perp n = \frac{\partial n}{\partial t} + [n, H], \tag{3.33}$$

where $[n, H]$ is a Poisson bracket[53].

The transport is understood to be due to small static field asymmetries[54], which exert an azimuthal drag force on the rotating plasma, causing a radially outward drift motion. In the experiments[2], the transport flux is varied (i.e., increased) by applying additional field asymmetries.

On general grounds, the flux is expected to be of the Fick's law form[55]

$$\Gamma_r = -\mu\frac{\partial \phi_0}{\partial r}n - \mathcal{D}\frac{\partial n}{\partial r}, \tag{3.34}$$

where the coefficient of mobility μ and the diffusion coefficient $\mathcal{D}$ satisfy the Einstein relation, $\mu = e\mathcal{D}/T < 0$. Here, $-\partial\phi_0/\partial r$ is the unperturbed radial electric field and T is the temperature in the halo region. The Fick's law form follows from the requirement that the flux vanish for a thermal equilibrium density profile, $n(r) = n_0 \exp[-e\phi_0(r)/T]$.

By changing variables from (r, θ, t) to (θ, P_θ, t), Eq. (3.32) takes the form

$$\frac{\partial n}{\partial t} + [n, H] = \frac{\partial}{\partial P_\theta}\left[-\dot{P}_\theta|_T n + \tilde{\mathcal{D}}\frac{\partial n}{\partial P_\theta}\right], \qquad (3.35)$$

where

$$\dot{P}_\theta|_T = -\mu\frac{eB}{c}r\frac{\partial\phi_0}{\partial r}, \tilde{\mathcal{D}} = -\frac{\dot{P}_\theta|_T P_\theta \cdot 2T}{re\partial\phi_0/\partial r}. \qquad (3.36)$$

Here $\dot{P}_\theta|_T$ is the rate at which mobility changes the value of P_θ of a particle. Note that $\tilde{\mathcal{D}}$ is proportional to $\dot{P}_\theta|_T$ and that $\dot{P}_\theta|_T < 0$ and $\tilde{\mathcal{D}} > 0$ since $e\partial\phi/\partial r$ is negative. We will need the transport equation in the resonant region where to a good approximation $er\partial\phi_0/\partial r$ is approximately $-2e^2N$ and P_θ is approximately $P_w \equiv eBR_w^2/2c$, where N is the number of particles per unit length. Thus the transport coefficients takes the simple form

$$\dot{P}_\theta|_T = \mu\frac{B}{c} \cdot 2e^2N, \tilde{\mathcal{D}} = \dot{P}_\theta|_T P_w\frac{T}{Ne^2}. \qquad (3.37)$$

For the experimental conditions, the factor T/Ne^2 in the diffusion coefficient is small (i.e., $T/Ne^2 \sim 10^{-2}$), so the transport is dominated by mobility everywhere except at the leading edge of the halo where a large density gradient enhances the effect of diffusion.

As noted in the last section, it is convenient to work in the rotating frame of

the wave. The generating function[53]

$$F(\theta, \bar{P}_\theta, t) = \bar{P}_\theta[\theta - \omega_1 - \alpha(t)] \tag{3.38}$$

yields a canonical transformation to this frame, with the new coordinate and momentum

$$\bar{\theta} = \theta - \omega_1 t - \alpha(t), \bar{P}_\theta = P_\theta \tag{3.39}$$

and the new Hamiltonian

$$\bar{H} = H + \frac{\partial F}{\partial t} = H - (\omega_1 + \Delta\omega)P_\theta, \tag{3.40}$$

where $\Delta\omega = \dot{\alpha}$. Since $\bar{P}_\theta$ and P_θ are equal, we continue to use P_θ in the new Hamiltonian. To work in the rotating frame, one only needs to replace H by $\bar{H}$ in Eq. (3.35); the Right Hand Side of the equation need not be changed since the radial flux is the same in both frames.

Since the transport flow is slow compared to the $\mathbf{E} \times \mathbf{B}$ drift flow, the halo particles very nearly follow curves of constant $\bar{H}$. Thus, changing independent variables from $(\bar{\theta}, P_\theta, t)$ to $(\bar{\theta}, \bar{H}, t)$ in Eq. (3.35) is useful. The result is the transport equation

$$\left.\frac{\partial n}{\partial t}\right|_{\bar{\theta},\bar{H}} + \left.\frac{\partial n}{\partial \bar{H}}\right|_{\bar{\theta},t} \left.\frac{\partial \bar{H}}{\partial t}\right|_{\bar{\theta},P_\theta} + \left.\frac{\partial n}{\partial \bar{\theta}}\right|_{\bar{H},t} \left.\frac{\partial \bar{H}}{\partial P_\theta}\right|_{\bar{\theta},t} = \left.\frac{\partial \bar{H}}{\partial P_\theta}\right|_{\bar{\theta},t} \frac{\partial}{\partial \bar{H}}[-\dot{P}_\theta|_T n + \tilde{\mathcal{D}} \left.\frac{\partial \bar{H}}{\partial P_\theta}\right|_{\bar{\theta},t} \left.\frac{\partial n}{\partial \bar{H}}\right|_{\bar{\theta},t}]. \tag{3.41}$$

To complete the description of the transport equation, the Hamiltonian $\bar{H}(\bar{\theta}, P_\theta, t)$ is needed. Formally, the Hamiltonian is given by the expression

$$\bar{H} = e\phi_0[r(P_\theta)] + e\delta\phi[r(P_\theta), \bar{\theta}] - (\omega_1 + \Delta\omega)P_\theta, \tag{3.42}$$

where $\phi_0(r)$ is the unperturbed potential and $\delta\phi(r,\bar{\theta})$ is the perturbation caused by the mode.

As mentioned in the introduction, the transport equation can be simplified by using the smallness of the halo density n_h in the resonant region. Our goal is to calculate the damping rate and frequency shift to first order in this small quantity. From Eqs. (3.22) and (3.23) one can see that the integral expressions for the damping rate and frequency shift are already first order small in n_h. Thus, the functional form of the perturbed halo density in the resonant region need only be accurate to zero order in n_h. Likewise, the transport equation, which determines the functional form, need only be accurate to zero order in the halo density.

Of course, n_h is not a dimensionless parameter on which to base a proper ordering scheme. The dimensionless ordering parameter is $N_h/N \equiv (n_h \pi R_w^2)/N$, which has the value 0.1 for typical experimental conditions. As we will see, even the largest of the neglected terms is down by this dimensionless factor.

Let us start by simplifying the Hamiltonian. In the resonant region, where the transport equation and Hamiltonian are needed, the dipole contribution to the perturbed potential is given by the expression

$$
\begin{aligned}
\delta\phi_1(r,t) & = -erD[N(R_1) - \pi R_1^2 n^{(0)}(R_1)]\left(\frac{1}{R_w^2} - \frac{1}{r^2}\right)e^{-i\omega_1 t - i\alpha} \\
& \quad -4\pi e \int_{R_1}^{R_w} 2\pi r' dr' G_1(r|r')\delta n_1'(r',t),
\end{aligned}
\tag{3.43}
$$

where use has been made of Eqs. (3.13) and (3.16). The first term is the contribution to the dipole potential from the non-resonant region, and the second is the contribution from the resonant region. Simple estimates show that the second term is smaller

than the first term by a factor of N_h/N, so we neglect the second term. The higher harmonic contributions to the perturbed potential are comparably small and also are neglected. The constant square bracket in the first term can be replaced by N with a relative error that is down by a factor N_h/N. Finally, there is a small $\bar{\theta}$-independent contribution to the perturbed potential, which we also neglect. The radial electric field from this potential is smaller than that from the unperturbed potential $\phi_0(r)$ by a factor that is much smaller than N_h/N. Thus, the perturbed potential reduces to the simple form

$$\delta\phi(r,\bar{\theta}) = -2eNDr\left(\frac{1}{R_w^2} - \frac{1}{r^2}\right)\cos\bar{\theta}. \tag{3.44}$$

In the resonant region, the Hamiltonian can be simplified further by Taylor expansion with respect to P_θ about $P_\theta = P_w$. Setting $\phi_0(R_w) = 0$, using $\partial\phi_0/\partial r \simeq -2Ne/r$ near the wall and using the resonance condition $\omega_1 = \omega_E(R_w) = (c/BR_w)(\partial\phi_0/\partial r)|_{R_w}$ yield the expansion

$$\bar{H} = \frac{Ne^2}{2}\left\{\left(\frac{P_\theta - P_w}{P_w}\right)^2 - \frac{4D}{R_w}\left(\frac{P_\theta - P_w}{P_w}\right)\left[\cos\bar{\theta} + \frac{R_w P_w \Delta\omega}{2DNe^2}\right]\right\}, \tag{3.45}$$

where higher than second order terms in the small quantity $|P_\theta - P_w|/P_w \sim 4D/R_w$ have been dropped and the purely time-dependent term $\Delta\omega P_w$ has been added.

We will see that the second term in the square bracket is a constant of value $0.6(N_h/N_c)$. This term can be retained in the analysis, but for consistency (and simplicity) is dropped here yielding the reduced Hamiltonian

$$\bar{H} = \frac{Ne^2}{2}\left[\left(\frac{P_\theta - P_w}{P_w}\right)^2 - \left(\frac{P_\theta - P_w}{P_w}\right)\cdot\frac{4D}{R_w}\cos\bar{\theta}\right]. \tag{3.46}$$

The time dependence of the transport equation also can be simplified by using

the smallness of N_h/N. In the introduction, we noted that the halo evolution can be divided into two stages. First the halo extends radially out to the wall. At the wall, particles are continuously absorbed and a quasi-steady state density distribution is established. We calculate the damping rate and frequency shift for this quasi-steady state density distribution.

The modifier "quasi" is used since the density continues to change slowly due to the slow damping, that is, due to the time dependence in $D(t)$, which enters the Hamiltonian. In Sections 4 and 5, we neglect this slow time dependence, that is, neglect the first two terms on the Left Hand Side of Eq. (3.41), to obtain the simplified transport equation

$$\frac{\partial n}{\partial \bar{\theta}}\bigg|_{\bar{H}} = \frac{\partial}{\partial \bar{H}}[-\dot{P}_\theta|_T n + \tilde{\mathcal{D}}\frac{\partial \bar{H}}{\partial P_\theta}\bigg|_{\bar{\theta}} \frac{\partial n}{\partial \bar{H}}\bigg|_{\bar{\theta}}]. \tag{3.47}$$

One expects the corrections due to the neglected time dependence to be small since $\dot{D}(t)$ is first order small in n_h. In Section 6, a perturbative treatment is used to show that the relative correction to the damping rate is approximately $\Delta\gamma/\gamma \simeq 2N_h/N$. The relative correction to the frequency shift is even smaller.

For plotting purposes, it is useful to re-write the reduced Hamiltonian in the scaled form

$$h = p^2 - p\cos\bar{\theta}, \tag{3.48}$$

where

$$p = \left(\frac{P_\theta - P_w}{P_w}\right)\left(\frac{R_w}{4D}\right), \tag{3.49}$$

$$h = \frac{2\bar{H}}{Ne^2}\left(\frac{R_w}{4D}\right)^2. \tag{3.50}$$

Likewise transport equation (3.47) takes the scaled form

$$\left.\frac{\partial n}{\partial \bar{\theta}}\right|_h = \frac{\partial}{\partial h}[\beta n - \delta \left.\frac{\partial h}{\partial p}\right|_{\bar{\theta}} \left.\frac{\partial n}{\partial h}\right|_{\bar{\theta}}]_{\bar{\theta}}, \tag{3.51}$$

where

$$\beta = -\frac{2\dot{P}_\theta|_T}{Ne^2}\left(\frac{R_w}{4D}\right)^2, \tag{3.52}$$

$$\delta = \beta\frac{T}{Ne^2}\left(\frac{R_w}{4D}\right). \tag{3.53}$$

To lowest order in the Taylor expansion, β and δ are treated as constant in the resonant region. Except for the smallest values of D accessed in the experiments, these constants are ordered as $\delta \ll \beta \ll 1$.

Fig. (3.2) shows a contour plot of $h(\bar{\theta}, p)$ in the resonant region near the wall. The ordinate of the plot ranges from $p = 0$, the location of the wall, to $p = -2$, which is enough of the $(\bar{\theta}, p)$ phase space to show the resonant region. Of course, the full phase space extends to much lower values of p where the plasma core is located.

The contours of constant $h(\bar{\theta}, p)$ are the trajectories that would be followed by a particle moving only under the $\mathbf{E} \times \mathbf{B}$ drift flow, and the arrows on the contours indicate the direction of the flow. There are open trajectories extending from $\bar{\theta} = 0$ to $\bar{\theta} = 2\pi$, closed trajectories, and a separatrix between the two. The value of h is positive on the open trajectories, zero on the separatrix, and negative on the closed trajectories. The closed trajectories are the $m = 1$ version of "cat's eye" trajectories, but they do not look like such trajectories since the resonance is at the wall where the mode potential goes to zero.
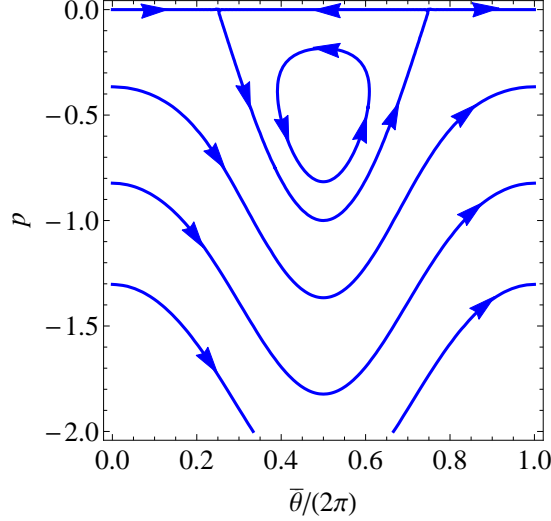
Figure 3.2: Contours of $h(\bar{\theta}, p)$

Solving Eq. (3.48) yields a solution for the trajectories

$$p_{\pm} = \frac{\cos\bar{\theta} \pm \sqrt{\cos^2\bar{\theta} + 4h}}{2}, \tag{3.54}$$

where the minus sign is to be used for the open trajectories, on which $p(\bar{\theta})$ is a single-valued function of $\bar{\theta}$. Both the plus and minus signs are needed for the closed trajectories, where $p(\bar{\theta})$ is double-valued.

Adjacent to the wall, there is a thin scrape-off layer where guiding center drift theory fails, and particles (electrons) are absorbed by the wall. The scrape-off layer is at least as thick as a cyclotron radius, which is of order 10^{-4} cm for the experiments. However, other effects, such as misalignment of and ripples in the magnetic field, likely increase the thickness of the scrape-off layer. In this regard, note that the particles undergo rapid axial bounce motion and azimuthal drift motion relative to the wall, so any region of the wall where the scrape-off mechanism reaches out furthest sets the overall thickness of the scrape-off layer.

The scrape-off mechanism and the thickness of the scrape-off layer Δr are not known experimentally, but we believe that the thickness Δr is small compared to the mode amplitude D, for the range of amplitudes in the experiments. This condition is necessary for the damping rate and the frequency shift to be independent of thickness. Note that a physical thickness Δr corresponds to a scaled momentum thickness $\Delta p = \Delta r / 2D$.

Figure 3.3: Contours of $h = h_c$ (blue solid), $k = h_c$ (red dot-dashed) and the scrape-off layer (black dashed) in the $(\bar{\theta}, p)$ plane.

Fig. (3.3) shows a blow up of the phase space near the scrape-off layer, which for the sake of the figure is taken to have the thickness $\Delta p = 10^{-2}$. The lower edge of the scrape-off layer is shown as the black dashed line at $p = -\Delta p = -10^{-2}$. The solid blue contour is the critical contour, $h(\bar{\theta}, p) = h_c$, which just misses the scrape-off layer at $\bar{\theta} = 0$ and $\bar{\theta} = 2\pi$. Eq. (3.48) implies that the value of h on the critical contour is given by $h_c = (\Delta p)^2 + \Delta p \simeq \Delta p = 10^{-2}$. Also shown is a red dot-dashed curve that will be explained in the next section.
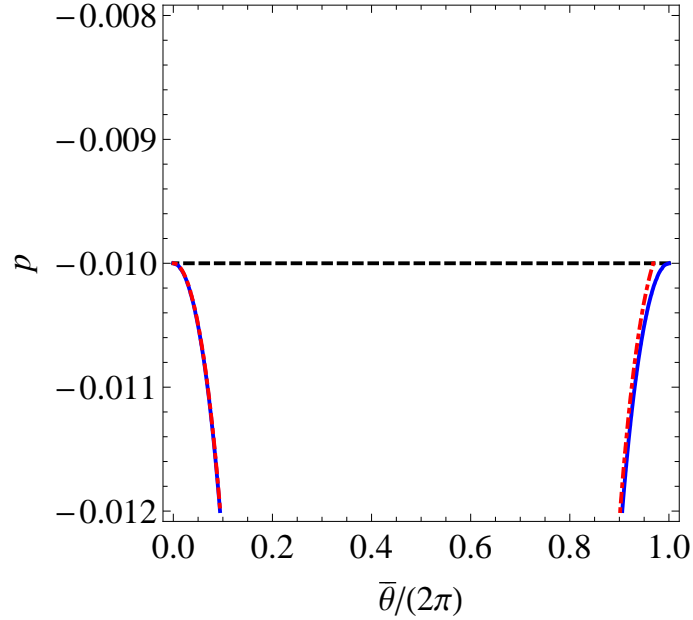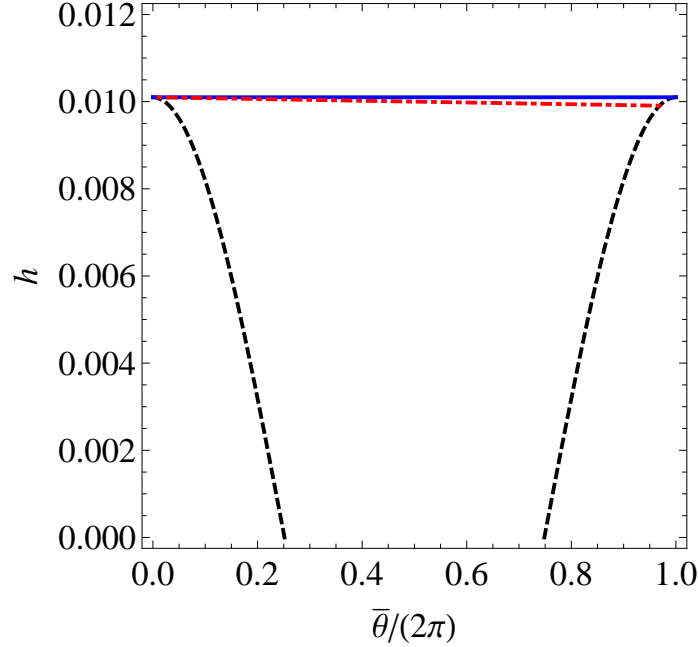
Figure 3.4: Contours of $h = h_c$ (blue solid), $k = h_c$ (red dot-dashed) and the scrape-off layer (black dashed) in the $(\bar{\theta}, h)$ plane.

Fig. (3.4) shows the scrape-off layer and critical contour in $(\bar{\theta}, h)$-space. The solid blue horizontal line is the critical contour $h = h_c \simeq 10^{-2}$, and the black dashed curve is the lower edge of the scrape-off layer at $h = h(\bar{\theta}, -\Delta p) \simeq \Delta p(\cos \bar{\theta})$. Also shown is the red dot-dashed curve of Fig. (3.3).

For orientation, note that p increases upward in Fig. (3.3) and that h increases upward in Fig. (3.4). Thus, the core plasma is below the region shown in Fig. (3.3) and above the region in Fig. (3.4).

In the region $h > h_c$ of Fig. (3.4), the contours of constant h extend from $\bar{\theta} = 0$ to $\bar{\theta} = 2\pi$. Since the points $(\bar{\theta} = 0, h)$ and $(\bar{\theta} = 2\pi, h)$ are the same point physically, we require that $n(\bar{\theta} = 0, h) = n(\bar{\theta} = 2\pi, h)$ in the region $h > h_c$. In the region $0 < h < h_c$, the contours of constant h encounter the scrape-off layer before reaching $\bar{\theta} = 0$ or $\bar{\theta} = 2\pi$. The particle density within the scrape-off layer is taken to be zero. This implies that no particles emerge from the scrape-off layer and, when

diffusion is taken into account, that the particle density at the surface of the scrape-off layer be zero. Otherwise, there would be an infinite density gradient at the surface, which is unsustainable in the face of diffusion.

3.5   Zero diffusion model

As was noted earlier, the scaled diffusion coefficient, δ, is small compared to the scaled mobility coefficient β. Motivated by this observation, the previous calculation[2, 3] of the damping rate assumed the limit of zero diffusion.

A review of this simple model is instructive since it admits a trivial analytic solution for the steady state density profile. Happily, the model yields the same answer for the damping rate and frequency shift as a more realistic model that includes small but finite diffusion [see Section 5].

Setting $\delta = 0$ and treating β as a constant reduces transport equation (3.51) to the simple form

$$\left.\frac{\partial n}{\partial \bar{\theta}}\right|_{h} - \beta \left.\frac{\partial n}{\partial h}\right|_{\bar{\theta}} = 0, \tag{3.55}$$

which immediately yields the solution

$$n(\bar{\theta}, h) = g[h + \beta \bar{\theta}]. \tag{3.56}$$

The flow is incompressible along trajectories of constant $k = h + \beta \bar{\theta}$.

To understand this result physically, note that constant β implies constant $\dot{P}_{\theta}|_{T}$, which in turn implies that the mobility flow is incompressible. The mobility flow can then be incorporated along with the incompressible $\mathbf{E} \times \mathbf{B}$ drift flow in a

Hamiltonian description. One can easily check that the Hamiltonian

$$K(\bar{\theta}, P_\theta) = H(\bar{\theta}, P_\theta) - \dot{P}_\theta|_T \bar{\theta} \tag{3.57}$$

generates both the $\mathbf{E} \times \mathbf{B}$ drift flow and the mobility flow. Since we are neglecting any explicit time dependence in this Hamiltonian, it is a constant of motion, that is, particles flow along curves of constant K. The equation $k = h(\bar{\theta}, p) + \beta \bar{\theta}$ is simply the scaled version of Eq. (3.57). Since the Hamiltonian flow is incompressible, the density is constant along the contour of constant k.

   The red dot-dashed curves in Figs. (3.3) and (3.4) are two views of the critical trajectory $k = h_c$, drawn for the value $\beta = 2 \times 10^{-4}$, which is characteristic of the experimental conditions. This trajectory just misses the scrape-off layer at $\bar{\theta} = 0$ but enters the scrape-off layer just to the left of $\bar{\theta} = 2\pi$.

   For the region $h > h_c$, the periodic boundary condition $n(\bar{\theta} = 0, h) = n(\bar{\theta} = 2\pi, h)$ plus the solution in Eq. (3.56) implies the relation $n(\bar{\theta} = 0, h) = n(\bar{\theta} = 2\pi, h+2\pi\beta)$. Thus, $n(\bar{\theta} = 0, h)$ must be constant in the region $h > h_c$. The possibility of a periodic component with the very short periodicity scale $\delta h \sim 2\pi\beta$ is ruled out by even small diffusion. This conclusion will be clarified in the next section.

   Every point above the red dot-dashed contour in Fig. (3.4), that is, above the trajectory $k = h_c$, lies on a trajectory that emerges from the line interval $(\bar{\theta} = 0, h > h_c)$, on which the density has a constant value. Thus, the density in the whole region above the red dot-dashed trajectory has this constant value. The density below the red dot-dashed trajectory is zero, because there the points lie on trajectories that

emerge from the scrape-off layer. Thus, the density is given by the expression

$$n(\bar{\theta}, h) = n^{(0)}(R_1)\mathcal{U}[h - h_c + \beta\bar{\theta}], \tag{3.58}$$

where $\mathcal{U}(x)$ is a step-function, and we have identified the value of the constant density as $n_0(R_1)$, the density at the beginning of the resonant region.

Eqs. (3.22) and (3.23) for the damping rate and frequency shift can be re-written in the form

$$\frac{\partial D}{\partial t} = \frac{ecR_w}{B}\left(\frac{4D}{R_w}\right)^2 \int_0^{2\pi} d\bar{\theta}\sin\bar{\theta}\int_{p(R_1)}^0 pdp \cdot n[\bar{\theta}, h(\bar{\theta}, p)], \tag{3.59}$$

$$D\Delta\omega = -\frac{ecR_w}{B}\left(\frac{4D}{R_w}\right)^2 \int_0^{2\pi} d\bar{\theta}\cos\bar{\theta}\int_{p(R_1)}^0 pdp \cdot n[\bar{\theta}, h(\bar{\theta}, p)], \tag{3.60}$$

where the relations

$$r'dr' = 2DR_w dp \tag{3.61}$$

$$\frac{G_1(r|r')}{r} = \frac{1}{4\pi r'}\left(\frac{r'^2}{R_w^2} - 1\right) \simeq \frac{Dp}{\pi R_w^2} \tag{3.62}$$

have been used, and the Green's function has been Taylor expanded about $r' = R_w$ in the last step of Eq. (3.62).

Substituting Eq. (3.58) for the density and carrying out the p-integrals yields the expressions

$$\frac{\partial D}{\partial t} = \frac{ecR_w}{B}\left(\frac{4D}{R_w}\right)^2 n^{(0)}(R_1)\int_0^{2\pi} d\bar{\theta}\frac{\sin\bar{\theta}}{2}\{p_-^2[\bar{\theta}, h_c - \beta\bar{\theta}] - p^2(R_1)\}, \tag{3.63}$$

$$D\Delta\omega = -\frac{ecR_w}{B}\left(\frac{4D}{R_w}\right)^2 n^{(0)}(R_1)\int_0^{2\pi} d\bar{\theta}\frac{\cos\bar{\theta}}{2}\{p_-^2[\bar{\theta}, h_c - \beta\bar{\theta}] - p^2(R_1)\}, \tag{3.64}$$

where $p_-(\bar{\theta}, h)$ is given by Eq. (3.54) with the minus sign chosen.

In the curly brackets of both integrals, the constant term $p^2(R_1)$ integrates to zero. Using the smallness of β, the other term in the curly brackets may be Taylor expanded yielding the expression

$$p_-^2[\bar{\theta}, h_c - \beta\bar{\theta}] = p_-^2(\bar{\theta}, h_c) - 2p_-(\bar{\theta}, h_c)\left[\frac{\partial p_-}{\partial h}(\bar{\theta}, h_c)\right]\beta\bar{\theta}. \tag{3.65}$$

The first term in this Taylor expansion does not integrate to zero when substituted into Eq. (3.64) for the frequency shift, so the smaller, second term may be neglected, yielding the expression

$$D\Delta\omega = -\frac{ecR_w}{B}\left(\frac{4D}{R_w}\right)^2 n^{(0)}(R_1)\int_0^{2\pi} d\bar{\theta}\frac{\cos\bar{\theta}}{2}p_-^2(\bar{\theta}, h_c). \tag{3.66}$$

For $h_c \ll 1$, Eq. (3.54) implies that $p_-^2(\bar{\theta}, h_c)$ is approximately given by $\cos^2\bar{\theta}$ in the interval $\pi/2 < \bar{\theta} < 3\pi/2$ and is nearly zero elsewhere. Thus, Eq. (3.66) reduces to the result

$$\begin{aligned}
\Delta\omega &= -\frac{ecR_w}{BD}\left(\frac{4D}{R_w}\right)^2 n^{(0)}(R_1)\int_{\pi/2}^{3\pi/2} d\bar{\theta}\frac{\cos^3\bar{\theta}}{2} \\
&= \frac{32}{3}\frac{ecn^{(0)}(R_1)}{B}\frac{D}{R_w}.
\end{aligned} \tag{3.67}$$

Eqs. (3.15) and (3.17) show that the frequency ω_1 has the value $\omega_E(R_w)$, assuming that the density has the constant value $n^{(0)}(R_1)$ in the resonant region $R_1 < r < R_w$. For the density solution given by Eq. (3.56), the density does not extend at the constant value $n^{(0)}(R_1)$ to the wall, but only to the dot-dashed trajectory in Figs. (3.3) and (3.4). The particles are excluded from the closed cat's eye orbits

adjacent to the wall. The frequency shift accounts for this exclusion, yielding an effective exclusion length of $\Delta r = (8/3\pi)D$.

In progressing from Eq. (3.45) to Eq. (3.46), the quantity $(R_w P_w \Delta\omega)/(2DNe^2)$ was dropped, anticipating that it would be small compared to unity. Substituting for $\Delta\omega$ from Eq. (3.67) shows that the quantity is indeed small:

$$\frac{R_w P_w \Delta\omega}{2DNe^2} = \frac{8}{3}\frac{R_w^2 n^{(0)}(R_1)}{N} \simeq 0.06. \tag{3.68}$$

In Eq. (3.63) for the damping rate, the first term in Taylor expansion (3.65) integrates to zero, since $p_-^2(\bar{\theta}, h)$ is even in $\bar{\theta}$ about $\bar{\theta} = \pi$ and $\sin\bar{\theta}$ is odd. Thus, the integral is determined solely by the second term in the Taylor expansion and reduces to the form

$$\frac{\partial D}{\partial t} = -\frac{ecR_w}{B}\left(\frac{4D}{R_w}\right)^2 n^{(0)}(R_1) \int_0^{2\pi} d\bar{\theta}\sin\bar{\theta} p_-(\bar{\theta}, h_c)\left[\frac{\partial p_-}{\partial h}(\bar{\theta}, h_c)\right]\beta\bar{\theta}. \tag{3.69}$$

Eqs. (3.48) and (3.54) imply the relation

$$p_-(\bar{\theta}, h_c)\left[\frac{\partial p_-}{\partial h}(\bar{\theta}, h_c)\right] = \frac{-\cos\bar{\theta} + \sqrt{\cos^2\bar{\theta} + 4h}}{2\sqrt{\cos^2\bar{\theta} + 4h}}. \tag{3.70}$$

For $h = h_c \simeq \Delta p \ll 1$, the Right Hand Side has the approximate value 1 for $\pi/2 < \bar{\theta} < 3\pi/2$ and is nearly zero elsewhere. Thus, Eq. (3.69) yields the result

$$\begin{aligned}\frac{\partial D}{\partial t} &= -\frac{ecR_w}{B}\left(\frac{4D}{R_w}\right)^2 n^{(0)}(R_1)\int_{\pi/2}^{3\pi/2} d\bar{\theta}\sin\bar{\theta}\beta\bar{\theta} \\ &= +\frac{ecR_w}{B}\left(\frac{4D}{R_w}\right)^2 n^{(0)}(R_1)\cdot 2\beta.\end{aligned} \tag{3.71}$$

By using Eq. (3.52) and the relation

$$n^{(0)}(R_1)\dot{P}_\theta|_T = \frac{eB}{2\pi c}\left|\frac{dN}{dt}\right|,$$ (3.72)

Eq. (3.71) reduces to the previous result for the damping rate[2, 3], as given by Eq. (3.2).

The second term in Taylor expansion (3.65) represents the particle density in the region between the solid and the dot-dashed curves of Figs. (3.3) and (3.4) [i.e., between $h = h_c$ and $k = h_c$], so the damping rate is determined exclusively by particles in this region. From Fig. (3.3), one can see that these are particles that are being swept around the cat's eye orbits to the scrape-off layer and wall.

The previous calculation[2, 3] guessed that the wave torque is dominantly applied to these particles, approximated that torque by the the rate of change of angular momentum of the particles, and evaluated the change in angular momentum using the zero diffusion orbits discussed in this section.

A particle enters the region between the solid and the dot-dashed curves when mobility transports the particle through the contour $h = h_c$. The rate at which particles flow through this contour between $\bar{\theta}$ and $\bar{\theta}+d\bar{\theta}$ is proportional to $\beta n d\bar{\theta}$. Since βn is constant, the flux is uniform in $\bar{\theta}$. Since all of the particles enter the scrape-off layer at $p = -\Delta p$, the average change in angular momentum for the particles is simply

$$\langle \Delta P_\theta \rangle = \int_0^{2\pi} \frac{d\bar{\theta}}{2\pi} P_w \frac{4D}{R_w}[-\Delta p - p_-(\bar{\theta}, h_c)].$$ (3.73)

Using the inequality $h_c \simeq \Delta p \ll 1$ and Eq. (3.54) yields the result

$$\Delta P_\theta \simeq -\frac{eBR_w}{\pi c} \int_{\pi/2}^{3\pi/2} d\bar{\theta} \cos\bar{\theta} = \frac{2}{\pi}\frac{eBR_w D}{c}, \qquad (3.74)$$

which is the result quoted in the introduction. The rate of change of angular momentum was then written as $|dN/dt|\langle\Delta P_\theta\rangle$ and used as the torque in the torque balance equation to obtain the damping rate in Eq. (3.2).

Since this previous calculation approximates the wave torque on the halo particles by the rate of change of halo particle angular momentum, omitting the torque due to the transport, one may ask why the present and previous calculations agree. The answer is that the torque exerted on a particle while it is being swept around the cat's eye orbit is small, of order β. Also, the quantity $|dN/dt|$ is first order in β, so the correction would be of order β^2. Likewise in the Taylor expansion of Eq. (3.65) only the term first order in β was retained. Thus, the two calculations are accurate only to order β, and differences would appear in order β^2.

3.6   Diffusive broadening

An obvious criticism of the zero-diffusion model is that it leads to an infinite density gradient at the leading edge of the halo [i.e. at $k = h_c$], and even a small diffusion gradient must broaden such a gradient. This broadening is worrisome since the damping rate in the zero diffusion model is determined by a thin ribbon of particles at the leading edge of the halo. Moreover, for the conditions of the experiments, the diffusively broadened layer is much wider than the ribbon. Nevertheless, we will find that the answer for the damping rate is not changed significantly, provided the

diffusive broadening is not too large, as will be specified by constraints on the size of the diffusion coefficient.

Numerical solutions of transport equation (3.51) are obtained in Appendix B. The boundary conditions imposed on the solution are that $n(\bar{\theta}, h)$ approaches the constant value $n^{(0)}(R_1)$ for sufficiently large h, that $n(\bar{\theta} = 0, h) = n(\bar{\theta} = 2\pi, h)$ for $h > h_c$ and that $n(\bar{\theta}, h)$ be zero at the surface of the scrape-off layer. The dynamics itself will prevent particles from reaching the contour $h = 0$.

Figure 3.5: Contour plot of the relative density $n(\bar{\theta}, h)/n^{(0)}(R_1)$. The black dashed line is the scrape-off layer. The solid blue line and the red dot-dashed line are the critical contours $h = h_c$ and $k = h_c$. The blue dotted line represents the diffusive broadening layer $(\Delta h)_2$.

Fig. (3.5) shows a contour plot of the relative density $n(\bar{\theta}, h)/n^{(0)}(R_1)$ obtained

for the transport coefficient values $\beta = 10^{-5}$ and $\delta = 4 \times 10^{-7}$, which are characteristic values for the experiments. Only the relative density need be specified since the transport equation is linear and the boundary conditions are homogeneous. The critical contour $h = h_c$ is again drawn as a solid blue line. Likewise, the red dot-dashed line is the trajectory $k = h_c$, and the dashed black curves are the surface of the scrape-off layer. Clearly the thin ribbon between the solid blue line and the dot-dashed red line is very narrow compared to the width of the diffusive broadening.

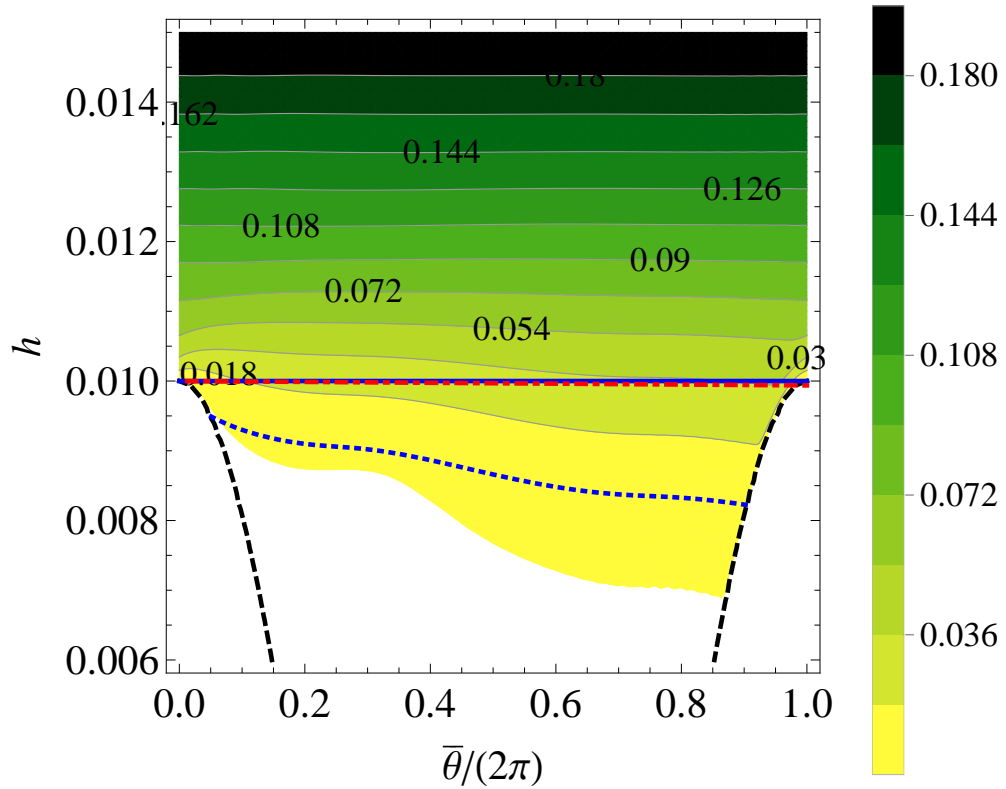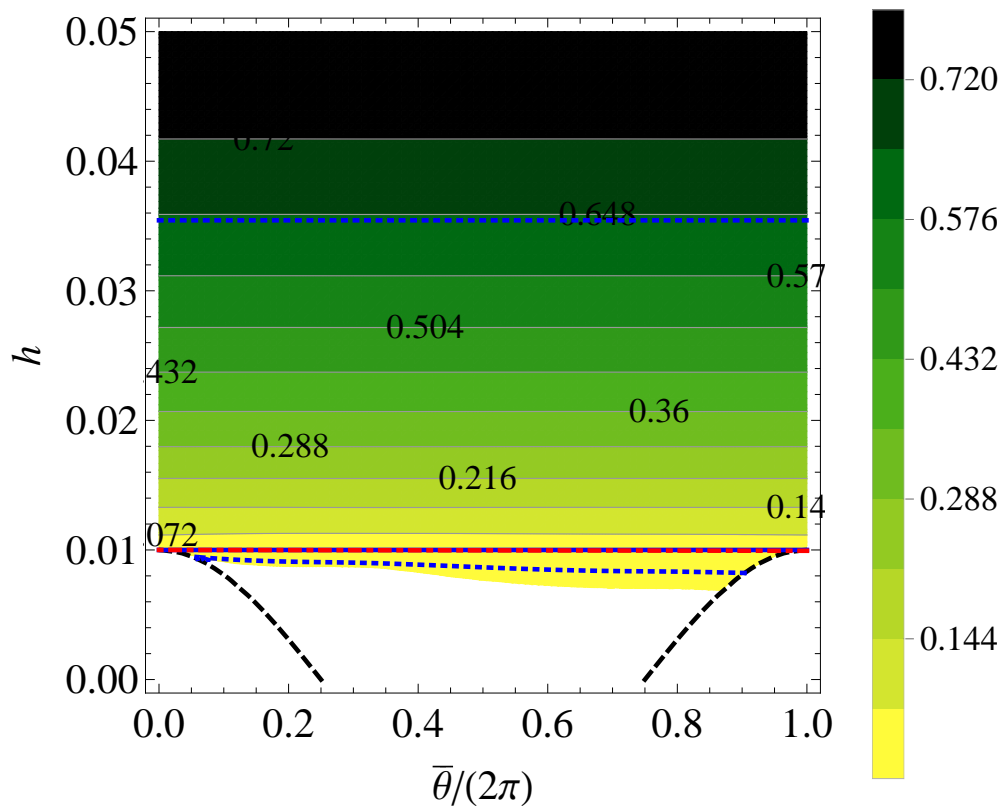**Figure 3.6**: Contour plot of the relative density $n(\bar{\theta}, h)/n^{(0)}(R_1)$. The black dashed line is the scrape-off layer. The solid blue line and the red dot-dashed line are the critical contours $h = h_c$ and $k = h_c$. The upper and lower blue dotted lines represent the diffusive broadening layer $(\Delta h)_1$ and $(\Delta h)_2$.

In order to show the full range of diffusive broadening, the range of h values

shown in Fig. (3.6) is larger than that in Fig. (3.5). The upper dotted blue curve in Fig. (3.6) shows the h-scale length for diffusive broadening in the region $h > h_c$, and the lower dotted blue curve shows the scale length in the region $0 < h < h_c$. The diffusive broadening scales are different in the two regions, since the boundary conditions of the transport equation (3.51) are different in the two regions.

To estimate the h-scale length for diffusive broadening in the region $h > h_c$, we use a perturbation expansion of Eq. (3.51) based on the smallness of β and δ. Substituting the expansion $n(\bar{\theta}, h) = n^{(0)}(\bar{\theta}, h) + n^{(1)}(\bar{\theta}, h)$, where $n^{(1)}/n^{(0)}$ is first order in β and δ, yields the zeroth-order equation $\partial n^{(0)}/\partial \bar{\theta} = 0$ and its simple solution $n^{(0)} = n^{(0)}(h)$.

In first order, the expansion yields the equation

$$\frac{\partial n^{(1)}}{\partial \bar{\theta}} = \frac{\partial}{\partial h}\left[\beta n^{(0)}(h) - \delta \frac{\partial h}{\partial p}\frac{\partial n^{(0)}}{\partial h}\right]. \tag{3.75}$$

Treating β and δ as constants and using the periodic boundary condition required for $n(\bar{\theta}, h)$ in the region $h > h_c$ yields the equation

$$0 = \int_0^{2\pi} \frac{d\bar{\theta}}{2\pi}\frac{\partial n^{(1)}}{\partial \bar{\theta}} = \frac{\partial}{\partial h}\left[\beta n^{(0)}(h) - \delta\left\langle\frac{\partial h}{\partial p}\right\rangle\frac{\partial n^{(0)}}{\partial h}\right], \tag{3.76}$$

where

$$\left\langle\frac{\partial h}{\partial p}\right\rangle \equiv \int_0^{2\pi} \frac{d\bar{\theta}}{2\pi}\frac{\partial h}{\partial p} = -\int_0^{2\pi} \frac{d\bar{\theta}}{2\pi}\sqrt{\cos^2\bar{\theta} + 4h}. \tag{3.77}$$

Here, the last expression follows from Eqs. (3.48) and (3.54).

Since the diffusion term will be significant only at the leading edge of the halo where $h \ll 1$, the last integral in Eq. (3.77) has the approximate value $\langle\partial h/\partial p\rangle \simeq$

$-2/\pi$. Thus, Eq. (3.76) reduces to the simple form

$$0 = \frac{\partial}{\partial h}\left[n^{(0)}(h) + (\Delta h)_1 \frac{\partial n^{(0)}}{\partial h}\right], \qquad (3.78)$$

where $(\Delta h)_1 = 2\delta/\pi\beta$. The solution is given by the expression

$$n^{(0)}(h) = C_1 + (C_2 - C_1)\exp\left[-\frac{h - h_c}{(\Delta h)_1}\right], \qquad (3.79)$$

where C_1 and C_2 are constants. For $h - h_c \gg (\Delta h)_1$, the density $n^{(0)}(h)$ has the constant value C_1, which we identify as the constant $n^{(0)}(R_1)$. The constant C_2 is the value of the $\bar{\theta}$-averaged density at $h = h_c$, $n^{(0)}(h_c)$. This latter constant must be determined by matching onto the solution for $h < h_c$.

One can continue with the perturbation analysis to determine the $\bar{\theta}$-dependent part of the density, but the conclusion is that $(\Delta h)_1$ sets the diffusive broadening scale. The upper blue dotted curve in Fig. (3.6) is the line $h = (\Delta h)_1 = 2\delta/\pi\beta$. Physically, this broadening scale is determined by a competition between diffusion and mobility.

In the region $0 < h < h_c$, a given particle makes a single pass through the $(\bar{\theta}, h)$ space and then is lost to the scrape-off layer, so the diffusive broadening in this region is determined by a competition between diffusion and $\mathbf{E} \times \mathbf{B}$ drift streaming. Neglecting the mobility term in Eq. (3.51) and using the small-h expansion $\partial h/\partial p \simeq -|\cos \bar{\theta}|$ in the diffusion term yields the diffusive broadening scale

$$(\Delta h)_2(\bar{\theta}) = [2\delta \int_0^{\bar{\theta}} d\bar{\theta}' |\cos \bar{\theta}'|]^{1/2}. \qquad (3.80)$$

The lower dotted blue curve in Figs. (3.5) and (3.6) is a plot of $(\Delta h)_2(\bar{\theta})$. For the

conditions of the experiment, $(\Delta h)_1$ is substantially larger than $(\Delta h)_2(\bar{\theta})$.

If the diffusive broadening scales $(\Delta h)_1$ and $(\Delta h)_2$ satisfy appropriate constraints, the details of the density distribution are not needed to calculate the damping rate and frequency shift. First, we require that there exists a contour $h = h_b$, where $h_b - h_c$ is a few times larger than $(\Delta h)_1$ and yet $h_b \ll 1$. This is possible if $(\Delta h)_1 \ll 1$. Recall that $h_c \simeq \Delta p \ll 1$. The density then has the constant value $n^{(0)}(R_1)$ for $h \geq h_b$.

Second, we require that $(\Delta h)_2(\bar{\theta} = 3\pi/2)$ be small compared to $h_c \simeq \Delta p$, so that particles can't reach the contour $h = 0$. Note here that the scrape-off layer on the Right Hand Side of Fig. (3.5) intersects the contour $h = 0$ at $\bar{\theta} = 3\pi/2$. Physically, the particles must be swept to the scrape-off layer by the $\mathbf{E} \times \mathbf{B}$ drift flow before the diffusive broadening can move the particles to $h = 0$.

In summary, the required inequalities are the following

$$(\Delta h)_1 \quad = \quad \frac{2\delta}{\pi\beta} = \frac{2}{\pi}\frac{T}{Ne^2}\frac{R_w}{4D} \ll 1 \tag{3.81}$$

$$1 \quad \gg \quad (\Delta p)^2 \simeq h_c^2 \gg [(\Delta h)_2(3\pi/2)]^2 = 6\delta = \frac{3}{2}\frac{T\beta}{Ne^2}\frac{R_w}{D}, \tag{3.82}$$

which are consistent with the experimental conditions except for the smallest values of D.

By using the constancy of $n(\bar{\theta}, h)$ for $h > h_b$, Eqs. (3.59) and (3.60) can be

re-written in the form

$$\frac{\partial D}{\partial t} = \frac{ecR_w}{B}\left(\frac{4D}{R_w}\right)^2 \int_0^{2\pi} d\bar\theta \sin\bar\theta \left\{\frac{n^{(0)}(R_1)}{2}[p_-^2(\bar\theta, h_b) - p^2(R_1)]\right.$$
$$\left. + \int_{h_b}^0 dh p_-(\bar\theta, h)\frac{\partial p_-(\bar\theta, h)}{\partial h}n(\bar\theta, h)\right\}, \tag{3.83}$$

$$D\Delta\omega = -\frac{ecR_w}{B}\left(\frac{4D}{R_w}\right)^2 \int_0^{2\pi} d\bar\theta \cos\bar\theta \left\{\frac{n^{(0)}(R_1)}{2}[p_-^2(\bar\theta, h_b) - p^2(R_1)]\right.$$
$$\left. + \int_{h_b}^0 dh p_-(\bar\theta, h)\frac{\partial p_-(\bar\theta, h)}{\partial h}n(\bar\theta, h)\right\}, \tag{3.84}$$

where the differential relation $dp = dh(\partial p/\partial h)_{\bar\theta}$ has been used in the integrals.

In both square brackets, the constant term $p_-^2(R_1)$ integrates to zero. By even-odd arguments, the term $p_-^2(\bar\theta, h_b)$ integrates to zero in Eq. (3.83), but not in Eq. (3.84). The integral over h makes the only contribution in Eq. (3.83) and may be neglected in Eq. (3.84). The integral is negligible there because $h_b \ll 1$. Thus, the equations reduce to the form

$$\frac{\partial D}{\partial t} = \frac{ecR_w}{B}\left(\frac{4D}{R_w}\right)^2 \int_0^{2\pi} d\bar\theta \sin\bar\theta \int_{h_b}^0 dh p_-(\bar\theta, h)\frac{\partial p_-(\bar\theta, h)}{\partial h}n(\bar\theta, h), \tag{3.85}$$

$$D\Delta\omega = -\frac{ecR_w}{B}\left(\frac{4D}{R_w}\right)^2 \frac{n^{(0)}(R_1)}{2} \int_0^{2\pi} d\bar\theta \cos\bar\theta p_-^2(\bar\theta, h_b). \tag{3.86}$$

The reason that the diffusive broadening makes only a negligible change in the frequency shift is easy to understand. The leading edge of the halo has the approximate $\bar\theta$-dependence $p_-(\bar\theta, 0)$, which varies by order unity as $\bar\theta$ varies over the interval $(0, 2\pi)$. On the other hand the diffusive broadening is small compared to unity, $(\Delta p_-)_{\text{broad}} \simeq (\partial p_-/\partial h)(\Delta h)_1 \sim 2\delta/\pi\beta \ll 1$, so the change produced by the broadening is negligible.

To evaluate the damping rate in Eq. (3.85) first recognize that $p_- \sin\bar\theta =$

$\partial h/\partial\bar{\theta}$, based on the form of h in Eq. (3.48). Such recognition, together with the chain rule $(\partial h/\partial\bar{\theta}|_{p_-})(\partial p_-/\partial h|_{\bar{\theta}}) = -\partial p_-/\partial\bar{\theta}|_h$, and an integration by parts over $\bar{\theta}$ since $p_-(\bar{\theta}, h)$ and $n(\bar{\theta}, h)$ are periodic in $\bar{\theta}$, allows us to rewrite Eq. (3.85) as

$$\frac{\partial D}{\partial t} = \frac{ecR_w}{B}\left(\frac{4D}{R_w}\right)^2 \int_0^{2\pi} d\bar{\theta} \int_{h_b}^0 dh\, p_-(\bar{\theta}, h) \left.\frac{\partial n}{\partial\bar{\theta}}\right|_h. \tag{3.87}$$

Since $h_b \ll 1$, $p_-(\bar{\theta}, h)$ can be approximated by $p_-(\bar{\theta}, 0)$, which is given by $p_-(\bar{\theta}, 0) = \cos\bar{\theta}$ from Eq. (3.54) for $\pi/2 < \bar{\theta} < 3\pi/2$ and is zero elsewhere. Thus, Eq. (3.87) reduces to the form

$$\frac{\partial D}{\partial t} = \frac{ecR_w}{B}\left(\frac{4D}{R_w}\right)^2 \int_{\pi/2}^{3\pi/2} d\bar{\theta}\cos\bar{\theta} \int_{h_b}^0 dh\, \left.\frac{\partial n}{\partial\bar{\theta}}\right|_h. \tag{3.88}$$

Substituting for $\partial n/\partial\bar{\theta}|_h$ from transport equation (3.51), carrying out the h-integral and using the relations $n(\bar{\theta}, h_b) = n^{(0)}(R_1)$ and $\partial n/\partial h(\bar{\theta}, 0) = 0$ yields the expression

$$\frac{\partial D}{\partial t} = -\frac{ecR_w}{B}\left(\frac{4D}{R_w}\right)^2 \int_{\pi/2}^{3\pi/2} d\bar{\theta}\cos\bar{\theta} \cdot \beta n^{(0)}(R_1), \tag{3.89}$$

which reduces to the result

$$\frac{dD}{dt} = \frac{ecR_w}{B}\left(\frac{4D}{R_w}\right)^2 n^{(0)}(R_1) \cdot 2\beta = -\frac{2}{\pi}\frac{|dN/dt|}{N}R_w, \tag{3.90}$$

This result is the same as the damping rate for zero-diffusion given in Eqs. (3.71) and (3.2).

This analytic solution for the damping rate approximates the $d\bar{\theta}dh$ integrals

in Eq. (3.85), denoted as

$$J \equiv \int_0^{2\pi} d\bar{\theta} \sin \bar{\theta} \int_{h_b}^0 dh p_- \frac{\partial p}{\partial h} \frac{n(\bar{\theta}, h)}{n^{(0)}(R_1)}, \tag{3.91}$$

by the value 2β, which significantly is independent of δ, provided δ is not too large. Fig. (3.7) shows a comparison of this analytical approximation for the integral J to a direct numerical evaluation using the numerical solutions for the diffusively broadened density found in Appendix B.
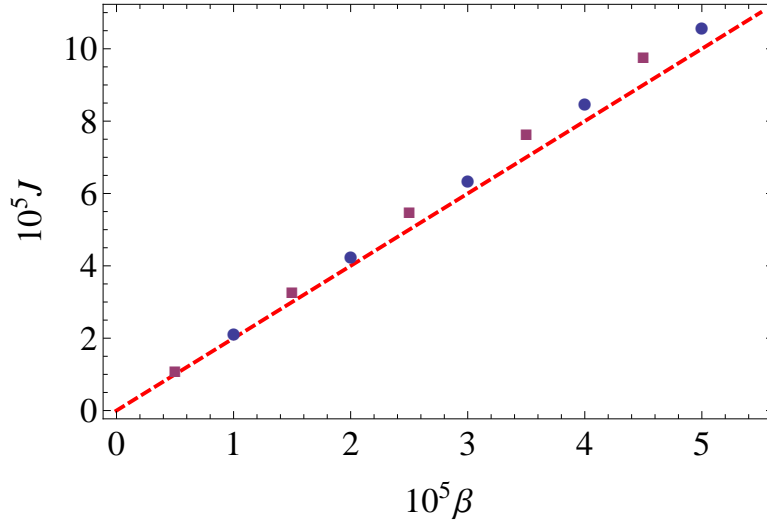
Figure 3.7: Values of damping integral J. Numerical results are in squares for $T = 4 \times 10^{-2} Ne^2$ and in circles for $T = 1.6 \times 10^{-2} Ne^2$, with $D = 0.1 R_w$. Red dashed line shows the approximate analytical result $J \simeq 2\beta$.

The numerical evaluations are obtained for many values of β, shown in the figure, and for $D = 0.1 R_w$ and two distinct values of T, $T = 1.6 \times 10^{-2} Ne^2$ and $T = 4 \times 10^{-2} Ne^2$. These values are characteristic of the experiment. The value of h_b is taken to be large enough that $n(\bar{\theta}, h)/n^{(0)}(R_1)$ is close to 1 and the integral J is independent of h_b.

Results for $T = 1.6 \times 10^{-2} Ne^2$ are shown as circles and for $T = 4 \times 10^{-2} Ne^2$

as squares. The red dashed line is the analytic result 2β. Significantly, the circles and squares lie close to the red line, with slightly larger values. The origin of the difference lies in the approximation made in Eq. (3.88) in the analytic evaluation. We neglected the small finite h in $p_-(\bar{\theta}, h)$. However, when the finite value of $0 < h < h_b$ is retained in the numerical evaluation, values slightly larger than the analytic approximation is obtained.

That diffusive broadening does not change the damping rate significantly, even when the broadening is much wider than the thin region responsible for damping in the zero-diffusive model [i.e. $(\Delta h)_1 \gg 2\pi\beta$] may be surprising. All that is needed is that $(\Delta h)_1$ and $(\Delta h)_2$ satisfy inequalities (3.81) and (3.82).

To understand the near equality of the two damping rates, first note that the scaled flow of particles through contour h_b is simply $2\pi\beta n^{(0)}(R_1)$, which is the same as the flow through contour h_c in the zero diffusion model. Provided that $(\Delta h)_2 \ll \Delta p$, all of the particles that pass through contour $h = h_b$ ultimately enter the scrape-off layer. To calculate the average change in angular momentum of the particles as they move from $h = h_b$ to the scrape-off layer, one need only replace h_c by h_b in Eq. (3.73). By inequality (3.82), h_b is small compared to unity and the modified version of Eq. (3.73) still reduces to the result in Eq. (3.74). Thus, the average rate of change of angular momentum for the particles is the same in the two cases.

The question remains as to whether or not the average rate of change of angular momentum is a good approximation to the torque exerted by the wave on the particles. In the zero diffusion model, particles cross the contour $h = h_c$ and then enter the scrape-off layer in a single pass through the $(\bar{\theta}, h)$ space. In scaled variables, the change in angular momentum of a particle caused by the transport during this period

is of order $\delta p \sim \beta$, which is much smaller than the average change $\delta p \sim 1$.

In the finite diffusion case, particles cross the contour $h = h_b$ and then make many passes through the $(\bar{\theta}, h)$ space before reaching the scrape-off layer, so torque due to transport has more time to act on the particle. The change in angular momentum due to the transport is of order $\delta p \sim h_b$, which is much larger than β, but according to inequality (3.82) is still small compared to the average change in angular momentum $\delta p \sim 1$. Thus, the rate of change of angular momentum of the particles still provides a good approximation to the torque exerted by the wave. Therefore, the damping rates for the two cases are nearly the same.

3.7 Correction for time dependence in $D(t)$

Here, we obtain a perturbative correction to the damping rate due to the explicit time dependence in the Hamiltonian, that is, due to the time dependence in $D(t)$. There are detailed calculations of other corrections of the same order of magnitude in Appendix . Unscaled equations must be used to obtain this correction since $D(t)$ enters the scaling. The first two terms on the Left Hand Side of Eq. (3.41) give rise to the correction.

To estimate the relative size of these two terms, we substitute the approximate zero-diffusion solution $n(\bar{\theta}, \bar{H}, t) = n^{(0)}(R_1)\mathcal{U}[\bar{H} - \bar{H}_c(t)]$, obtaining the relation $\partial n/\partial t|_{\bar{\theta},\bar{H}} = (-\partial \bar{H}_c/\partial t)(\partial n/\partial \bar{H})_{\bar{\theta},t}$. One can show that $|\partial \bar{H}_c/\partial t|$ is small compared to $|\partial \bar{H}/\partial t|$ for $\Delta p \ll 1$, so the first term may be neglected in comparison to the

second. The equation then takes the form

$$
\left.\frac{\partial n}{\partial\bar{\theta}}\right|_{\bar{H},t} = \frac{\partial}{\partial\bar{H}}\left[-\dot{P}_\theta|_T n + \left.\frac{\partial\bar{H}}{\partial P_\theta}\right|_{\bar{\theta},t}\tilde{\mathcal{D}}\left.\frac{\partial n}{\partial\bar{H}}\right|_{\bar{\theta}}\right] + \left.\frac{\partial P_\theta}{\partial t}\right|_{\bar{H},t}\left.\frac{\partial n}{\partial\bar{H}}\right|_{\bar{\theta},t},
\tag{3.92}
$$

where

$$
\left.\frac{\partial P_\theta}{\partial t}\right|_{\bar{\theta},\bar{H}} = -\frac{\partial\bar{H}/\partial t|_{\bar{\theta},P_\theta}}{\partial\bar{H}/\partial P_\theta|_{\bar{\theta},t}}
\tag{3.93}
$$

is the rate at which a contour $\bar{H}(\bar{\theta}, P_\theta, t) = $ constant moves upward in the $(\bar{\theta}, P_\theta)$ phase space.

Anticipating that we will need Eq. (3.92) only for $\bar{\theta}$ in the range $\pi/2 < \bar{\theta} < 3\pi/2$ and only for small values of h, Eq. (3.54) implies that

$$
\frac{P_\theta - P_w}{P_w} \simeq \frac{4D(t)}{R_w}\cos\bar{\theta},
\tag{3.94}
$$

which in turn implies the relation

$$
\left.\frac{\partial P_\theta}{\partial t}\right|_{\bar{\theta},\bar{H}} \simeq \frac{4\dot{D}(t)}{R_w}P_w\cos\bar{\theta}.
\tag{3.95}
$$

Changing to scaled variables, choosing an angle in the range $\pi/2 < \bar{\theta} < 3\pi/2$ and integrating with respect to h from $h = h_b$ to $h = 0$ yields the result

$$
\int_{h_b}^0 dh\left.\frac{\partial n}{\partial\bar{\theta}}\right|_{h,t} = -\beta n^{(0)}(R_1)[1 - \frac{4\dot{D}P_w}{R_w\dot{P}_\theta|_T}\cos\bar{\theta}].
\tag{3.96}
$$

Comparing this result to Eqs. (3.88) and (3.89) shows that the square bracket is a correction to the flux through the contour $h = h_b$ to account for the the fact that the contour moves in time.

Substituting this result into Eq. (3.88) and carrying out the $\bar{\theta}$-integration yields the damping rate

$$\frac{dD}{dt} = -\frac{\gamma}{1 + 2N_h/N} \simeq -\gamma(1 - 2N_h/N), \tag{3.97}$$

where γ is the zero-diffusion damping rate in Eq. (3.71) and $N_h/N \simeq 0.1$.

3.8 Discussion

How general is the flux-driven damping mechanism discussed here? First note that the mechanism is not limited to the case of an $m = 1$ mode. Subsequent to the experimental discovery of the damping for an m=1 diocotron mode, similar damping was observed for an $m = 2$ mode[2]. Again, algebraic damping began when the halo particles reached the resonant layer, which for the $m = 2$ mode is well separated from the wall.

Because the resonant layer for the $m = 2$ mode is well separated from the wall, one may ask what plays the role of the wall in truncating particle orbits? Put another way, what prevents the resonant particles from giving back angular momentum that they have received from the mode? We believe that the answer is simply passage of the particles through the "cat's-eye" orbits in the resonant layer. Because of transport, the particles cannot come back through these structures, and in the one-way passage, the particles pick up significant angular momentum from the mode, causing the damping. In principle, this mechanism also would apply for $m = 3$ and higher, but the resonant layer is closer to and even inside the core for higher m modes, and such modes typically suffer large ordinary Landau damping.

In this chapter we do not treat the damping of the $m = 2$ mode in parallel with the damping of the m=1 mode, because there are technical differences between $m = 1$ and $m = 2$ cases. The $m = 1$ mode admits an analytic solution for a general monotonically decreasing density profile, while the $m = 2$ mode does not. The structure of the "cat's-eye" orbits differ, since the potential goes to zero at the resonant radius for an $m = 1$ mode (i.e. at the wall), but not for the $m = 2$ mode. Also, the truncation of the orbits by the wall is different than simply passing through the "cats eye orbits. The theory for the higher order modes must wait for a later paper.

Broader than the flux-driven damping mechanism itself is the idea that all Landau-type damping (or growth), that is, damping (or growth) due to interaction with resonant particles, can be thought of as resulting from the action of the bare electric field from the resonant particles back on the mode. The resonant particles travel at the mode phase velocity so the electric field from the resonant particles drives the mode resonantly. The idea is not limited to the case where the azimuthal mode number is unity and the field from the resonant particles is uniform, but applies for arbitrary mode number. This general idea is elaborated in Chapter 4.

Chapter 3, in full, is a reprint of the material as it appears in Physics of Plasmas. C.Y. Chim, T.M. O'Neil, *Physics of Plasmas* **23**, 072113 (2016). The dissertation author was the primary investigator and author of this paper.

Chapter 4

A mechanistic interpretation of the resonant wave-particle interaction

4.1 Abstract

This chapter provides a simple mechanistic interpretation of the resonant wave-particle interaction of Landau. For the simple case of a Langmuir wave in a Vlasov plasma, the non-resonant electrons satisfy an oscillator equation that is driven resonantly by the bare electric field from the resonant electrons, and in the case of wave damping, this complex driver field is of a phase to reduce the oscillation amplitude. The wave-particle resonant interaction also occurs in waves governed by 2D $\mathbf{E} \times \mathbf{B}$ drift dynamics, such as a diocotron wave. In this case, the bare electric field from the resonant electrons causes $\mathbf{E} \times \mathbf{B}$ drift motion back in the core plasma, reducing the amplitude of the wave.

4.2   Introduction

This chapter provides a re-interpretation of the resonant wave-particle interaction of Landau[30]. There are two halves to this interaction: first there is the influence of the wave on the resonant particles and second the influence of the resonant particles back on the wave. The mechanisms for the two halves of the interaction are usually described differently. For the first half, the mechanism is obvious; the wave electric field acts on the resonant particles and produces a perturbation in the resonant particle charge density. The mechanism for the second half of the interaction is usually described through Poisson's equation, or equivalently, a dispersion relation that follows from Poisson's equation; the perturbed charge density from the resonant particles makes a small correction to the dispersion relation, and this correction yields a small imaginary frequency shift, which is the damping decrement for the wave. In contrast, here we provide a mechanical interpretation of the second half of the interaction that is similar to the interpretation of the first half.

Consider the simple case of a Langmuir wave that is excited in a collisionless, Maxwellian plasma, with the wave phase velocity well out on the tail of the velocity distribution. We will see that the wave induced displacement of the non-resonant electrons, that is, the electrons in the main part of the Maxwellian, satisfies an oscillator equation that is driven by the bare electric field from the perturbed charge density of the resonant electrons. This field drives the oscillator resonantly, since the resonant electrons travel at the phase velocity of the wave. From this perspective, the wave damping simply results from the action of the driver field from the resonant electrons back on the oscillator.

The interpretation does not specify the perturbed charge density of the reso-

nant particles, so the interpretation applies equally well to the cases of linear Landau damping and growth and to the case of a large amplitude wave with nonlinear, trapped particle orbits. In general, the portion of the drive field that is 90° out of phase with the oscillator produces damping or growth and the portion that is in phase produces a frequency shift.

Because Landau's analysis of the damping was rather formal and did not offer a physical interpretation, other authors have provided physical interpretations[31, 32, 33, 34]. Here, we find a particularly simple interpretation by focusing on only half of the wave-particle interaction: namely, the influence of the resonant particles back on the wave.

One usually thinks of Landau resonances in connection with waves in a collisionless plasma, that is, waves that are described by Vlasov dynamics, but such resonances also occur for waves that are described by 2D $\mathbf{E} \times \mathbf{B}$ drift dynamics. A simple example is a diocotron wave that is excited on a nonneutral plasma column in a Penning-Malmberg trap[14, 15, 35, 23]. The analysis is simplest for the case where the plasma column consists of a high-density core surrounded by a relatively low-density halo. The diocotron wave can be thought of as a surface wave that propagates azimuthally around the core. At some critical radius in the halo, the azimuthal $\mathbf{E} \times \mathbf{B}$ drift rotation velocity of the halo fluid elements matches the phase velocity of the wave potential, and the resonant interaction of the wave potential and fluid elements gives rise to Landau damping.

In the standard analysis, the linearized continuity equation for the $\mathbf{E} \times \mathbf{B}$ drift flow is combined with Poisson's equation to obtain a dispersion relation. When the resonant region is in the low density halo, the perturbed charge density of the

resonant electrons makes a small correction to the dispersion relation, yielding a small imaginary frequency shift, which is the wave damping decrement. To understand more clearly how the resonant particles act back on the wave, we focus on the equation of motion for the surface ripple on the plasma core. As we will see, the bare electric field from the perturbed charge density of the resonant electrons acts back on the core, causing $\mathbf{E} \times \mathbf{B}$ drifts that reduce the amplitude of the surface ripple, that is, damp the wave. Again, we find a simple mechanistic description of the manner in which the resonant electrons act back on the wave.

4.3 Langmuir Wave

First, we consider the case of a Langmuir wave that propagates in the x-direction, writing the perturbed electric field in the form

$$\delta E(x, t) = \delta E_k(t) \exp(ikx) + \text{c.c.}, \tag{4.1}$$

where c.c. stands for the complex conjugate. It is convenient to write the field as the sum

$$\delta E_k(t) = \delta E_k^{\text{non-res}}(t) + \delta E_k^{\text{res}}(t), \tag{4.2}$$

where

$$\delta E_k^{\text{non-res}}(t) = -\frac{4\pi e \delta n_k^{\text{non-res}}(t)}{ik} \tag{4.3}$$

$$\text{and } \delta E_k^{\text{res}}(t) = -\frac{4\pi e \delta n_k^{\text{res}}(t)}{ik} \tag{4.4}$$

are the fields produced by the perturbed charge densities of the non-resonant and resonant electrons, $-e\delta n_k^{\text{non-res}}(t)$ and $-e\delta n_k^{\text{res}}(t)$, following Guass's Law. The non-resonant electrons are those in the bulk of the velocity distribution, and the resonant electrons are assumed to be well out on the tail of the distribution.

For the non-resonant electrons, it is convenient to introduce a displacement $\delta x(x,t)$ defined through the relation $\partial \delta x(x,t)/\partial t = \delta v$, where $\delta v(x,t)$ is the velocity perturbation. The spatial Fourier transform of this relation is the equation $\partial \delta x_k/\partial t = \delta v_k(t)$, which allows the continuity equation to be written in the form

$$0 = \frac{\partial n_k^{\text{non-res}}}{\partial t} + ikn\delta v_k = \frac{\partial}{\partial t}[\delta n_k^{\text{non-res}} + ikn\delta x_k], \tag{4.5}$$

where n is the unperturbed density of the non-resonant electrons. The last form yields the solutions

$$\delta n_k^{\text{non-res}}(t) \;=\; -ikn\delta x_k(t) \tag{4.6}$$

$$\text{and } \delta E_k^{\text{non-res}}(t) \;=\; 4\pi e n\delta x_k(t). \tag{4.7}$$

The linearized Euler equation for the non-resonant electrons governed by fluid theory takes the form

$$nm\frac{\partial \delta v_k}{\partial t} = -ne\delta E_k - ik\gamma T\delta n_k^{\text{non-res}}, \tag{4.8}$$

where m is the electron mass, T is the electron temperature and γ has the value 3 for a one-dimensional adiabatic compression[56]. By using the definition $\partial \delta x_k/\partial t = \delta v_k$ and Eqs. (4.1), (4.6) and (4.7), Eq. (4.8) can be rewritten as the driven oscillator

equation

$$\left(\frac{\partial^2}{\partial t^2} + \omega_p^2 + 3k^2\bar{v}^2\right)\delta x_k(t) = -\frac{e}{m}\delta E_k^{\mathrm{res}}(t), \tag{4.9}$$

where $\omega_p^2 = 4\pi n e^2/m$ is the square of the plasma frequency, $\bar{v}^2 = T/m$ is the square of the thermal velocity, and the quantity $k^2\bar{v}^2/\omega_p^2 = k^2\lambda_D^2$ is assumed to be small. Here λ_D is the Debye length. Physically, Eq. (4.9) states that the non-resonant electrons moving in the wave field may be thought as an oscillator that is driven by the bare electric field from the resonant electrons. Of course, Eq. (4.9) also can be obtained from the coupled Vlasov and Poisson equation.

To understand the effect of the driver field on the amplitude of the oscillations, we look for a solution to Eq. (4.9) of the form $\delta x_k(t) = \delta\tilde{x}_k(t)\exp(-i\omega_0 t)$, where $\omega_0^2 = \omega_p^2 + 3k^2\bar{v}^2$ is the original Langmuir wave frequency squared and $\delta\tilde{x}_k(t)$ is a slowly varying complex amplitude. This solution yields the expected form for a Langmuir wave traveling in the positive x-direction. Since the resonant particles travel at the wave phase velocity ω_0/k, the driving field due to these particles can be written as $\delta E_k^{\mathrm{res}}(t) = \delta\tilde{E}_k^{\mathrm{res}}(t)\exp(-i\omega_0 t)$, where $\delta\tilde{E}_k^{\mathrm{res}}(t)$ again is a slowly varying complex amplitude. Substituting these forms into Eq. (4.9) and neglecting $|\delta\ddot{\tilde{x}}_k/\delta\tilde{x}_k|$ compared to ω_0^2, yields the reduced equation

$$-2i\omega_0\frac{d\delta\tilde{x}_k}{dt} = -\frac{e}{m}\delta\tilde{E}_k^{\mathrm{res}}(t). \tag{4.10}$$

Thus, when the ratio $\delta\tilde{E}_k^{\mathrm{res}}/\delta\tilde{x}$ is imaginary, the driver produces damping or growth, and when the ratio is real the driver produces a frequency shift.

As noted in the introduction, this paper focuses on only half of the wave-particle interaction, namely, the influence of the resonant particles back on the wave,

and Eq. (4.10) solves that problem for the case of a Langmuir wave. The other half of the problem determines the influence of the wave on the resonant particles, that is, determines the perturbed charge density of the resonant particles. As a simple application of Eq. (4.10), we use the well-known perturbed charge density for resonant particles in a weakly damped, linear Langmuir wave[31]

$$
\begin{aligned}
\delta\tilde{n}_k^{\text{res}}(t) &= n\int_{\text{res}} dv\,\frac{e}{m}\frac{\delta\tilde{E}_k}{i(kv-\omega_0)}\frac{\partial f_0}{\partial v} \\
&\simeq n\int_{\text{res}} dv\,\frac{e}{m}\pi\delta(kv-\omega_0)\delta\tilde{E}_k\frac{\partial f_0}{\partial v} \\
&= \frac{\pi n e}{m}\frac{\delta\tilde{E}_k(t)}{k}\frac{\partial f_0}{\partial v}\bigg|_{\omega_0/k},
\end{aligned}
\tag{4.11}
$$

where $f_0(v)$ is the unperturbed velocity distribution, and the Plemelj formula has been used in the second step[57].

Since $\partial f_0/\partial v|_{\omega_0/k}$ is first order in the small number of resonant particles, $\delta\tilde{E}_k(t)$ need only be accurate ot zero order, and we can use Eq. (4.7) to obtain the relation

$$
\delta\tilde{E}_k(t) \simeq \delta\tilde{E}_k^{\text{non-res}}(t) = 4\pi n e\,\delta\tilde{x}_k(t).
\tag{4.12}
$$

Eq. (4.4) then yields the equation

$$
-\frac{e}{m}\delta\tilde{E}_k^{\text{res}}(t) = -\pi i\frac{\omega_p^4}{k^2}\frac{\partial f_0}{\partial v}\bigg|_{\omega_0/k}\delta\tilde{x}_k(t).
\tag{4.13}
$$

Eq. (4.10) then implies the oscillator damping rate

$$
\begin{aligned}
\gamma_k = \frac{d\delta\tilde{x}_k/dt}{\delta\tilde{x}_k(t)} &= \left. \frac{\pi}{2\omega_0} \frac{\omega_p^4}{k^2} \frac{\partial f_0}{\partial v} \right|_{\omega_0/k} \\
&= -\sqrt{\frac{\pi}{8}} \frac{\omega_p}{k^3 \lambda_D^3} \exp[-\frac{1}{2k^2\lambda_D^2}(1+3k^2\lambda_D^2)],
\end{aligned}
\qquad (4.14)
$$

where the last form is the well-known form of the damping rate for a Maxwellian velocity distribution[31].

Of course, the use of Eq. (4.10) is not limited to the case where the resonant particle density perturbation is determined by the linearized Vlasov equation. For a large amplitude wave where trapping of resonant particles in wave troughs is important[58, 59], Eq. (4.10) can still be used to determine the influence of the resonant particles back on the wave.

4.4   Diocotron Wave

To illustrate the wave-particle interaction that can occur in 2D $\mathbf{E}\times\mathbf{B}$ dynamics, we consider a diocotron wave that is excited on a pure electron plasma column in a Malmberg-Penning trap[14, 60, 23]. An analytic treatment is possible for the case where the electron column consists of a uniform density central core surrounded by a relatively low-density halo. Such a density profile often is said to be of the "top hat" form. We assume that the unperturbed density has the constant value $n(r) = n_c$ out to the radius $r = R_c$, and there drops abruptly to the much lower density $n(R_c^+) = n_h$, where the subscripts c and h refer to the core and halo, respectively. Consistent with the standard trap configuration, we assume that the electron column is immersed in a uniform, axial magnetic field $\mathbf{B} = B\hat{z}$, where (r, θ, z) is a cylindrical coordinate

system with the z-axis coincident with the axis of the trap.

Since the 2D $\mathbf{E} \times \mathbf{B}$ drift flow is incompressible and since the unperturbed density profile for the core is uniform with an abrupt fall off at the surface, the diocotron wave can be characterized by specifying the ripple on the surface of the core. For a diocotron wave of azimuthal wave number m, the θ- and t-dependent radial position of the core surface can be written as

$$r_s(\theta, t) = R_c + D(t) \exp[i(m\theta - \omega_m t)] + \text{c.c.}, \tag{4.15}$$

where ω_m is the still-to-be-determined wave frequency and $D(t)$ is a complex wave amplitude. The slow time dependence in the complex amplitude is due to the interaction with the resonant particles.

The total time derivative of $r_s(\theta, t)$ is given by the equation

$$
\begin{aligned}
\frac{dr_s(\theta, t)}{dt} &= \left[\frac{\partial}{\partial t} + \omega_E(R_c) \frac{\partial}{\partial \theta} \right] r_s(\theta, t) \\
&= \{\dot{D}(t) + i[m\omega_E(R_c) - \omega_m]D(t)\} \exp[i(m\theta - \omega_m t)] + \text{c.c.,} \tag{4.16}
\end{aligned}
$$

where $\omega_E(r)$ is the $\mathbf{E} \times \mathbf{B}$ drift rotation frequency at radius r.

Since the motion of the surface is due to $\mathbf{E} \times \mathbf{B}$ drifts caused by the mode potential, we also can write the time derivative as the drift velocity

$$\frac{dr_s(\theta, t)}{dt} = -\frac{c}{BR_c} \frac{\partial \delta\phi(R_c, \theta, t)}{\partial \theta}, \tag{4.17}$$

where $\delta\phi = \delta\phi(r, \theta, t)$ is the mode potential.

The m-th Fourier components of the potential and the density perturbation

are related by the Green's function integral[23]

$$\delta\phi_m(r,t) = 4\pi e \int_0^{R_w} 2\pi r' dr' G_m(r,r')\delta n_m(r',t), \tag{4.18}$$

where

$$G_m(r,r') = \frac{1}{4\pi m} \begin{cases} \dfrac{r^m}{r'^m}\left(\dfrac{r'^{2m}}{R_w^{2m}} - 1\right) & \text{for } r < r' \\[2ex] \dfrac{r'^m}{r^m}\left(\dfrac{r^{2m}}{R_w^{2m}} - 1\right) & \text{for } r' < r \end{cases} \tag{4.19}$$

is the Green's function and $-e$ is the electron charge. Here, R_w is the radius of a conducting wall that bounds the confinement region, and the Green's function vanishes at $r = R_w$ in accord with the boundary condition on the wave potential.

It is convenient to write the perturbed density as the sum of a term from the non-resonant region and a term from the resonant region, $\delta n_m^{\text{non-res}}(r,t)$ and $\delta n_m^{\text{res}}(r,t)$, and to write the potential as the sum of the corresponding terms $\delta\phi_m(r,t) = \delta\phi_m^{\text{non-res}}(r,t) + \delta\phi_m^{\text{res}}(r,t)$. Because the unperturbed core density is uniform out to the core surface and because the halo density is relatively low, the dominant contribution to $\delta n^{\text{non-res}}(r,\theta,t)$ comes from the surface of the core and is given by the expression

$$\begin{aligned} \delta n^{\text{non-res}}(r,\theta,t) &= -D(t)\exp[i(m\theta - \omega_m t)]\frac{\partial n}{\partial r} + \text{c.c.} \\ &= D(t)\exp[i(m\theta - \omega_m t)](n_c - n_h)\delta(r - R_c) + \text{c.c.,} \tag{4.20} \end{aligned}$$

where $\delta(r - R_c)$ is a delta function.

The Green's function integral then implies the non-resonant potential

$$
\begin{aligned}
\delta\phi^{\text{non-res}}(R_c, \theta, t) &= 8\pi^2 e R_c (n_c - n_h) G_m(R_c, R_c) D(t) \exp[i(m\theta - \omega_m t)] + \text{c.c.} \\
&= -\frac{2\pi e}{m} R_c (n_c - n_h) \left(1 - \frac{R_c^{2m}}{R_w^{2m}}\right) D(t) \exp[i(m\theta - \omega_m t)] + \text{c.c..}
\end{aligned}
$$

$$(4.21)$$

Combining Eqs. (4.16) and (4.17) and substituting Eq. (4.21) for the non-resonant potential yields the relation

$$
\begin{aligned}
&-\frac{c}{BR_c} \frac{\partial \delta\phi^{\text{res}}(R_c, \theta, t)}{\partial \theta} + \frac{2i\pi e c(n_c - n_h)}{B}\left(1 - \frac{R_c^{2m}}{R_w^{2m}}\right) D(t) \exp[i(m\theta - \omega_m t)] + \text{c.c.} \\
&= \{\dot{D}(t) + i[m\omega_E(R_c) - \omega_m]D(t)\} \exp[i(m\theta - \omega_m t)] + \text{c.c..}
\end{aligned}
$$

$$(4.22)$$

It is instructive to examine Eq. (4.22) in the limit where there is no resonance, and $\delta\phi^{\text{res}}$ and $\dot{D}(t)$ are zero. The equation then implies the dispersion relation for a diocotron wave on a "top-hat" density profile

$$
\omega_m - m\omega_E(R_c) = -\omega_E(R_c)(1 - \frac{n_h}{n_c})(1 - \frac{R_c^{2m}}{R_w^{2m}}),
\tag{4.23}
$$

using that fact that $\omega_E(R_c) = 2\pi e c n_c / B$ at the surface of the core. This dispersion relation is well-known in the limit $n_h = 0$.[14, 15] By using this dispersion relation, Eq. (4.22) reduces to the form

$$
-\frac{c}{BR_c} \frac{\partial \delta\phi^{\text{res}}}{\partial \theta} = \dot{D}(t) \exp[i(m\theta - \omega_m t)] + \text{c.c..}
\tag{4.24}
$$

Thus, we obtain the rate of change of the complex wave amplitude

$$
\begin{aligned}
\dot{D}(t) &= -\int_0^{2\pi} \frac{d\theta}{2\pi} \frac{c}{BR_c} \frac{\partial \delta\phi^{\mathrm{res}}(R_c,\theta,t)}{\partial\theta} \exp[-i(m\theta - \omega_m t)] \\
&= -\frac{imc}{BR_c} \delta\phi_m^{\mathrm{res}}(R_c,t) \exp[i\omega_m t].
\end{aligned}
\tag{4.25}
$$

Physically, the electric field from the resonant particles acts back on the core causing $\mathbf{E} \times \mathbf{B}$ drift motion, and this motion produces a slow rate of change of the complex wave amplitude.

Since the resonant particles travel at the wave phase speed, the perturbed density $\delta n_m^{\mathrm{res}}(R_c,t)$ can be written in the form $\delta\tilde{n}_m^{\mathrm{res}}(R_c,t)\exp[-i\omega_m t]$, where $\delta\tilde{n}_m^{\mathrm{res}}(R_c,t)$ is slowly varying. Likewise, the perturbed potential $\delta\phi_m^{\mathrm{res}}(R_c,t)$ can be written in the form $\delta\tilde{\phi}_m^{\mathrm{res}}(R_c,t)e^{-i\omega_m t}$, where $\delta\tilde{\phi}_m^{\mathrm{res}}(R_c,t)$ is slowly varying. Eqs. (4.18) and (4.19) then imply the relationship

$$
\delta\tilde{\phi}_m^{\mathrm{res}}(R_c,t) = \frac{e}{m} \int_{\mathrm{res}} 2\pi r' dr' \frac{R_c^m}{r'^m} \left(\frac{r'^{2m}}{R_w^{2m}} - 1 \right) \delta\tilde{n}_m^{\mathrm{res}}(r',t),
\tag{4.26}
$$

and Eq. (4.25) reduces to the result

$$
\dot{D}(t) = -\frac{icm}{BR_c} \delta\tilde{\phi}_m^{\mathrm{res}}(R_c,t).
\tag{4.27}
$$

To obtain Eq. (4.25), we projected out the m-th Fourier component of Eq. (4.24), but one may worry about other Fourier components in the potential $\delta\phi^{\mathrm{res}}(r,\theta,t)$. When the perturbed resonant particle density, $\delta n^{\mathrm{res}}(r,\theta,t)$, is obtained by linear theory, as is the case in linear Landau damping, there is only the m-th Fourier component, so there is no issue. However, when the resonant particle dynamics is nonlinear,

say, when particle trapping is involved, higher harmonics typically are present in $\delta n^{\text{res}}(r, \theta, t)$ and correspondingly in $\delta \phi^{\text{res}}(r, \theta, t)$. Why are these harmonic terms not balanced by such terms on the Right Hand Side of Eq. (4.24)? The reason is that we neglected small harmonic terms in the surface ripple of Eq. (4.15). These higher harmonic ripples are indeed small because the higher harmonics in $\delta \phi^{\text{res}}(r, \theta, t)$ do not drive the core surface resonantly. One can easily show that the harmonic ripple amplitudes are smaller than $D(t)$ by the factor $n_h/n_c \ll 1$.

As a simple application of Eq. (4.27), we evaluate $\delta \tilde{\phi}_m^{\text{res}}(R_c, t)$ for the case of a diocotron mode that experiences a linear Landau resonance in the low-density halo[18, 23]. We work only to first order in the small quantity $n_h/n_c \ll 1$. The resonant radius then need only be calculated to zero order in n_h/n_c. To this order, the $\mathbf{E} \times \mathbf{B}$-drift rotation frequency in the halo region $(r > R_c)$ is $\omega_E(r) = \omega_E(R_c) R_c^2/r^2$. Substituting this expression and dispersion relation (4.23) into the resonance condition $\omega_m = m\omega_E(r_{\text{res}})$ and dropping first order terms in n_h/n_c yields the expression for the resonant radius

$$\frac{R_c^2}{r_{\text{res}}^2} = 1 - \frac{1}{m}\left(1 - \frac{R_c^{2m}}{R_w^{2m}}\right). \tag{4.28}$$

Note that $r_{\text{res}} > R_c$ for all m.

From the linearized continuity equation and the Plemelj formula[57], one finds the expression for the perturbed density at the resonance

$$\delta \tilde{n}_m^{\text{res}}(r, t) = \frac{mc}{Br}\frac{\partial n}{\partial r}\delta \tilde{\phi}_m^{\text{non-res}}(r, t) i\pi\delta[\omega_m - m\omega_E(r)], \tag{4.29}$$

where $\delta \tilde{\phi}_m^{\text{non-res}}(r, t)$ is the potential due to the perturbed charge density on the surface of the core. Here we ignore $\delta \tilde{\phi}_m^{\text{res}}(r, t)$ set up by the fewer resonant particles, similar

to the case in Section 4.3. For $r > R_c$, this latter potential can be written as

$$\delta\tilde{\phi}_m^{\text{non-res}}(r,t) = \delta\tilde{\phi}_m^{\text{non-res}}(R_c,t)\frac{G_m(r,R_c)}{G_m(R_c,R_c)}, \tag{4.30}$$

where $\delta\tilde{\phi}_m^{\text{non-res}}(R_c,t)$ is easily extracted from Eq. (4.21). Substituting Eqs. (4.29) and (4.30) into Eq. (4.26) and evaluating the Green's function with Eq. (4.19) yields the result

$$\delta\tilde{\phi}_m^{\text{res}}(R_c,t) = \frac{(2\pi e)^2}{m}\frac{cR_c}{B}\frac{R_c^{2m}}{r_{\text{res}}^{2m}}\left(1 - \frac{r_{\text{res}}^{2m}}{R_w^{2m}}\right)^2\frac{n'(r_{\text{res}})}{m|\omega_E'(r_{\text{res}})|}i\pi D(t)n_c. \tag{4.31}$$

Substituting into Eq. (4.27) then yields the well-known damping rate[18, 23]

$$\frac{\dot{D}(t)}{D(t)} = \omega_E(R_c)\frac{n'(r_{\text{res}})R_c}{n_c}\frac{\pi}{2m}\left(\frac{R_c}{r_{\text{res}}}\right)^{2m-3}\left(1 - \frac{r_{\text{res}}^{2m}}{R_w^{2m}}\right)^2. \tag{4.32}$$

The case of an $m = 1$ diocotron wave provides a particularly clear illustration of this mechanical approach to the wave-particle interaction[4]. First, note that the $m = 1$ wave is special in that an analytic description of the wave is not limited ot the case of a "top-hat" density profile, but also is possible for any monotonically decreasing density profile, $n(r)$, that vanishes at the conducting wall. For many years it was thought that there can be no resonant wave-particle resonance for the $m = 1$ wave since the resonant radius is at the wall, and the unperturbed density is zero at the wall. However, recent experiments have observed a novel algebraic damping of the $m = 1$ wave when transport sweeps a low density halo of particles out from a central core to the wall[2]. The damping begins when the halo reaches the wall and is thought to be due to a nonlinear wave particle interaction in the region of the wall.

In the absence of a wave-particle interaction, the self-consistent density perturbation and wave potential for the $m = 1$ wave are given by the expressions

$$
\begin{aligned}
\delta n^{\text{non-res}}(r, \theta, t) &= -\frac{\partial n}{\partial r}[D \exp[i(\theta - \omega_1 t)] + \text{c.c.}] \\
&= -\frac{\partial n}{\partial r} A \cos(\theta - \omega_1 t - \alpha) \quad\quad (4.33)
\end{aligned}
$$

and

$$
\delta \phi^{\text{non-res}}(r, \theta, t) = -\frac{rB}{c}[-\omega_1 + \omega_E(r)] A \cos(\theta - \omega_1 t - \alpha). \quad\quad (4.34)
$$

Here, we have set $D = (A/2) \exp(-i\alpha)$, where A and α are real. By using the Green's function integral in Eq. (4.18) one can easily show that the density perturbation and potential are self-consistent, that is, substituting the density perturbation into the Green's function integral yields potential. The wave frequency is given by $\omega_1 = \omega_E(R_w)$, so the wave potential vanishes at the conducting wall.

Physically, such a density perturbation results when the plasma column is displaced off the trap axis by the amount A in the instantaneous direction $\theta = \omega_1 t + \alpha$. The displaced column produces an image in the conducting wall, and for small displacement (i.e. $A \ll R_w$) the image is well outside the wall, producing an image electric field that is nearly uniform in the region of the column. The uniform field produces a uniform $\mathbf{E} \times \mathbf{B}$ drift velocity of the column transverse to the instantaneous displacement off axis, and in turn this produces a rotation of the column around the trap axis at the mode frequency ω_1. In the wave potential, the term proportional to ω_1 is the potential due to the uniform image electric field, and the term proportional to $\omega_E(r)$ is the correction to the radial space charge potential due the shift of the column off axis.

We postulate that the non-resonant density perturbation still can be described as a displacement of the column off the trap axis even when the potential due to the resonant electrons acts back on the column. The reason for this simplification is easy to understand. The resonant particles are near the wall, so the field from these particles in the non-resonant region is a vacuum field, and the dipole component of such a field is uniform, as will be explained shortly. Thus, the field due to the resonant particles simply produces an increment to the uniform $\mathbf{E} \times \mathbf{B}$ drift motion produced by the non-resonant potential, and we will see that the increment can be accomodated simply by allowing a slow time dependence in $A(t)$ and $\alpha(t)$.

Formally, the condition that the postulate be satisfied is that continuity equation in the non-resonant region,

$$\left[\frac{\partial}{\partial t} + i\omega_E(r)\right]\delta n_1^{\text{non-res}}(r,t) = \frac{ic}{Br}[\delta\phi_1^{\text{non-res}}(r,t) + \delta\phi_1^{\text{res}}(r,t)]\frac{\partial n}{\partial r}, \qquad (4.35)$$

be satisfied when the Fourier components $\delta\phi_1^{\text{non-res}}(r,t)$ and $\delta n_1^{\text{non-res}}(r,t)$ are evaluated using the functional forms for the potential and density perturbation in Eqs. (4.33) and (4.34), allowing only that D, or equivalently A and α, are time-dependent. Substituting the Fourier components yields the equation

$$\dot{A}(t) - iA(t)\dot{\alpha}(t) = 2\dot{D}(t)e^{i\alpha(t)} = \frac{-2ic}{Br}\delta\phi_1^{\text{res}}(r,t)e^{i\omega_1 t + i\alpha(t)}. \qquad (4.36)$$

Since the Left Hand Side of the equation is independent of r it is necessary that the Right Hand Side be independent of r, or equivalently that $\delta\phi_1^{\text{res}}(r,t)$ be proportional

to r, and the Green's function solution,

$$\delta\phi_1^{\text{res}}(r,t) = -er \int_{\text{res}} 2\pi r' dr' \left(1 - \frac{r'^{2m}}{R_w^{2m}}\right) \delta n_1^{\text{res}}(r,t), \qquad (4.37)$$

does imply the required proportionality. In choosing the correct form of the Green's function from Eq. (4.18), we used the fact that $r < r'$ in the non-resonant region. Proper choice of the time-dependence in $A(t)$ and $\alpha(t)$ then allows both the real and imaginary parts of the equation to be satisfied.

Since $\delta\phi^{\text{res}}(r,\theta,t)$ is a vacuum potential in the non-resonant region, the dipole portion of the potential can be written in the form

$$\delta\phi^{\text{res}}(r,\theta,t) = -\delta E_x^{\text{res}}(t)r\cos(\theta - \omega_1 t - \alpha) - \delta E_y^{\text{res}}(t)r\sin(\theta - \omega_1 t - \alpha), \qquad (4.38)$$

where a rotating (x,y) coordinate system has been introduced, with the x-axis directed along the instantaneous displacement of the plasma column. The Fourier component of this expression is simply

$$\delta\phi_1^{\text{res}}(r,t) = \left[\frac{-\delta E_x^{\text{res}}(t)r}{2} + i\frac{\delta E_y^{\text{res}}(t)r}{2}\right]\exp[-i(\omega_1 t + \alpha)], \qquad (4.39)$$

so the real and imaginary parts of Eq. (4.36) take the form

$$\dot{A}(t) = \frac{c\delta E_y^{\text{res}}(t)}{B}, \qquad (4.40)$$

$$\dot{\alpha}(t)A(t) = \Delta\omega_1 A(t) = -\frac{c\delta E_x^{\text{res}}(t)}{B}. \qquad (4.41)$$

Here, we have identified $\dot{\alpha} \equiv \Delta\omega_1$ as a frequency shift. Physically, the uniform field that is transverse to the instantaneous displacement of the column (i.e., δE_y^{res})

produces an $\mathbf{E} \times \mathbf{B}$ drift motion of the plasma column parallel to the displacement, that is a damping or growth of the wave amplitude, and the component that is parallel to the displacement (i.e. $\delta E_x^{\mathrm{res}}$) produces an increment to the rotation velocity of the column around the trap-axis, that is, a wave frequency shift.

Chapter 4, in full, is a reprint of the material as it appears in Physics of Plasmas. C.Y. Chim, T.M. O'Neil, *Physics of Plasmas* **23**, 050801 (2016). The dissertation author was the primary investigator and author of this paper.

Appendix A

Evaluation of integrals Λ_1 and Λ_2

In this appendix, we evaluate the integrals

$$\Lambda_1(\bar{\kappa}) = \int_0^\infty \frac{d\sigma}{\sigma} \int_0^\infty \eta^3 d\eta f_1^2(\frac{\bar{\kappa}}{\sigma^3}, \eta) e^{-\sigma^2/2}, \tag{A.1}$$

$$\Lambda_2(\bar{\kappa}) = \int_0^\infty d\sigma \sigma^3 \int_0^\infty \eta d\eta f_2^2(\frac{\bar{\kappa}}{\sigma^3}, \eta) e^{-\sigma^2/2}, \tag{A.2}$$

where

$$f_1(\kappa, \eta) = \int_{-\infty}^\infty \frac{\cos(\kappa\xi)d\xi}{[\eta^2 + \zeta^2(\xi)]^{3/2}}, \tag{A.3}$$

$$f_2(\kappa, \eta) = \int_{-\infty}^\infty \frac{\cos(\kappa\xi)d\xi}{[\eta^2 + \zeta^2(\xi)]^{3/2}}(1 - \frac{3\eta^2}{2[\eta^2 + \zeta^2(\xi)]}). \tag{A.4}$$

Here, $\zeta(\xi)$ satisfies the differential equation

$$(\frac{d\zeta}{d\xi})^2 + \frac{1}{\sqrt{\eta^2 + \zeta^2(\xi)}} = 1, \tag{A.5}$$

where $\xi\;=$ is chosen so that $\zeta^2(\xi)$ is even in ξ. This is the case when $\zeta^2(0) = \max(0, 1 - \eta^2)$. Also, note that in Eqs. (A.3) and (A.4) κ stands in for $\kappa = \bar{\kappa}/\sigma^3$.

For large $\bar{\kappa}$, the integrands in Eqs. (A.3) and (A.4) involve the product of a rapidly oscillating function and a slowly varying function, and efficient evaluation of such integrals can be effected through analytic continuation. Following the earlier work of O'Neil and Hjorth[9], we define $x = \sqrt{\eta^2 + \zeta^2(\xi)}$, which satisfies the differential equation

$$\frac{dx}{d\xi} = \frac{i\sqrt{x - \eta}\sqrt{x + \eta}\sqrt{x - 1}}{x\sqrt{-x}}, \tag{A.6}$$

where $x(\xi = 0) = \max(\eta, 1)$. In the square roots of Eq. (A.6), the branch cut for any function $\sqrt{w(x)}$ is taken along $\arg w(x) = 0$. The Right Hand Side of Eq. (A.6) then has branch cuts for $x < -\eta$, $0 < x < \min(\eta, 1)$ and $x > \max(\eta, 1)$.

We first consider the case where $\eta < 1$, that is, where there is reflection. The case of no reflection ($\eta > 1$) follows similarly. For $\eta < 1$, the branch cuts are indicated by the thick solid lines in Fig. A.1(b). As ξ moves from $-\infty$ to ∞ along the dashed contour in Fig. A.1(a), $x(\xi)$ moves along the dashed contour in Fig. A.1(b), reaching the turning point $x = 1$ at $\xi = 0$, i.e. $x(0) = 1$. Because $x(\xi)$ is even in ξ, the integrals in Eqs. (A.3) and (A.4) can be rewritten as

$$f_1(\kappa, \eta) = \int_C \frac{\exp(i\kappa\xi)d\xi}{x^3(\xi)}, \tag{A.7}$$

$$f_2(\kappa, \eta) = \int_C \frac{\exp(i\kappa\xi)d\xi}{x^3(\xi)}[1 - \frac{\eta^2}{x^2(\xi)}]. \tag{A.8}$$

The goal here is to analytically continue the ξ-contour so that the integrands themselves exhibit the exponentially small value of the integrands, so we push the
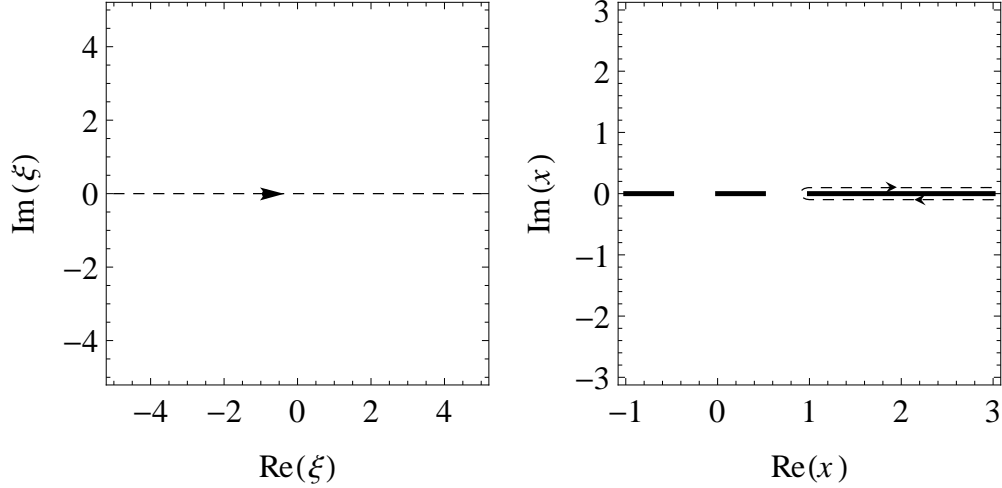
Figure A.1: Path (dashed curve) of the original contour in ξ-plane (a) and x-plane (b). Branch cuts are denoted by thick solid lines, and in this figure, $\eta = 0.5$.

ξ-contour toward positive imaginary values. The deformation can continue until the $x(\xi)$ contour collides with the branch cut ending at $x = \eta$ as shown in Figs. A.2(a) and A.2(b).

During the deformation, the turning point moves from $x = 1$ to $x = \eta$, and ξ-image of the turning point moves from $\xi = 0$ to

$$\xi = ig(\eta) = i \int_\eta^1 \frac{x^{2/3}dx}{\sqrt{1-x}\sqrt{x^2 - \eta^2}}, \tag{A.9}$$

where use has been made of Eq. (A.6). The two points around which the x-contour loop are the images of $x = 0$ approached from opposite sides of the branch cut between $x = 0$ and $x = \eta$. From Eq. (A.6), we see that the coordinates of these two points in the complex ξ-plane are $\xi = ig(\eta) \pm r(\eta)$, where

$$r(\eta) = \int_0^\eta \frac{x^{2/3}dx}{\sqrt{1-x}\sqrt{\eta^2 - x^2}}. \tag{A.10}$$
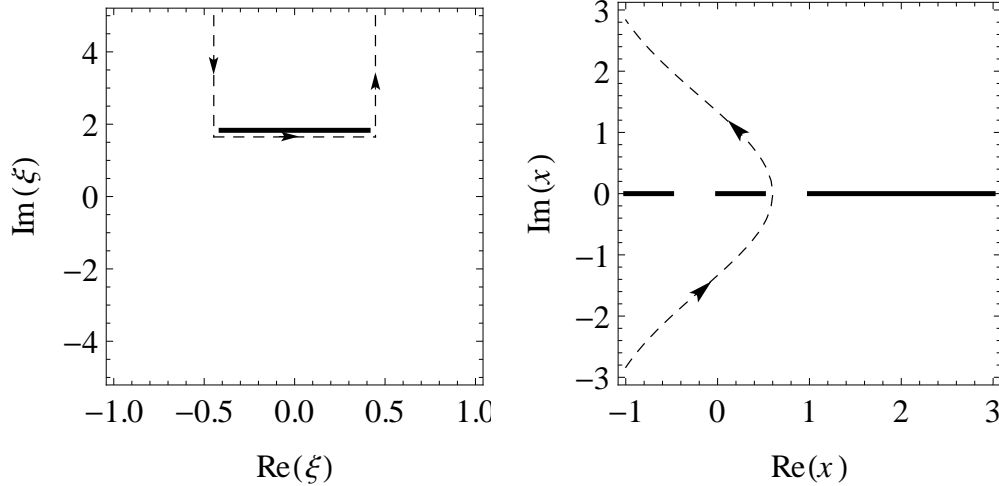
Figure A.2: Path (dashed curve) of the deformed contour in ξ-plane (a) and x-plane (b). Branch cuts are denoted by thick solid lines, and in this figure, $\eta = 0.5$.

There is a branch cut between the two points in the function $x(\xi)$.

Since the singularities of the integrands in Eqs. (A.7) and (A.8) involve more than just isolated poles, the integrals cannot be expressed as the sum of residues. Nevertheless, for sufficiently large κ, one can see that the integrals are of order $\exp[-g(\eta)\kappa]$, that is, one obtains the asymptotic forms $f_j(\kappa, \eta) = h_j(\kappa, \eta) \exp[-g(\eta)\kappa]$ quoted in Eqs. (2.35) and (2.36) of Section 2.3. Here, the quantities $h_j(\kappa, \eta)$ are neither exponentially small nor large, and for small η are given by[9] $h_j(\kappa, \eta) \simeq 8\pi\kappa/9$.

The integrals also are evaluated by numerically carrying out the ξ-integral along the deformed contour in Fig. A.2(a). Fig. (2.1) of Section 2.3 shows a comparison of the numerical and asymptotic evaluations of $f_1(\kappa, \eta = 0) = f_2(\kappa, \eta = 0)$.

Returning to an evaluation of integrals (A.3) and (A.4), we first note that $g(\eta)$ is an increasing function of η. Thus, for sufficiently large values of $\bar{\kappa}$, only small values of η contribute to the integrals, and we may use the approximation $h_j(\kappa, \eta) \simeq h_j(\kappa, 0) = 8\pi\kappa/9$, or $h_j(\bar{\kappa}/\sigma^3, \eta) \simeq h_j(\kappa, 0) = 8\pi\bar{\kappa}/(9\sigma^3)$. Also, for small
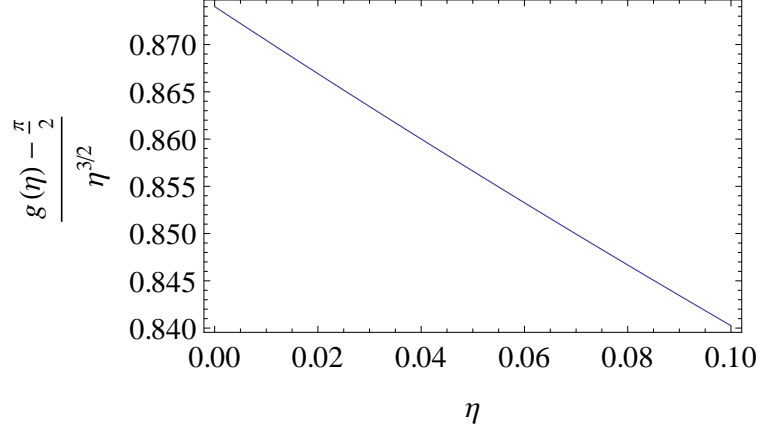
Figure A.3: Curve fitting of $g(\eta)$ against η, showing that $g(\eta) - g(0) \sim \mathcal{O}(\eta^{3/2})$.

values of η, one can see by curve fitting that $g(\eta) \simeq \pi/2 + \lambda\eta^{3/2}$, where $\lambda = 0.874$ (see Fig. A.3). The integrations over η can then be carried out in Eqs. (A.3) and (A.4) yielding the integrals

$$\Lambda_1(\bar{\kappa}) = (\frac{8\pi}{9})^2 \frac{\bar{\kappa}^2}{(2\bar{\kappa}\lambda)^{8/3}} \cdot \frac{2}{3}\Gamma(\frac{8}{3}) \int_0^\infty d\sigma\sigma e^{-\sigma^2/2} e^{-\pi\bar{\kappa}/\sigma^3}, \tag{A.11}$$

$$\Lambda_2(\bar{\kappa}) = (\frac{8\pi}{9})^2 \frac{\bar{\kappa}^2}{(2\bar{\kappa}\lambda)^{4/3}} \cdot \frac{2}{3}\Gamma(\frac{4}{3}) \int_0^\infty d\sigma\sigma e^{-\sigma^2/2} e^{-\pi\bar{\kappa}/\sigma^3}. \tag{A.12}$$

The σ-integrals in these two equations are identical and involve the product of an exponentially decreasing function, $\exp(-\sigma^2/2)$, and an exponentially increasing function, $\exp(-\pi\bar{\kappa}/\sigma^3)$. Evaluating the integrals by the saddle point method yields the large $\bar{\kappa}$ asymptotic formulae

$$\Lambda_1(\bar{\kappa}) = 3.10\bar{\kappa}^{-7/15} e^{-5(3\pi\bar{\kappa})^{2/5}/6}, \tag{A.13}$$

$$\Lambda_2(\bar{\kappa}) = 3.87\bar{\kappa}^{13/15} e^{-5(3\pi\bar{\kappa})^{2/5}/6}. \tag{A.14}$$

Numerical evaluations of $\Lambda_1(\bar{\kappa})$ and $\Lambda_2(\bar{\kappa})$ have been carried out for a series of

$\bar{\kappa}$ values. At each of these values, the quantities $h_j(\bar{\kappa}/\sigma^3, \eta)$ are evaluated for an array of (σ, η) values using the analytic continuation described earlier. The integrands are peaked near some values (σ_0, η_0), and the (σ, η) integrands are evaluated by choosing (σ, η) values near the peak and smoothly interpolating the integrand between these points. The results of the integration are given for a series of $\bar{\kappa}$ values in Table (A.1) and (A.2). Also, Figs. (A.4) and (A.5) show a comparison of the numerical evaluations (dots) and the asymptotic formulae (solid curves).

Table A.1: Numerically integrated values of $\Lambda_1(\bar{\kappa})$ for different values of $\bar{\kappa}$

$\bar{\kappa}$	$\Lambda_1(\bar{\kappa})$	$\bar{\kappa}$	$\Lambda_1(\bar{\kappa})$
5	0.222	200	5.06×10^{-8}
10	5.06×10^{-2}	300	6.92×10^{-10}
20	7.71×10^{-3}	500	1.29×10^{-11}
50	2.41×10^{-4}	700	2.89×10^{-13}
100	5.95×10^{-6}	1000	3.15×10^{-15}

Table A.2: Numerically integrated values of $\Lambda_2(\bar{\kappa})$ for different values of $\bar{\kappa}$

$\bar{\kappa}$	$\Lambda_2(\bar{\kappa})$	$\bar{\kappa}$	$\Lambda_2(\bar{\kappa})$
0.01	3.250	20	2.837×10^{-1}
0.05	3.230	50	3.074×10^{-2}
0.1	3.201	100	2.338×10^{-3}
0.7	2.850	200	4.989×10^{-5}
2	2.419	350	1.685×10^{-6}
6	1.251	500	4.195×10^{-8}
10	7.523×10^{-1}		

We can compare our results with previous work. If we consider equipartition of a strongly magnetized single-species plasma, where $n = n_1$ and $n_2 = 0$, $T_{\perp 1}$ equilibrates with $T_{\parallel}$ following the rate equation

$$\frac{dT_{\perp 1}}{dt} = (T_{\parallel} - T_{\perp 1})\bar{n}_1 \bar{b}^2 \bar{v}_{11} I(\bar{\kappa}_{11}), \tag{A.15}$$
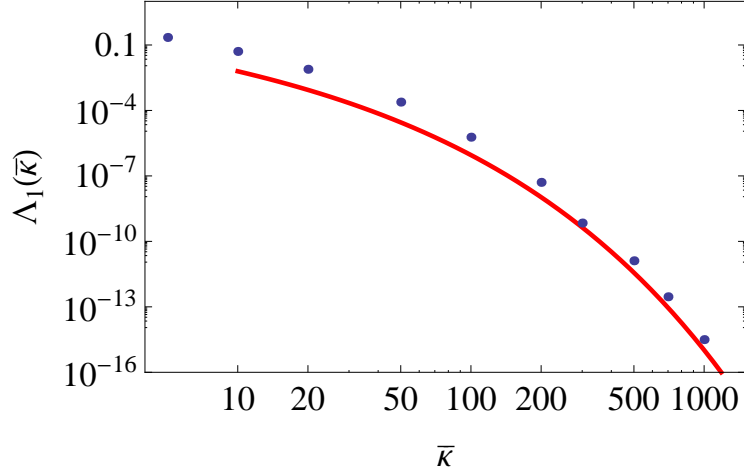
Figure A.4: Numerically integrated values of $\Lambda_1(\bar{\kappa})$ (dots) and its asymptotic graph (red line).

where $I(\bar{\kappa}_{11}) = \sqrt{2\pi}\Lambda_1(\bar{\kappa}_{11})/8$ from Eqn. (2.63). The function $I(\bar{\kappa})$ was evaluated in the work of O'Neil and Hjorth[9] and Glinksy *et. al.*[8]. In Fig. (A.6), numerical values of $I(\bar{\kappa})$ in our work are plotted as points together with values obtained by Glinsky *et. al.* using Monte Carlo simulations. The different sets of values follow very close trends. Furthermore, in the limit of large $\bar{\kappa}$, O'Neil and Hjorth obtained an asymptotic formula for $I(\bar{\kappa})$

$$I(\bar{\kappa}) = 0.47\bar{\kappa}^{-1/5}\exp[-\frac{5}{6}(3\pi\bar{\kappa})^{2/5}], \tag{A.16}$$

while the asymptotic formula from Glinsky *et. al.* is

$$
\begin{aligned}
I(\bar{\kappa}) &= (1.83\bar{\kappa}^{-7/15} + 20.9\bar{\kappa}^{-11/15} + 0.347\bar{\kappa}^{-13/15} + 87.8\bar{\kappa}^{-15/15} + 6.68\bar{\kappa}^{-17/15}) \\
&\quad \cdot \exp[-\frac{5}{6}(3\pi\bar{\kappa})^{2/5}]. \tag{A.17}
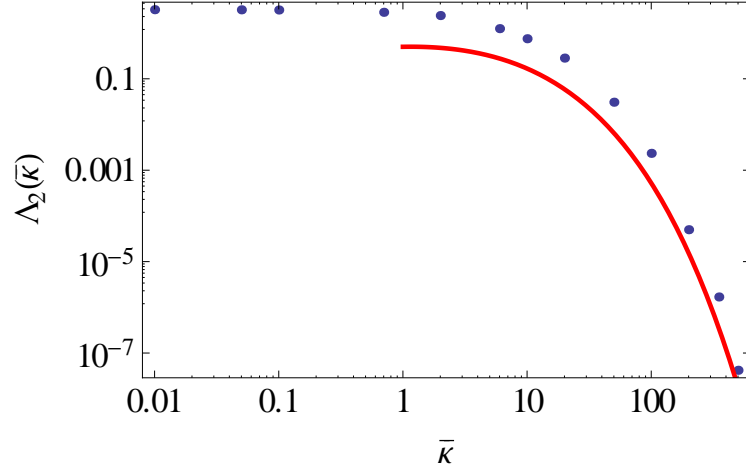\end{aligned}
$$

Figure A.5: Numerically integrated values of $\Lambda_2(\bar{\kappa})$ (dots) and its asymptotic graph (red line).

From Eqn. (A.13), our version is

$$I(\bar{\kappa}) = 0.97\bar{\kappa}^{-7/15} \exp[-\frac{5}{6}(3\pi\bar{\kappa})^{2/5}]. \tag{A.18}$$

Our asymptotic formula is an improved version of the work of O'Neil and Hjorth. We approximate $g(\eta)$ with $\eta^{3/2}$ as the lowest-order non-constant term, which is more accurate than η^2 in the work of O'Neil and Hjorth. However, we believe the result from Glinsky *et. al.* is even better, since their work investigated the cyclotron motion in much greater detail. In the same Fig. (A.6), we plot the graphs of the three asymptotic expressions together with the points of numerically integrated values mentioned above. All the plotted graphs and data points show the similar exponential decrease of $I(\bar{\kappa})$ with increasing $\bar{\kappa}$.
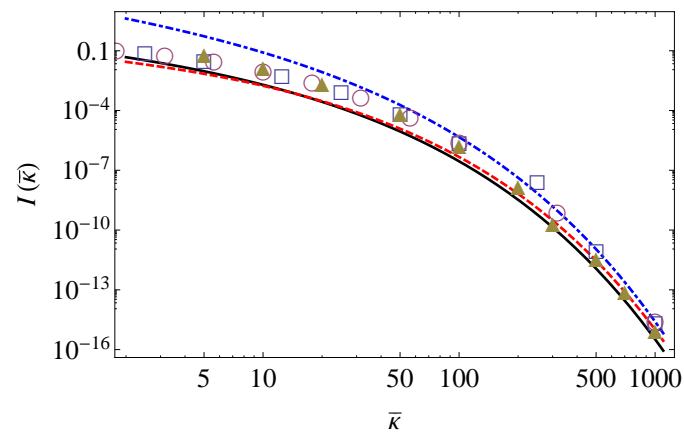
Figure A.6: Numerical values and asymptotic graphs of $I(\bar{\kappa})$. Solid triangles correspond to our calculated values. Empty circles and squares are values calculated by Glinsky *et. al.* using two different sets of Monte Carlo simulations[8]. The solid line is the graph of our asymptotic expressions. The dashed and dot-dashed curves corresponds to the asymptotic expressions from O'Neil and Hjorth and Glinsky *et. al.* respectively.

Appendix B

Numerical solution for diffusive broadening

This appendix describes a numerical solution of the transport equation (3.51) using an eigenfunction expansion. This solution follows a similar approach in the work of Dubin and Tsidulko[61].
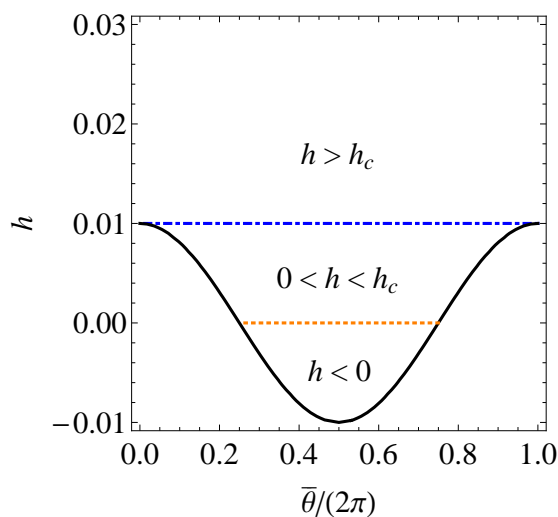

Figure B.1: Illustration of the region for which Eq. (3.51) is solved. The black solid curve is the scrape-off layer. The blue dot-dashed curve is the critical contour $h = h_c$. The orange dotted curve is the contour $h = 0$.

Fig. (B.1) illustrates the region of the solution of Eq. (3.51). In this figure, we set $p = \Delta p = 10^{-2}$ to be the scrape-off layer. The scrape-off layer is the black solid contour $h = \Delta p \cos \bar{\theta}$, with smaller term $(\Delta p)^2$ dropped. The critical contour, which is the blue dot-dashed curve, is $h = h_c = \Delta p$. The orange dotted curve is the contour $h = 0$.

The region for which $n(\bar{\theta}, h)$ is solved is bounded in the figure by the scrape-off layer and the straight lines $\bar{\theta} = 0$ and $\bar{\theta} = 2\pi$. It can be divided into three region of interests, which are $h > h_c$, $0 < h < h_c$ and $h < 0$. The three regions are to be explained in the paragraphs that follow. Meanwhile three boundary conditions of Eq. (3.51) will be introduced in the explanation.

The first region, $h > h_c$, is taken to extend to infinite h, since we are interested in the regime $h < h_b \ll 1$ and the non-resonant region is far from the wall. At large h, the density is equal to that at the edge of the non-resonant region. Therefore

$$\lim_{h \to \infty} n(\bar{\theta}, h) = n^{(0)}(R_1), \tag{B.1}$$

which is our first boundary condition.

Our second boundary condition is the periodic boundary condition $f(\bar{\theta} = 0, h) = f(\bar{\theta} = 2\pi, h)$, as $\bar{\theta} = 0$ and $\bar{\theta} = 2\pi$ refers to the same physical point. It only applies in the region $h > h_c$, which is the only region that can access $\bar{\theta} = 0$ and $\bar{\theta} = 2\pi$.

The second region, $0 < h < h_c$, is the region of open orbits in contact with the scrape-off layer, where the density must be zero, i.e.

$$n(\bar{\theta}, h = \Delta p \cos \bar{\theta}) = 0. \tag{B.2}$$

In this region, the range of $\bar{\theta}$ that a particle can access is bounded by the scrape-off layer.

The third region, $h < 0$, differs from the first and second region in that the contours are closed in this region. We continue to apply Eq. (3.51) in this region, and use the same zero-density boundary $h = \Delta p \cos \bar{\theta}$ as in the second region. However in Eq. (3.51), the factor $\partial h / \partial p$ takes $p = p_-(\bar{\theta}, h)$ from Eq. (3.54) when $p(\bar{\theta}, h)$ is expressed, and misses the $p = p_+(\bar{\theta})$ part of the closed contour for $h < 0$. Fortunately, the error is negligible because this region is dynamically inaccessible to the particles, as discussed in the small-diffusion condition (3.82) in Section 3.6. There are literally no particles for $h < 0$, and thus n is vanishingly small in this region.

Since Eq. (3.51) is linear and the boundary conditions are homogeneous, the density may be normalized as $f \equiv n / n^{(0)}(R_1)$ and the equation rewritten as

$$\left. \frac{\partial f}{\partial \bar{\theta}} \right|_h = \frac{\partial}{\partial h} [\beta f - \delta \left. \frac{\partial h}{\partial p} \right|_{\bar{\theta}} \left. \frac{\partial f}{\partial h} \right|_{\bar{\theta}}]. \tag{B.3}$$

In order to fit the boundary condition more easily, we change variables from $(\bar{\theta}, h)$ to $(\bar{\theta}, x)$, where $x \equiv h - \Delta p \cos \bar{\theta}$. Fig. (B.2) shows the region of solution in the $(\bar{\theta}, x)$ space. The black solid line is the scrape-off layer. The blue dot-dashed curve is the critical contour $h = h_c$ and the orange dotted curve is the contour $h = 0$. As we see from the figure, the region of solution in Fig. (B.1) is reshaped to the semi-infinite rectangular region in Fig. (B.2). The boundaries of the region of solution are lines $x = 0$, $\bar{\theta} = 0$, and $\bar{\theta} = 2\pi$, and the region extends to infinite x. As discussed when the region was described in $(\bar{\theta}, h)$-space, the solution is solved considering the three subregions $h > h_c$, $0 < h < h_c$ and $h < 0$ as a whole, although we expect the value of f in the dynamically inaccessible region $h < 0$ to be vanishingly small.
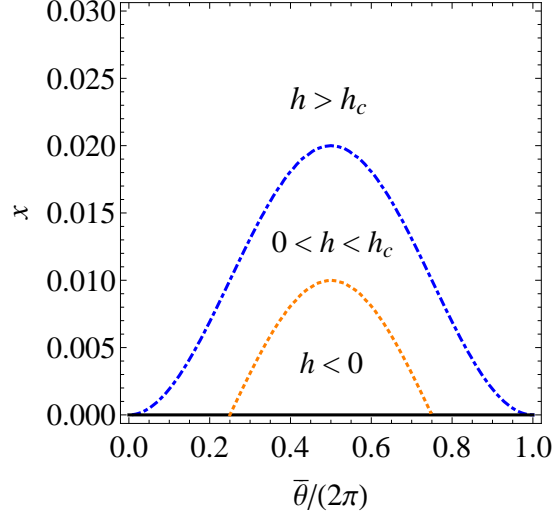
Figure B.2: Illustration of the region of solution in $(\bar{\theta}, x)$-space. The black solid line is the scrape-off layer. The blue dot-dashed curve is the critical contour $h = h_c$. The orange dotted curve is the contour $h = 0$.

In this new set of variables and the normalized density, the first boundary condition, which is the large-h limit (B.1), is expressed as

$$\lim_{x \to \infty} f = 1. \tag{B.4}$$

The second boundary condition, which is the periodic boundary condition, is rephrased as $f(\bar{\theta} = 0, x) = f(\bar{\theta} = 2\pi, x)$. It applies only to the region $h > h_c$, the same as when the region was described in terms of $(\bar{\theta}, h)$. Since the region $h > h_c$ reaches all values of $x > 0$, the periodic boundary condition applies for all $x > 0$.

More importantly, at the scrape-off layer, the third boundary condition (B.2) is now expressed as

$$f(\bar{\theta}, x = 0) = 0, \tag{B.5}$$

which is much easier to work with as the scrape-off layer is straightened to be the horizontal line $x = 0$, and $\bar{\theta}$-dependence is avoided.

By using the relations $\partial_h|_{\bar\theta} = (\partial x/\partial h)\partial_x|_{\bar\theta}$ and $\partial_{\bar\theta}|_h = (\partial x/\partial\bar\theta)\partial_x|_{\bar\theta} + \partial_{\bar\theta}|_x$ Eq. (B.3) is rewritten in the form

$$\left.\frac{\partial f}{\partial\bar\theta}\right|_x + \Delta p\sin\bar\theta\left.\frac{\partial f}{\partial x}\right|_{\bar\theta} = \frac{\partial}{\partial x}[\beta f - \delta\cdot\eta(x,\bar\theta)\left.\frac{\partial f}{\partial x}\right|_{\bar\theta}]. \tag{B.6}$$

Here $\eta(\bar\theta, x) \equiv \partial h/\partial p$ is explicitly expressed as

$$\eta(\bar\theta, x) = -\sqrt{\cos^2\bar\theta + 4h(\bar\theta, x)} \tag{B.7}$$

using the relations (3.48) and (3.54). The fact that we are interested in the region $0 < h < h_b \ll 1$ permits us to remove the x-dependence in η by neglecting h and thus approximating

$$\eta(\bar\theta, x) \simeq \eta(\bar\theta) \equiv -|\cos\bar\theta|. \tag{B.8}$$

Since $f(\bar\theta, x)$ and $\eta(\bar\theta)$ are both periodic in $\bar\theta$ for all values of x, they may be expressed as the Fourier Series

$$f(\bar\theta, x) = \sum_{\mu=-\infty}^{+\infty} f_\mu(x)e^{i\mu\bar\theta}, \tag{B.9}$$

$$\eta(\bar\theta) = \sum_{\nu=-\infty}^{+\infty} \eta_\nu e^{i\nu\bar\theta}, \tag{B.10}$$

where $\eta_\nu = -\int_0^{2\pi} d\bar\theta|\cos(\bar\theta)|e^{-i\nu\bar\theta}/(2\pi)$. Note that $f_{-\mu} = f_\mu^*$ and $\eta_{-\nu} = \eta_\nu^*$ as f and η are real functions. In practice, both series must be truncated when solving numerically for [i.e. $f_\mu = 0$ if $|\mu| > N_f$, and $\eta_\nu = 0$ if $|\nu| > N_\eta$]. N_f and N_η are positive integers chosen to be sufficiently large to resolve $\eta(\bar\theta)$ and to obtain a converged solution of $f(\bar\theta, x)$.

Substituting Fourier expansions (B.9) and (B.10) into Eq. (B.6), using the relation $\sin\bar\theta = (e^{i\bar\theta} - e^{-i\bar\theta})/(2i)$ and equating coefficients of $e^{i\mu\bar\theta}$ on both sides yields the differential equations

$$i\mu f_\mu(x) + i\frac{\Delta p}{2}[f'_{\mu+1}(x) - f'_{\mu-1}(x)] = \beta f'_\mu(x) - \delta \sum_{\nu=-N_\eta}^{N_\eta} \eta_{-\nu} f''_{\mu+\nu}(x). \qquad (B.11)$$

This is a set of $2N_f + 1$ linear coupled ODEs, as the subscript μ counts from $-N_f$ to N_f. Since the coefficients are constants, we seek a solution of the form $f_\mu(x) = C_\mu e^{-sx}$. Substituting this form of solution into Eq. (B.11) yields a set of eigenvalue equations

$$i\mu C_\mu - is\frac{\Delta p}{2}[C_{\mu+1} - C_{\mu-1}] = -s\beta C_\mu + s^2\delta \sum_{\nu=-N_\eta}^{N_\eta} \eta_{-\nu} C_{\mu+\nu}, \qquad (B.12)$$

with s as the eigenvalue and C_μ as the μ-th element of the eigenvector. By inspection, there is an obvious eigenvalue $s = 0$ with the coefficient $C_\mu = \delta_{\mu 0}$ as the eigenvector. This eigenvector corresponds to the a constant eigenfunction $f_\mu(x) = \delta_{\mu 0}$, and we set C_0 to be 1 so as to satisfy Eq. (B.4) for large x. Other physically admissible eigenvalues are the ones with positive real parts, denoted as $\{s_r\}$ with the eigenvector $\{C_{\mu,r}\}$, since the eigenfunctions die out in the form of $e^{-\mathrm{Re}[s_r]x}e^{-i\mathrm{Im}[s_r]x}$ when x is large. The subscript r refers to the r-th eigenvalue and eigenvector.

Both the eigenvalues and the eigenvectors are obtained numerically. It is noteworthy that in the numerical solutions, the eigenvalue with the smallest positive real part is equal to $\pi\beta/(2\delta)$, which is the reciprocal of the diffusive broadening scale $(\Delta h)_1$ in Eq. (3.81). Its eigenfunction, which then has the form $e^{-x/(\Delta h)_1}$, is responsible for the change of density over that broadening region. Other eigenvalues are not as recognizable though, and the respective eigenfunctions superpose, together

with that for the scale $(\Delta h)_1$, to produce the delicate density structure around $h = h_c$ in Fig. (3.6).

The total solution is a superposition of all the eigenfunctions

$$f(\bar{\theta}, x) = 1 + \sum_r \sum_{\mu=-N_f}^{N_f} A_r C_{\mu,r} e^{-s_r x} e^{i\mu\bar{\theta}}, \tag{B.13}$$

where A_r is the coefficient of the r-th eigenfunction.

We have to satisfy the boundary condition at the scrape-off layer, therefore by following Eq. (B.5), we obtain the condition

$$0 = f(\bar{\theta}, x = 0) = 1 + \sum_r \sum_{\mu=-N_f}^{N_f} A_r C_{\mu,r} e^{i\mu\bar{\theta}}. \tag{B.14}$$

Collecting coefficients for every Fourier component yields the set of coupled equations

$$0 = \delta_{\mu 0} + \sum_r A_r C_{\mu,r} \tag{B.15}$$

from which $\{A_r\}$ is solved numerically.

References

[1] C. Y. Chim, T. M. O'Neil, and D. H. Dubin, Phys. Plasmas **21**, 042115 (2014).

[2] A. Kabantsev, C. Chim, T. O'Neil, and C. Driscoll, Phys. Rev. Lett. **112**, 115003 (2014).

[3] C. Y. Chim and T. M. O'Neil, Flux-driven algebraic damping of diocotron modes, in *NON-NEUTRAL PLASMA PHYSICS IX: 11th International Workshop on Non-Neutral Plasmas*, edited by H. Himura, A. Sanpei, and Y. Soga, volume 1668, p. 020004, AIP Publishing, 2015.

[4] C. Y. Chim and T. M. O'Neil, Phys. Plasmas **23**, 072113 (2016).

[5] C. Y. Chim and T. M. O'Neil, Phys. Plasmas **23**, 050801 (2016).

[6] B. Beck, J. Fajans, and J. Malmberg, Phys. Rev. Lett. **68**, 317 (1992).

[7] B. Beck, J. Fajans, and J. Malmberg, Phys. Plasmas **3**, 1250 (1996).

[8] M. E. Glinsky, T. M. O'Neil, M. N. Rosenbluth, K. Tsuruta, and S. Ichimaru, Phys. Fluids B **4**, 1156 (1992).

[9] T. O'Neil and P. Hjorth, Phys. Fluids **28**, 3241 (1985).

[10] T. O'Neil, P. Hjorth, B. Beck, J. Fajans, and J. Malmberg, Collisional relaxation of strongly magnetized pure electron plasma (theory and experiment), in *Strongly coupled Plasma Physics, Proceedings of the Yamada Conference*, number 24, p. 313, 1990.

[11] M. Affolter, F. Anderegg, C. Driscoll, and D. Dubin, Cyclotron resonances in a non-neutral multispecies ion plasma, in *AIP Conference Proceedings*, volume 1521, p. 175, 2013.

[12] E. Sarid, F. Anderegg, and C. Driscoll, Phys. Plasmas **2**, 2895 (1995).

[13] L. Landau and E. Lifshitz, *Statistical Physics*, Number v. 5, Elsevier Science, 1996.

[14] R. C. Davidson, chapter 6, pp. 289–343, Imperial College Press, 2001.

[15] R. Levy, Phys. Fluids **8**, 1288 (1965).

[16] C. Driscoll and K. Fine, Phys. Fluids B **2**, 1359 (1990).

[17] J. Fajans, E. Gilson, and L. Friedland, Phys. Rev. Lett. **82**, 4444 (1999).

[18] R. Briggs, J. Daugherty, and R. Levy, Phys. Fluids **13**, 421 (1970).

[19] N. J. Balmforth, S. G. Llewellyn Smith, and W. R. Young, J. Fluid Mech. **426**, 95 (2001).

[20] W. D. White, J. H. Malmberg, and C. F. Driscoll, Phys. Rev. Lett. **49**, 1822 (1982).

[21] R. C. Davidson and E. H. Chao, Phys. Plasmas **3**, 3279 (1996).

[22] A. Kabantsev and C. Driscoll, Fus. Sci. and Tech. **51**, 96 (2007).

[23] D. Schecter, D. Dubin, A. Cass, C. Driscoll, I. Lansky, and T. O'Neil, Phys. Fluids **12**, 2397 (2000).

[24] S. Crooks and T. ONeil, Phys. Plasmas **2**, 355 (1995).

[25] B. Cluggish and C. Driscoll, Phys. Rev. Lett. **74**, 4213 (1995).

[26] E. Sarid, E. P. Gilson, and J. Fajans, Phys. Rev. Lett. **89**, 105002 (2002).

[27] A. Kabantsev, C. Driscoll, T. Hilsabeck, T. O'Neil, and J. Yu, Phys. Rev. Lett. **87**, 225002 (2001).

[28] T. M. O'Neil, Phys. Fluids **23**, 2216 (1980).

[29] T. M. O'Neil and R. A. Smith, Phys. Fluids B **4**, 2720 (1992).

[30] L. Landau, Sov. Phys. JETP **16**, 574 (1946).

[31] F. Chen, *Kinetic Theory*, chapter 7, pp. 225–285, Volume 1 of [62], 2nd edition, 1974.

[32] J. Dawson, Phys. Fluids **4**, 869 (1961).

[33] T. Stix, *Waves in plasmas*, chapter 8, pp. 169–216, American Institute of Physics, 1992.

[34] R. Kulsrud, *Plasma Physics for Astrophysics*, chapter 10, pp. 286–290, Princeton University Press, 2005.

[35] C. Driscoll and K. Fine, Phys. Fluids B **2**, 1359 (1990).

[36] H. Goldstein, C. Poole, and J. Safko, *Classical Mechanics*, Addison-Wesley Longman, Incorporated, 2002.

[37] G. R. Smith and A. N. Kaufman, Phys. Fluids **21**, 2230 (1978).

[38] R. G. Littlejohn, J. Plasma Phys. **29**, 111 (1983).

[39] J. Taylor, Phys. Fluids **7**, 767 (1964).

[40] J. C. Butcher, J. Austr. Math. Soc. **4**, 179 (1964).

[41] D. H. Dubin and T. O'Neil, Rev. Mod. Phys. **71**, 87 (1999).

[42] S. Ichimaru, *Basic Principles of Plasma Physics: A Statistical Approach*, Frontiers in Physics, Benjamin, 1973.

[43] D. J. Evans and G. Morriss, *Statistical mechanics of nonequilibrium liquids*, Cambridge University Press, 2008.

[44] F. Anderegg, X.-P. Huang, E. Sarid, and C. Driscoll, Rev. Sci. Instrum. **68**, 6 (1997).

[45] D. H. Dubin and T. O'Neil, Phys. Fluids **29**, 11 (1986).

[46] D. Larson, J. Bergquist, J. Bollinger, W. M. Itano, and D. Wineland, Phys. Rev. Lett. **57**, 70 (1986).

[47] T. M. O'Neil, Phys. Fluids **24**, 1447 (1981).

[48] T. G. Northrop, *The adiabatic motion of charged particles*, volume 21, Interscience Publishers New York, 1963.

[49] R. Levy, Phys. Fluids **11**, 920 (1968).

[50] J. Taylor, Phys. Fluids **7**, 767 (1964).

[51] T. O'Neil and R. Smith, Phys. Plasmas **1**, 2430 (1994).

[52] H. Goldstein, C. Poole, and J. Safko, chapter 8, pp. 334–367, Addison–Wesley, 3rd edition, 2002.

[53] H. Goldstein, C. Poole, and J. Safko, chapter 9, pp. 368–429, Addison–Wesley, 3rd edition, 2002.

[54] C. Driscoll, K. Fine, and J. Malmberg, Phys. Fluids **29**, 2015 (1986).

[55] M. Balkanski and R. F. Wallis, volume 8, chapter 8, pp. 159–160, Oxford University Press, 2000.

[56] F. Chen, *Plasmas as Fluids*, chapter 3, p. 63, Volume 1 of [62], 2nd edition, 1974.

[57] A. Zangwill, chapter 1, p. 13, Modern Electrodynamics, Cambridge University Press, 2013.

[58] T. O'Neil, Phys. Fluids **8**, 2255 (1965).

[59] J. Danielson, F. Anderegg, and C. Driscoll, Phys. Rev. Lett. **92**, 245003 (2004).

[60] J. deGrassie and J. Malmberg, Phys. Fluids **23**, 63 (1980).

[61] D. H. Dubin and Y. A. Tsidulko, Phys. Plasmas **18**, 062114 (2011).

[62] F. Chen, *Introduction to Plasma Physics and Controlled Fusion*, volume 1, Plenum Press, 2nd edition, 1974.